

Characterization of Phase Behavior and Protein Interactions of Monoclonal Antibodies

zur Erlangung des akademischen Grades eines
DOKTORS DER INGENIEURWISSENSCHAFTEN (Dr.-Ing.)

der Fakultät für Chemieingenieurwesen und Verfahrenstechnik des
Karlsruher Institut für Technologie (KIT)

genehmigte

DISSERTATION

von

Dipl.-Ing. Natalie Rakel, geb. Schnabel

aus Herscheid

Referent: Prof. Dr. Jürgen Hubbuch

Korreferent: Prof. Dr.-Ing. Matthias Kind

Tag der mündlichen Prüfung: 24.04.2015

Nicht Kunst und Wissenschaft allein,

Geduld will bei dem Werke sein.

Johann Wolfgang von Goethe (1749-1832): Faust I

Danksagungen

An dieser Stelle möchte ich mich ganz herzlich bei meinem Doktorvater Prof. Jürgen Hubbuch bedanken. Er hat mir die Möglichkeit gegeben, an seinem Institut ein hochinteressantes Thema zu bearbeiten und mir dabei sowohl den Freiraum für meine eigenen Ideen gelassen als auch mich bei der Umsetzung meiner Ziele unterstützt.

Darüber hinaus bedanke ich mich bei Prof. Dr.-Ing. Matthias Kind für die nette Zusammenarbeit im Projekt und für seine Arbeit, Mühen und Zeit als Korreferent.

Ohne die finanzielle Unterstützung des BMBFs, sowie der Firmen Boehringer Ingelheim GmbH & Co. KG und Rentschler Biotechnologie GmbH wäre diese Arbeit nicht möglich gewesen. Die Zusammenarbeit mit den Firmen und Instituten im gesamten Projekt war sowohl persönlich als auch wissenschaftlich sehr bereichernd für mich. Besonders bedanken möchte ich mich auf Firmenseite bei Dorothee Ambrosius, Franz Nothelfer, Katrin Lohr und Nicole Knoll, sowie Roland Wagner, Sybille Ebert und Mario Metzger. Auf Institutsseite danke ich Hans Kiefer, Yuguo Zang und Maike Eisenkolb von der Hochschule in Biberach, sowie Matthias Kind, Hermann Nirschl und insbesondere Stefanie Alten und Bianca Cornehl vom KIT für die herzliche Zusammenarbeit und den regen fachlichen Austausch.

Vielen Dank euch allen vom Institut für die tolle gemeinsame Zeit und das angenehme Klima sowohl während der Arbeit als auch in der Freizeit. Insbesondere möchte ich mich bedanken bei:

- Kristina Schleining: für die herzliche und produktive Zusammenarbeit im Labor und die Unterstützung in allen Lebenslagen.
- den fleißigen studentischen Helfern, die mich in Form von Diplomarbeiten, Studienarbeiten und als Hiwi unterstützt haben: insbesondere Mark Fresewinkel, Lara Galm, Miriam Baum, Katharina Bauer, Andrea Schaller, Frank Hämmerling, Philipp Schumacher, Doreen Liebich und Viktoriya Petrushova.
- Katharina Lang: dafür, dass unser Büro immer wieder ein „zu Hause“ war, die Ablenkung von der Arbeit, die Einführung in MD und die Unterstützung auch in schwierigen Stunden.
- Carolin Richter: für dein immer offenes Ohr, für die ständige Motivation und die moralische Unterstützung auf dem Endspurt.
- Frieder Kröner, Katrin Treier, Benjamin Maiser und Jörg Kittelmann: dafür, dass ich in euch nicht nur Kollegen sondern auch Freunde gefunden habe.

Einen ganz besonderen Dank richte ich an meine Eltern, die mir schon so vieles ermöglicht haben und mich bei allem, was ich getan habe, unterstützt haben. Meine Tochter Lara hat das Beenden dieser Arbeit vielleicht nicht leichter gemacht, aber dafür war die freie Zeit umso schöner. Vielen Dank, dass du da bist! Ich möchte keine Sekunde missen. Mein größter Dank geht an meinen Mann Thomas. Du hast mich bedingungslos unterstützt und in vielerlei Hinsicht zurückstecken müssen. Vielen Dank für deine Geduld und dass du an mich geglaubt hast.

Abstract

One of the fastest growing and most important product classes in biological pharmaceuticals and therapeutics is the group of monoclonal antibodies (mAb). They are applied mainly for cancer and autoimmune therapy, such as for the treatment of leukemia or rheumatism. While substantial progress was made in designing specific antibodies, the challenging recovery and purification of mAbs in downstream processing are still the most cost-intensive tasks. Even though current platform processes are highly optimized in terms of yield and achieved purity, they lack in performance when it comes to processing high titers and when long-term stability of the molecule becomes a critical issue. In this context crystallization of antibodies is a promising strategy to generate highly concentrated and stable products.

The objective of this work was to develop the scientific basis for the implementation of protein crystallization as an alternative process to other downstream steps like the common used chromatography. Since crystallization conditions influence process development, crystal separation and subsequent upscale, the main focus of this work was the optimization of screening strategies as well as the establishment of fundamental understanding for the phase behavior of monoclonal antibodies. In literature, it is attempted to describe and correlate protein phase behavior with protein interactions. Empirical correlations as well as thermodynamic approaches exist, which arise from physical chemistry and simplify the complexity of the analyzed system. Therefore another focus was set on the investigation if experimentally determined protein interactions allow a general description and prediction of phase behavior of complex and large molecules such as monoclonal antibodies.

After the introduction and the research proposal, the work is split into 4 main parts followed by the conclusion and outlook:

Protein-protein interactions are analyzed using the osmotic second virial coefficient (B_{22}). This parameter is experimentally determinable and describes the magnitude and direction of non-ideality of the osmotic pressure in a dilute solution. According to George and Wilson, the crystallization probability of proteins at conditions with slight negative B_{22} -values is high. In the **first part** of this work, an appropriate method had to be found to determine the B_{22} . The self-interaction chromatography (SIC) is very attractive due to its low protein consumption. It is a chromatographic method in which the analyzed protein is immobilized on the adsorber. Protein-protein interactions can be determined from the shift in retention time of a protein sample (same protein as immobilized) in the SIC-column compared to that in a protein-free column. The time and experimental effort of the column

preparation was successfully reduced with a novel established preparation procedure in pre-packed columns. The protein immobilization under continuous flow and the quantification of the surface load with a partial least squares regression resulted in a fast and reliable procedure. As SIC is an invasive method, influencing parameters including the effects of absolute surface load, injected protein concentration and distribution of protein orientation on the results were analyzed with the model protein lysozyme. Directed interactions between the proteins in the mobile phase and the immobilized proteins were measured. These results disprove the consistency of the SIC method regarding a randomized orientation of immobilized proteins on adsorber particles. This explains significant deviations in published SIC results. Moreover, the solely qualitative character of SIC could be confirmed by a comparison of the results from SIC with B_{22} -values determined with the traditional static light scattering (SLS) method. Hence, for a quantitative analysis of B_{22} -values the SLS as a non-invasive method is the method of choice in this work.

Protein phase behavior characterization is often conducted in trial and error experiments in a multivariate parameter space due to the high amount of influencing parameters, the unlimited number of precipitants and the diversity of the proteins. The influence of single factors on the protein is yet not understood and fundamental knowledge remains to be obtained. For this purpose, a systematic screening method was developed in the **second part** of this work to characterize the influence of fluid phase conditions on the phase behavior of antibodies. The establishment and application of a buffer system with a constant buffer capacity from pH 5 to 9 enables one to set up multi-dimensional phase diagrams and to analyze protein phase behavior dependent on single parameters like the pH, protein- and precipitant concentration as well as the precipitant type. Separate experiments were conducted to characterize the precipitant influence on the pH-value prior to protein studies. Phase behavior after 40 days, the crystal size and the nucleation kinetics in form of the onset of first visible structures were determined by combining the established semi-automated process with the sophisticated analysis on an imaging system. This approach was applied to three different monoclonal antibodies to investigate influences of pH, protein and salt concentrations, with five salts being tested. Although differences between the antibodies exist and the net charge of the antibodies is positive over a broad range, this extensive study confirmed the general applicability of the Hofmeister series to characterize the salt influence over the analyzed parameter range. Thereby the anion influence of the salt on antibody phase behavior is stronger than the cation influence. The pH influences mainly the range in which the protein crystallized respectively gelled. The type of protein is responsible whether gelation or needle crystallization occurs, whereby a pH close to the isoelectric point (pI) of the protein resulted in the highest probability of crystallization, a faster crystallization kinetic and lower solubility for the monoclonal antibody mAb04c. The influence of the different salts

on the aggregation probability was described qualitatively using the Hofmeister series, with no differentiation between crystallization and precipitation, however.

In the **third part**, the conditions investigated in the second part were analyzed by means of the osmotic second virial coefficient (B_{22}) to shed light into the protein-protein interactions and thereby into antibody phase behavior on a molecular basis. The B_{22} was determined with SLS for all three antibodies. The resulting B_{22} -values follow qualitatively the phenomenological Hofmeister series, which describes the aggregation probability of antibodies for various solvent compositions with salts. However, a direct correlation between the crystallization probability and the B_{22} in form of a crystallization slot as postulated by George and Wilson does not seem to be feasible for antibodies. Only some crystallization conditions fit in the crystallization slot. Others were below and above this range. Moreover there are some conditions showing no phase transition in the crystallization slot. A possible reason is the high anisotropy of antibodies attributed to the molecular size and complexity of the molecules, which could be experimentally confirmed. Hence, the nucleation and crystal growth kinetics are key parameters. This could be confirmed by a comparison of experimental B_{22} and phase behavior data with a theoretical phase diagram using a Haas and Drenth model. The theoretically determined binodal and spinodal do not represent the reality. On the other hand a universal correlation between the solubility and the B_{22} was found for salt systems with the HDW (Haas, Drenth and Wilson)-model as well as the RSL (Ruppert, Sandler and Lenhoff)-model. The resulting solubility line is independent of parameters like pH-value, precipitant substance and concentration describing the solubility only as a function of B_{22} . Hence, the solubility in different solvent compositions seems to be solely thermodynamically driven.

The systematic screening method was applied to analyze the influence of macromolecular precipitants namely PEG on antibody phase behavior in the **fourth part**. Three-dimensional phase diagrams were developed to find appropriate conditions for downstream processing in terms of fast kinetics and crystal sizes. Molecular weight and concentration were varied at different pH-values. Overall, the use of PEG as precipitant for antibodies is more promising compared to salts. The easy variation of depth and range of the osmotic attraction by simply changing the polymer size and concentration is the success factor for finding appropriate crystallization conditions. Thereby the molecular weight of PEG is, besides the pH-value, the most important parameter. PEG molecular weights of 1000 or 3350 in combination with mAb04c are preferred due to resulting large crystal sizes, fast phase transitions and broad crystallization ranges. To gain a deep insight view in the phase behavior on a molecular basis, B_{22} -values as parameters for protein-protein interactions were determined experimentally with static light scattering. The PEG-protein solutions were analyzed as a pseudo-one-compartment system. As before the crystallization slot was not applicable to describe the phase behavior of monoclonal antibodies. Additionally to the

results for salts, conditions of antibody crystallization with positive B_{22} -values exist. A reason for this fact might be the neglect of cross-interactions between protein and PEG. Therefore the SLS was applied to prove the interactions between these two macromolecules with the second osmotic cross-virial coefficient (B_{23}). This parameter further increases the knowledge for the antibody phase behavior on a molecular basis. However, a correlation to phase behavior was neither with the B_{22} nor with the B_{23} possible.

Overall, this thesis presents detailed experimental data and elaborated approaches to understand the fundamentals of complex systems containing different buffer components, precipitants and proteins. A newly developed systematic screening method in combination with a novel buffer system shed light on the phase behavior of monoclonal antibodies. In particular for mAb04c suitable crystallization conditions for downstream processing could be found. The here established method and sophisticated analysis is flexible and can be expanded to a higher number of proteins and precipitants. It was also shown, that SLS is the method of choice to determine protein-protein interactions using the B_{22} . Furthermore, a comparison of B_{22} and B_{23} -values with protein phase behavior resulted in a detailed understanding of processes on a molecular basis. Hence, the phase behavior of monoclonal antibodies is better understood in detail and the here gained knowledge will simplify the analysis of protein phase behavior in the future. Moreover, this work points out the limits of existing empirical and theoretical models. Based on these findings, new applications as well as investigation strategies were suggested. A fundamental understanding of protein phase behavior is not only the key to reduce experimental effort in crystallization condition screening, but also in optimization of all steps in downstream processing.

Zusammenfassung

In den letzten Jahren haben monoklonale Antikörper immer mehr an Bedeutung als Therapeutika und Diagnostika zur Behandlung beispielsweise von Krebs- oder Immunkrankheiten in der biopharmazeutischen Medizin gewonnen. Die Anforderungen an diese Produkte in Bezug auf Langzeitstabilität, Reinheit und Konzentration sind hoch. Durch die Verwendung von Chromatographie-Verfahren, wie die Protein-A-Chromatographie in der Aufreinigung, dem Downstream Processing, ist die Herstellung monoklonaler Antikörper kostspielig. Insbesondere in der Aufreinigung und Formulierung können die Prozesse optimiert werden, um Produktqualität und Ausbeuten zu steigern. Hier bietet sich die Proteinkristallisation als alternativer Prozessschritt an, da durch die kristalline Form das Protein sowohl stabilisiert als auch aufkonzentriert wird.

Ziel dieser Arbeit war es, Strategien zu entwickeln, um auf lange Sicht die Kristallisation von monoklonalen Antikörpern als Alternativverfahren zu weiteren Aufreinigungsprozessen, wie der Chromatographie konkurrenzfähig zu machen. Da die Wahl der Kristallisationsbedingungen stark die weiteren Schritte beim Scale-up der Prozessbedingungen und bei der Abtrennung der Kristalle beeinflusst, wurde ein Schwerpunkt dieser Arbeit auf die Optimierung des Screenings von Kristallisationsbedingungen sowie dem allgemeinen Verständnisaufbau für das Phasenverhalten von Proteinen gelegt. Darüber hinaus gibt es in der Literatur verschiedene Studien, die versuchen über Protein-Wechselwirkungen das Phasenverhalten von Proteinen zu beschreiben. Daher wurde ein weiterer Schwerpunkt auf die Überprüfung gelegt, ob dies auch für monoklonale Antikörper möglich ist. Dazu wurde analysiert, in wie weit experimentell bestimmbare Protein-Wechselwirkungen mit dem Phasenverhalten empirisch oder mittels thermodynamischer Modelle korreliert werden können.

Die Arbeit unterteilt sich nach einer Einleitung und der Beschreibung des Forschungsziels in vier Hauptteile, gefolgt von der Zusammenfassung und dem Ausblick:

Für die Beschreibung von Protein-Protein-Wechselwirkungen wurde der experimentell bestimmbare zweite osmotische Virialkoeffizient (B_{22}) genauer untersucht. Er leitet sich aus der Nichtidealität des osmotischen Druckes einer verdünnten Lösung ab. Leicht negative B_{22} -Bedingungen (Crystallization Slot) bedeuten laut George und Wilson eine hohe Kristallisationswahrscheinlichkeit für Proteine. Daher wurde im **ersten Teil** mit dem Modellprotein Lysozym überprüft, welche Analytik-Methode geeignet ist, um B_{22} -Werte experimentell in der gewünschten Genauigkeit zu bestimmen. Die Self-Interaction Chromatographie (SIC) ist aufgrund ihres niedrigen Proteinkonsums attraktiv und wird in der Literatur häufig angewendet. Mit dieser Methode wird untersucht, wie sich das

Retentionsverhalten einer Proteinprobe in einer mit dem gleichen Protein immobilisierten Säule im Vergleich zu einer nicht immobilisierten Säule verändert. Jedoch ist das Herstellen der benötigten Säulen aufwändig. Deswegen wurde ein neuartiges Verfahren entwickelt, um das Protein direkt in vorgepackten Säulen auf dem Adsorber zu immobilisieren. Der experimentelle und zeitliche Aufwand konnte zusätzlich durch die Charakterisierung des gebundenen Proteins mittels einer Partial-Least-Squares Regression erfolgreich reduziert werden. Durch eine intensive Analyse verschiedener Einflussparameter konnte jedoch gezeigt werden, dass das Protein nicht entsprechend der Grundvoraussetzung der Methode in zufälliger Anordnung auf der Adsorberoberfläche gebunden werden kann. Dies führt zu gerichteten Wechselwirkungen zwischen dem gebundenen Protein und dem Protein in Lösung. Diese Erkenntnis wird durch signifikant abweichende Messwerte in der Literatur bestätigt. Demnach handelt es sich bei der SIC um ein rein qualitatives Verfahren. Im Gegensatz dazu stellte sich die statische Lichtstreuung (SLS) aufgrund ihres nicht-invasiven Charakters als geeignete quantitative Methode heraus.

Im **zweiten Teil** wurde für das Kristallisations-Screening ein Puffersystem entwickelt, welches eine konstante Pufferkapazität über den pH-Bereich von 5 bis 9 besitzt. Dadurch konnte der Einfluss einzelner Faktoren wie der pH-Wert, Präzipitantenart sowie -konzentration und Antikörperart auf das Phasenverhalten der Antikörper in mehrdimensionalen Phasendiagrammen systematisch untersucht werden. Um das Screening im Hochdurchsatz unter charakterisierten Bedingungen durchführen zu können, wurde vorab der Präzipitaneinfluss auf den pH-Wert untersucht. Das eigentliche Screening beinhaltete die automatisierte Präparation der verschiedenen Bedingungen auf einer Roboterplattform und die visuelle Auswertung mittels eines bildgebenden Systems. Neben dem Phasenverhalten nach 40 Tagen wurden zusätzlich die Kristallgröße, als auch das erste Auftreten von sichtbaren Strukturen als Maß für die Nukleations- und Kristallisationskinetik ausgewertet. Somit resultiert aus einem Screening eine Vielzahl an Informationen, die Aufschluss über die Anwendbarkeit der Bedingungen für den Downstream geben. Das Screening wurde auf drei verschiedene Antikörper mAb04c, mAb05a und mAb02a angewendet, um einen Antikörper spezifischen Einfluss der beschriebenen Parameter zu überprüfen. Es konnte gezeigt werden, dass die Einteilung der benutzten Salze nach der Hofmeister Serie erfolgen kann, obwohl die Antikörper über einen weiten pH-Bereich eine positive Nettoladung tragen. Dabei haben die Anionen einen deutlich stärkeren Einfluss auf das Phasenverhalten des Proteins als die Kationen. Der pH-Wert beeinflusst hauptsächlich den Kristallisations-, bzw. Gelierungsbereich für die verschiedenen Salze. Ob das jeweilige Protein nadelförmig kristallisiert oder Gelierung auftritt, hängt zusätzlich vom Protein selbst ab.

Im **dritten Teil** wurde der Zusammenhang von Proteinphasenverhalten und Protein-Protein-Wechselwirkungen in Form des B_{22} analysiert. Die systematische Vorgehensweise beim Screening macht die verschiedenen Einflussfaktoren zugänglich. Mittels SLS gemessene B_{22} -Werte für die Antikörper spiegeln die Wechselwirkungen zwischen den Proteinen wider. Durch die B_{22} -Werte konnten die Trends in Bezug auf die Hofmeister Serie bestätigt werden. Beim direkten Vergleich der B_{22} -Werte mit dem Phasenverhalten, kann die hohe Kristallisationswahrscheinlichkeit im Bereich leicht negativer B_{22} -Werte, dem sogenannten Crystallization Slot, für komplexe Proteine, wie es die Antikörper sind, nicht bestätigt werden. Einige kristallisierende Bedingungen liegen innerhalb des Crystallization Slots, andere deutlich unterhalb. Darüber hinaus gab es viele Bedingungen die im Crystallization Slot lagen, jedoch keine Änderung im Phasenverhalten zeigten. Ein Grund dafür ist die hohe Anisotropie der Antikörper. Dies konnte experimentell bestätigt werden. Folglich bestimmen kinetische Einflussfaktoren entscheidend das Proteinphasenverhalten. Jedoch konnte durch den Vergleich von B_{22} -Werten und dem Phasenverhalten von mAb04c in Salzlösungen die Löslichkeit mit dem B_{22} über das HDW-Modell und das RSL-Modell allgemein korreliert werden. Die resultierende universelle Löslichkeitslinie beschreibt die Löslichkeit als Funktion des B_{22} unabhängig von Einflussfaktoren wie dem pH-Wert, der Präzipitantenart und deren Konzentrationen. Demnach ist die Löslichkeit thermodynamisch bestimmt. Eine Beschreibung weiterer Phasenzustände über die Binodale und Spinodale war nicht mit einem universellen thermodynamischen Modell von Haas und Drenth möglich. Zusätzliche Einflussfaktoren, wie kinetische Phänomene und die Komplexität der Proteine beeinflussen stark das Proteinphasenverhalten und müssen dementsprechend mit berücksichtigt werden.

Im **vierten Teil** wurde untersucht, wie Polymere das Phasenverhalten von Antikörpern beeinflussen. Dazu wurde als Präzipitant PEG (Polyethylenglykol) mit verschiedenen Molekulargewichten gewählt. Neben dem pH-Wert, beeinflusst insbesondere das PEG-Molekulargewicht das Phasenverhalten von mAb04c. Je größer das Molekulargewicht des PEG, desto geringer ist die benötigte Konzentration um Kristallisation beziehungsweise Präzipitation hervorzurufen. Eine einfache Variation der Stärke und Reichweite der osmotischen Anziehung durch die Veränderung der Polymergröße und -konzentration ist ein wichtiger Erfolgsfaktor auf der Suche nach Kristallisationsbedingungen. Im Vergleich zu dem Proteinphasenverhalten mit Salzen als Präzipitant war der Kristallisationsbereich mit PEG größer und eine kompakte Kristallstruktur wurde erzielt. In Bezug auf geeignete Bedingungen für den Downstream wurde die Kombination von mAb04c mit mittleren PEG-Molekulargewichten von 1000 und 3350 aufgrund der kompakten Kristallform, des breiten Kristallisationsbereichs, der Kristallgröße und der schnellen Kinetik ausgewählt. Um weitere Informationen über das Phasenverhalten zu erhalten, wurden Protein-Protein Wechselwirkungen bestimmt, wobei die PEG-Lösung als eine pseudo-Einkomponenten-Lösung angenommen wurde. Die Überprüfung der Anwendbarkeit des Crystallization

Slots führt wie zuvor bei Salzen als Präzipitanten zu einem negativen Ergebnis. Zusätzlich gab es auch Phasenübergänge bei positiven B_{22} -Werten. Dies legt nahe, dass die Wechselwirkungen zwischen Protein und dem zweiten Makromolekül nicht vernachlässigt werden dürfen. Daher wurden mittels SLS Kreuzinteraktionen zwischen Proteinen und makromolekularen Präzipitanten in Form des zweiten osmotischen Kreuzvirialkoeffizienten (B_{23}) bestimmt und die Kreuzinteraktionen nachgewiesen. Dieser Parameter hilft bei dem weiteren Verständnis aufbau für das Phasenverhalten von Proteinen. Jedoch konnten auch mit diesem Faktor keine zusätzlichen Aussagen über die Art von Phasenverhalten und Konzentrationsabhängigkeiten getroffen werden.

Insgesamt konnte die systematische Suche nach Kristallisationsbedingungen durch die Verwendung einer neuen Screening-Methode mit einem neuartigen Puffersystem grundlegend vereinfacht werden. Es wurden detaillierte experimentelle Daten generiert die als Basis für mehrdimensionale Phasendiagramme dienen. Dadurch konnten die Einflüsse verschiedener Faktoren auf das Phasenverhalten von monoklonalen Antikörpern in komplexen Systemen aus Pufferkomponenten, Präzipitanten und Proteinen analysiert werden. Für mAb04c konnten so geeignete Kristallisationsbedingungen für den Downstream gefunden werden. Diese Methode ist flexibel und kann beliebig um weitere Präzipitanten und Faktoren erweitert werden. Die SLS hat sich als geeignete Methode für die Bestimmung von Protein-Protein Wechselwirkungen in Form des B_{22} herausgestellt. Über den Vergleich von Proteinphasenverhalten und Protein-Protein-Interaktionen (B_{22}), beziehungsweise Protein-PEG-Interaktionen (B_{23}) konnten weitere tiefgreifende Erkenntnisse über die Vorgänge auf molekularer Ebene gewonnen werden. In Bezug auf die Vorhersagbarkeit von Proteinphasenverhalten mittels empirischer und thermodynamischer Modelle wurden die Grenzen der Anwendbarkeit des B_{22} aufgezeigt. Anhand dieser detaillierten Ergebnisse wurden erfolgreich grundlegende Zusammenhänge für das Phasenverhalten von monoklonalen Antikörpern aufgezeigt. Somit wurde sowohl eine konzeptionelle Basis als auch eine detaillierte Datenbasis für zukünftige Arbeiten geschaffen. Darauf aufbauend wurden weitere Vorgehensweisen empfohlen. Eine solch umfassende Wissensbasis ist nicht nur notwendig, um den experimentellen Aufwand während des Kristallisations-Screenings zu reduzieren, sondern auch, um andere Verfahrensschritte beispielsweise in Bezug auf eine hohe Löslichkeit des Proteins zu optimieren.

Abbreviations

| | |
|---------------------------------|---|
| A | Adjustable parameter in HDW-model |
| \bar{a} | Average polarizability of molecules |
| A_C, K | Adjustable parameters in RSL-model |
| B_{22}, B_{ii}, B_{jj} | Osmotic second virial coefficient |
| B_{23}, B_{ij} | Osmotic second cross virial coefficient |
| c | Concentration |
| c_p^* | Saturated protein concentration |
| d | Distance between detector and molecule |
| d, d_{max} | (Maximal) adsorber particle diameter |
| dn/dc_P | Refractive index increment |
| f | Factor of polarization |
| G | Free energy/ Gibbs energy |
| G_λ | Gibbs energy |
| g_λ | Parameter for protein-protein interactions |
| H | Enthalpy |
| I_0 | Irradiated intensity |
| i_s | Intensity of scattered light |
| k | Boltzmann constant |
| K, K^* | (Modified) optical constant |
| $K_{SEC}, K_{overall}, K_{aff}$ | Distribution coefficient for SEC, for SIC and the for the weak interaction |
| m, m_P | Mass (of immobilized protein) |
| $m = \Omega/\omega$ | Number of water molecules, which have the equivalent volume as one protein molecule |
| M_W | Molecular weight |
| n | Aggregate size |
| N | Molecule number density |
| n_0 | Refractive index of the solvent |
| N_A | Avogadro constant |
| p | Anisotropy |
| q | Surface load SIC |
| R | Universal gas constant |
| r | Center-to-center distance of two protein molecules |
| r_{pH} | Ratio of pH 5 to pH 9 buffer |
| r_{Salt} | Salt ratio |
| R_Θ | Rayleigh ratio |
| s | Solubility |

| | |
|--------------------------|--|
| S | Entropy |
| s^* | Grade of saturation |
| T | Temperature |
| V_0, V_t, V_i | Interstitial, total mobile phase and intraparticle volume |
| $V_P = \Omega \cdot N_A$ | Partial molar volume of the protein at infinite dilution in the aqueous solution |
| V_r | Retention volume of the mobile protein |
| V_W | Molar volume of water |
| W | Potential of mean force |
| z | Coordination number of the protein crystals |
| $\Delta V_{r,aff}$ | Change in retention volume caused by interaction |
| θ | Surface coverage |
| Θ | Detector angle |
| λ | Wave length |
| ν | Range of interaction |
| π | Osmotic pressure |
| ρ | Density |
| ϕ | Volume fraction |
| Ω | Volume of one protein molecule |
| ω | Molar volume of water V_W divided by the Avogadro number N_A |
| Ω_1 | possible angular positions/orientations immobilized interacting molecules |
| Ω_2 | possible angular positions/orientations mobile interacting molecules |

Indices

| | |
|--------------|--|
| * | Spinodal |
| c | Crystal or critical aggregate size |
| $i, j, 2, 3$ | Different species |
| max | Maximal |
| p, pro | Protein |
| pH | pH-Value |
| s | At saturation |
| $Salt$ | Salt |
| α | Protein lean phase |
| γ | Protein rich phase |
| crs | Crystal |
| eql | After phase separation and equilibration |
| ini | Initial |
| liq | Obtained filtrate |

Methods

| | |
|---------|---|
| CG-MALS | Composition gradient multi-angle light scattering |
| CLSM | Confocal laser scanning microscopy |
| FID | Free interface diffusion |
| FPLC | Fast protein liquid chromatography |
| HDW | Haas-Drenth-Wilson |
| HPLC | High-performance liquid chromatography |
| PLS | Partial Least Squares |
| RSL | Ruppert-Sandler-Lenhoff |
| SEC | Size exclusion chromatography |
| SIC | Self-interaction chromatography |
| SLS | Static light scattering |

Chemicals

| | |
|------------------------------|--|
| $(\text{NH}_4)_2\text{SO}_4$ | Ammonium sulfate |
| BCA | Bicinchoninic acid |
| BSA | Bovine serum albumin |
| CHES | 2-(N-Cyclohexylamino)-Ethanesulfonic Acid |
| CNBr | Cyaongen bromide |
| HEPPSO | 4-(2-Hydroxyethyl)-Piperazine-1-(2-Hydroxy)-Propanesulfonic Acid |
| Li_2SO_4 | Lithium sulfate |
| Lys | Lysozyme |
| mAb02a | Monoclonal antibody |
| mAb04c | Monoclonal antibody |
| mAb05a | Monoclonal antibody |
| MES | 2-(N-morpholino)ethanesulfonic |
| MOPSO | 3-Morpholino-2-Hydroxy-Propanesulfonic Acid |
| Na_2SO_4 | Sodium sulfate |
| NaCl | Sodium chloride |
| NaOAc | Sodium acetate |
| NaOH | sodium hydroxide |
| NaPi | Sodium phosphate |
| NH_4Cl | Ammonium chloride |
| NHS | N-hydroxysuccinimide |
| PEG | Polyethylene glycol |

Outline

| | |
|---|-------------|
| Abstract | V |
| Zusammenfassung | IX |
| Abbreviations | XIII |
| 1 Introduction | 1 |
| 1.1 Monoclonal antibodies and their purification..... | 1 |
| 1.2 Protein interactions | 2 |
| 1.2.1 Hard sphere potential | 2 |
| 1.2.2 Van der Waals and electrostatic potential..... | 2 |
| 1.2.3 Osmotic potential..... | 3 |
| 1.2.4 Hydration forces and hydrophobic potential..... | 3 |
| 1.2.5 Influence of solution parameters on protein interactions..... | 4 |
| 1.2.5.1 pH-value, buffer capacity and temperature | 4 |
| 1.2.5.2 Electrolytes and polymers as precipitants | 4 |
| 1.3 Osmotic virial coefficients..... | 5 |
| 1.3.1 Osmotic second virial coefficient (B_{22}) | 5 |
| 1.3.2 Osmotic second cross virial coefficient (B_{23}) | 5 |
| 1.4 Phase behavior of proteins in solution..... | 6 |
| 1.4.1 Protein crystallization | 6 |
| 1.4.2 Liquid-liquid separation..... | 8 |
| 1.4.3 Phase diagrams | 9 |
| 1.4.4 Theoretical calculation of phase diagrams..... | 11 |
| 1.5 Screening of protein crystallization conditions | 13 |
| 1.5.1 Empirical screening approaches | 14 |
| 1.5.2 Screening of thermodynamic properties | 15 |
| 1.5.2.1 Static light scattering | 16 |
| 1.5.2.2 Self-interaction chromatography..... | 17 |
| 2 Motivation and Research Proposal | 20 |
| 3 Self-interaction Chromatography in Pre-packed Columns: A Critical Evaluation of SIC Methodology to Determine the Second Virial Coefficient | 24 |
| 3.1 Introduction..... | 26 |
| 3.2 Theory..... | 28 |
| 3.2.1 Osmotic second virial coefficient (B_{22}) | 28 |
| 3.3 Materials and Methods..... | 30 |
| 3.3.1 Materials and Apparatus | 30 |
| 3.3.2 Preparation of SIC- and SEC-Columns | 30 |
| 3.3.3 Determination of uniform protein distribution in adsorber particles | 31 |

| | | |
|----------|---|-----------|
| 3.3.4 | Determination of surface load..... | 32 |
| 3.3.5 | Self-interaction-chromatography | 32 |
| 3.3.6 | Determination of isoform distribution | 33 |
| 3.3.7 | Static light scattering | 33 |
| 3.4 | Results and Discussion | 34 |
| 3.4.1 | Homogeneity of immobilized lysozyme in the column..... | 34 |
| 3.4.2 | Surface coverage of immobilized protein..... | 35 |
| 3.4.3 | B_{22} -determination using the prepared SIC-columns | 36 |
| 3.4.4 | Protein-protein interactions in the mobile phase | 38 |
| 3.4.5 | Multi-body interactions – Surface coverage of immobilized protein..... | 38 |
| 3.4.6 | Influence of protein orientation on B_{22} -determination..... | 40 |
| 3.4.7 | B_{22} -determination comparing SIC and SLS | 43 |
| 3.5 | Conclusions..... | 44 |
| 3.6 | References..... | 45 |
| 4 | Moving Through Three-dimensional Phase Diagrams of Monoclonal Antibodies..... | 48 |
| 4.1 | Introduction..... | 50 |
| 4.2 | Materials and Methods..... | 51 |
| 4.2.1 | Materials | 51 |
| 4.2.2 | Buffer system preparation and pH characterization..... | 52 |
| 4.2.3 | Screening buffer preparation | 54 |
| 4.2.4 | Antibody phase behavior analysis | 56 |
| 4.3 | Results..... | 56 |
| 4.3.1 | Influence of sulfate salts on mAb04c phase behavior: Ammonium, lithium, and sodium sulfate..... | 56 |
| 4.3.2 | Influence of sulfate salts on mAb05a and mAb02a phase behavior: Ammonium, lithium, and sodium sulfate | 58 |
| 4.3.3 | Influence of chloride salts on mAb04c, mAb05a and mAb02a phase behavior: Ammonium and sodium chloride | 59 |
| 4.3.4 | Time-dependent analysis of the phase behavior | 60 |
| 4.3.5 | Size of crystals | 61 |
| 4.4 | Discussion..... | 63 |
| 4.4.1 | Phase behavior of the three antibodies | 64 |
| 4.4.2 | Influence of the different anions | 65 |
| 4.4.3 | Influence of different cations | 66 |
| 4.5 | Conclusions..... | 67 |
| 4.6 | Acknowledgements..... | 68 |
| 4.7 | Literature Cited | 68 |
| 5 | From Osmotic Second Virial Coefficient (B_{22}) to Phase Behavior of a Monoclonal Antibody..... | 72 |
| 5.1 | Introduction..... | 74 |
| 5.2 | Material and Methods | 79 |

| | | |
|----------|---|------------|
| 5.2.1 | Chemicals..... | 79 |
| 5.2.2 | Determination of B_{22} | 80 |
| 5.2.3 | Determination of macroscopic phase behavior..... | 80 |
| 5.2.4 | Determination of solubility (s)..... | 81 |
| 5.2.5 | Determination of volume fractions (ϕ_P)..... | 82 |
| 5.2.6 | Model application | 83 |
| 5.3 | Results and Discussion | 84 |
| 5.3.1 | Electrostatic interactions: Influence of pH on B_{22} -values..... | 84 |
| 5.3.2 | Hydrophobic interactions: Influence of kosmotropic salts on B_{22} -values | 85 |
| 5.3.3 | Detailed analysis: Salt and pH influence on B_{22} -values of mAb04c | 86 |
| 5.3.4 | Crystallization slot: Correlation of B_{22} -values and macroscopic phase behavior..... | 89 |
| 5.3.5 | Phase diagram: Correlation of B_{22} -values and solubility..... | 91 |
| 5.3.6 | Phase diagram of mAb04c | 94 |
| 5.4 | Conclusion | 99 |
| 5.5 | Acknowledgements..... | 99 |
| 5.6 | Abbreviations..... | 99 |
| 5.7 | Literature Cited | 101 |
| 6 | Influence of Macromolecular Precipitants on Phase Behavior of Monoclonal Antibodies..... | 106 |
| 6.1 | Introduction..... | 108 |
| 6.2 | Material and Methods | 110 |
| 6.2.1 | Materials | 110 |
| 6.2.2 | Determination of phase diagrams | 110 |
| 6.2.3 | Determination of B_{22} , B_{33} and B_{23} with SLS | 112 |
| 6.3 | Results and Discussion | 113 |
| 6.3.1 | Macroscopic phase behavior of mAb04c in dependency of macromolecular precipitants | 113 |
| 6.3.2 | Nucleation kinetics, crystal size and form | 115 |
| 6.3.3 | Comparison of PEG and salt influence on antibody phase behavior..... | 118 |
| 6.3.4 | Characterization of macroscopic phase behavior of mAb04c using the osmotic second virial coefficient..... | 119 |
| 6.3.5 | Characterization of phase behavior using cross-interaction determination | 121 |
| 6.4 | Conclusion | 123 |
| 6.5 | Acknowledgements..... | 123 |
| 6.6 | Literature Cited | 123 |
| 7 | Conclusion and Outlook..... | 128 |
| | References..... | 130 |
| | Curriculum Vitae..... | 136 |
| | Publications..... | 137 |

1 Introduction

1.1 Monoclonal antibodies and their purification

In recent years the interest for monoclonal antibodies (mAb) raised in the biopharmaceutical industry as therapeutics and diagnostics. As part of the modern medicine this multifunctional product class helps against different indications and diseases like cancer, immunology or infection diseases. Unique properties make the mAb save, effective and versatile. In 2006 already 18 products against diseases like asthma, transplant rejection, acute myeloid leukemia or Non-Hodgkin's lymphoma were approved with a raising tendency.¹⁻⁴ To increase the benefit from antibody research the engineering of the antibody has to be optimized, the manufacturing and formulation to be improved, better pre-clinical models for behavior prediction found and new ideas of for the applications developed.⁵ In designing specific antibodies substantial progress is made, whereas the bottleneck is the recovery, purification and formulation of the antibodies.^{4,6} During the manufacturing process deamidation, chemical instability and glycosylation differences mainly generate the heterogeneity of antibodies.⁷⁻⁹ Combined with their large size and their high degree of segmental flexibility the process gets further complicated. The resulting inhomogeneous products are challenging tasks for the Food and Drug Administration (FDA) approval in respect to the purity and stability.¹⁰ Furthermore, the obtained low concentrated mAb-solutions stay in contrast to the requirements based on the sterile doses weekly for long periods of time. For tens of thousands of patients per year grams of sterile doses for intravenous administration are needed.⁵ As consequence higher manufacturing rates are necessary, while the costs for goods and facilities should be affordable. At the moment more than 80 percent of the overall process costs are produced by the downstream processing.⁹ The most cost intensive task during the purification are the chromatographic steps, foremost the application of a Protein A-step.^{10,11} These chromatographic steps are limited by the space of equipment, material and facilities, the volume of buffers, as well as cleaning and sanitization solutions. But limitations also exist from the techniques themselves. Research projects foster the reduction of purification steps, try to avoid complex steps, or to use alternatives for chromatographic steps like simulated moving bed, expanded bed as well as membrane chromatography. Further developments are flocculation, precipitation, crystallization or aqueous two phase systems.^{4,10,12,13}

With further progress in mAb research online analytics and strategies like Quality by Design (QbD) and Process Analytical Technology (PAT) more perspectives will open.^{8,9} Examples are patient tailored mAbs by combining diagnostics with therapeutics, targeted

drug delivery or the enhancement of properties by using fragments, conjugates, fusion as well as multi specific mAbs.^{1,3}

1.2 Protein interactions

Protein molecules interactions are comparable to those of small molecules. But proteins are complex molecules due to their large size, their high degree of segmental flexibility and potentially variable patterns.¹⁰ The surface consists of charged groups as well as hydrophobic and hydrophilic patches, which are inhomogeneously distributed. Therefore the interactions between two protein molecules are strongly dependent on their orientation to each other.¹⁴ The potential of mean force is generally used to characterize this anisotropic nature of the interactions. It describes the potential energy between two molecules in a diluted solution integrated over their distance and all possible orientations to each other.¹⁵ The potential of mean force comprises various single potentials, such as the hard sphere potential, the van der Waals potential, the electrostatic potential and the osmotic potential.¹⁶⁻¹⁸ Other potentials are often neglected, because theoretical explanations and possibilities for their calculations are still missing. It is neither possible to determine every single potential nor the complete potential of mean force. It is only possible to approximate the different potentials with theoretical approaches. This includes always neglect and simplifications.¹⁶ The first approaches were developed by Derjaguin and Landau¹⁹ and Verwey²⁰ as DLVO (Derjaguin, Landau, Verwey, Overbeek)-theory. Only the hard sphere, the van der Waals and the electrostatic potentials were included.

1.2.1 Hard sphere potential

Hard spheres are characterized as impenetrable spheres that cannot overlap in space. The hard sphere potential describes extremely strong repulsive interactions at close distances between the protein molecules. These forces cause, a distance of at least twice the protein radius.

1.2.2 Van der Waals and electrostatic potential

Van der Waals and electrostatic forces are the result of charged patterns on the surface of proteins. The interactions can be from repulsive or attractive nature. According to Leckband and Israelachvili¹⁶ van der Waals interactions between similar molecules are always attractive, whereas electrostatic interactions are generally repulsive. Van der Waals interactions result from fluctuations of the electric dipole moment and are from short range. They can be estimated with the approach of Hamaker.²¹

Electrostatic interactions between two proteins are dependent on their charge and the ambience conditions. The net charge of proteins can be varied via the pH-value. Protein molecules of the same kind have an equivalent net charge and therefore the interactions are repulsive. Even at the proteins isoelectric point (pI) of the protein with a zero net charge local charged groups at the molecule surface exist. Moreover the ionic strength can influence the electrostatic potential. For ionic strength of less than 500 mM the electrostatic potential can be approximated with the Debye-Hückel theory.²²

1.2.3 Osmotic potential

The attractive force of the osmotic potential is present in protein solutions with additional macromolecules, like PEG or with high electrolyte concentrations. When the distance between two protein molecules is smaller than the diameter of the solute macromolecules, none of these can enter the intermediate space. This space is then filled with pure solvent and local concentration gradients are the result.^{23,24} Out of the developed osmotic pressure an attractive potential between the protein molecules arises. The protein molecules attempt to further decrease the distance between each other to reduce the osmotic pressure. This osmotic potential can be calculated according to Asakura and Oosawa.²³

1.2.4 Hydration forces and hydrophobic potential

A liquid in contact with a surface acts as a non-random medium.¹⁶ On hydrophilic and charged patches on the protein surface a stable hydration layer develops. This layer can consist out of more than one layer, depending on number and distribution of the hydrophilic patches. As a result slight repulsive interactions occur due to steric hindrance.²⁵

On the other hand hydrophobic patches on the protein surface can interact with each other. The resulting interactions are negligible when these patches are not freely accessible due to concavities or clefts.¹⁸ As well from minor influence are hydrophobic patches below a particular threshold size. The protein will precipitate, if these hydrophobic patches are bigger than 1 nm and freely accessible.¹⁸ The proteins minimize the total energy by aggregation to reduce the amount of exposed hydrophobic patches. According to van Oss¹⁸ these hydrophobic interactions are the strongest and from longest range within the non-covalent interactions.

Hydrophobic interactions are strongly dependent on the protein properties. For comparison, the interactions between antibodies are besides van der Waals mainly from hydrophobic nature. On the other hand the protein BSA (Bovine Serum Albumin) consists of a high amount of hydrophilic patches. Therefore the interactions are mainly from hard

sphere potential and repulsive hydration forces, whereas hydrophobic interactions are negligible.

1.2.5 Influence of solution parameters on protein interactions

1.2.5.1 pH-value, buffer capacity and temperature

The net charge of proteins in solution is dependent on the pH-value. At the isoelectric point of a protein, the net charge is neutral. For pH-values below the pI the net charge is positive and equivalently for pH-values above the pI negative. With low salt concentrations in solution these charges on the surface are not shielded. Hence, the pH-value influences the electrostatic interactions. The electrostatic interactions are more repulsive the higher the distance to the pI is.

The buffer capacity can influence the protein interactions, especially in solutions of low ionic strength. A higher buffer capacity can result in a stronger shielding effect of charged surface groups due to the buffer salt ions. Thus, the repulsive interactions are reduced.

Elevated temperatures reduce in particular hydrophobic interactions between the protein molecules.²⁶ Nevertheless, proteins denature irreversible at the melting point and the denatured protein molecules aggregate.²⁷

1.2.5.2 Electrolytes and polymers as precipitants

Protein molecules are charged depending on the pH-value of the solution. Repulsion between protein molecules is induced due to the same net charge. With the addition of salts an electrostatic double layer around the charges can be induced at the protein surface on the one hand. The charges of the protein are shielded and the repulsive electrostatic interactions reduced. On the other hand the protein surface is surrounded by a hydration layer, as mentioned in chapter 1.2.4. This hydration layer can be influenced in its structure as well by the addition of salts. In concentrated salt solutions salt ions compete with the charged protein patches for water molecules. When the interaction of the salt ions with water molecules is stronger, the protein will be dehydrated. Then the repulsive hydration forces are reduced and the attraction increases. The degree of interactions depends on the properties of the protein surface and on the salt ions themselves.²⁸

Further influencing factors are polymers. A sufficient concentration produces an osmotic potential, which has been mentioned in chapter 1.2.3. The higher the molecular weight or the concentration of the polymer is, the higher the attractive interactions of the protein molecules.²⁹

1.3 Osmotic virial coefficients

As mentioned before, it is neither possible to measure the potential of mean force nor to calculate it without approximations. However, there is a relation between the potential of mean force and the non-ideality in osmotic pressure of solutions. Ideal behavior describes a solution without any molecule interactions. To describe the non-ideality of fluids thermodynamically, virial equations expand the ideal equation of state with terms to comprehend the non-ideality. Osmotic virial coefficients are parts of these additional terms. They describe the magnitude and the direction of the overall apparent interactions. Its theoretical background is explained in detail in the subsequent two chapters.

1.3.1 Osmotic second virial coefficient (B_{22})

The origin of virial coefficients is a virial series expansion of the osmotic pressure. The non-ideality of the osmotic pressure π for a solution of one kind of macromolecules in a dilute solution can be expressed by:

$$\pi = RTc_P \left(\frac{1}{M_W} + B_{22}c_P + \dots \right) \quad (1.1)$$

Parameters are the universal gas constant R , the temperature T , the protein concentration c_P and the molecular weight of the protein M_W . The non-ideality results from weak interactions between two molecules of the same kind. As mentioned before (chapter 1.3) the magnitude and direction is described by the osmotic second virial coefficient (B_{22}). Repulsive interactions between molecules result in positive, attractive ones in negative B_{22} -values. The overall potential of mean force $W(r, \Omega_1, \Omega_2)$, which is not directly measurable can be determined with this B_{22} as follows:^{15,30,31}

$$B_{22} = -\frac{N_A}{M_W^2} \int_{\Omega_1} \int_{\Omega_2} \int_0^{\infty} \left[\exp\left(\frac{-W(r, \Omega_1, \Omega_2)}{k T}\right) - 1 \right] r^2 dr d\Omega_2 d\Omega_1 \quad (1.2)$$

Where k is the Boltzmann constant, N_A is the Avogadro constant, r the center-to-center-distance of two protein molecules in solution and Ω_1 as well as Ω_2 the rotation angles defining the orientation of both molecules towards each other.

1.3.2 Osmotic second cross virial coefficient (B_{23})

The result of two different (protein) macromolecules interacting with each other is a non-ideal behavior of the solution. Via virial expansion of the osmotic pressure π , the equation of state can be described with the equation:

$$\pi = RT \left(\frac{c_2}{M_{W,2}} + \frac{c_3}{M_{W,3}} + B_{22}c_2^2 + B_{33}c_3^2 + 2B_{23}c_2c_3 \dots \right) \quad (1.3)$$

The parameters c_2 and c_3 represent the concentrations of two different macromolecules, $M_{W,2}$ and $M_{W,3}$ the corresponding molecular weights. The B_{ii} are the osmotic second virial coefficients of molecules from the same kind. The B_{23} is the osmotic second cross-virial coefficient and characterizes the interactions between two different molecules. The expansion can be truncated for diluted solutions. Over the B_{23} the potential of mean force can be approximated:

$$B_{23} = -\frac{N_A}{M_{W,2}M_{W,3}} \int_{\Omega_1} \int_{\Omega_2} \int_0^\infty \left[\exp\left(\frac{-W(r, \Omega_1, \Omega_2)}{kT}\right) - 1 \right] r^2 dr d\Omega_2 d\Omega_1 \quad (1.4)$$

Where Ω_1 and Ω_2 are the possible angular positions/orientations of the two different and interacting molecules.

1.4 Phase behavior of proteins in solution

The phase behavior of proteins differs corresponding to properties and size of the molecule. Proteins do not have a triple point with coexisting gas, liquid and solid states, due to their complex molecular structure.³² They show in fact additional polymer like behavior. Proteins can remain stable in solution, precipitate reversibly as well as irreversibly, can crystallize, separate into a protein dense and poor phases and build a gel phase. Whereas gelation and irreversible precipitation are kinetically induced,³³ the others can be thermodynamically described.

1.4.1 Protein crystallization

The phase behavior is dependent on the grade of saturation s^* , which is defined as:³⁴

$$s^* = \frac{c_P}{c_P^*} \quad (1.5)$$

With the protein concentration c_P and the saturated protein concentration c_P^* .

A solution is undersaturated or respectively saturated with $s^* \leq 1$ and the protein remains stable in solution, as the thermodynamic equilibrium is given. For solutions in the supersaturated range with $s^* > 1$, the equilibrium concentration is exceeded. This is an essential but not mandatory requirement for a phase transition. The driving force enables

crystallization or precipitation. The theoretical background is given by the Gibbs energy ΔG :

$$\Delta G = \Delta H - T \Delta S \quad (1.6)$$

The change in the Gibbs energy ΔG is equal to the change in enthalpy ΔH minus the product of Temperature T and change in entropy ΔS . The energy reference is always the state with monomers in solution. Aggregation is only possible, if the equilibrium energy state is reduced ($\Delta G < 0$). The entropy of an aggregate is always smaller than in solution and thereby $-T \Delta S > 0$. Thus, the change in enthalpy from solution to aggregate has to be negative and in absolute terms larger than the entropy term. In figure 1.1 the free energy of aggregates is plotted in dependency of their size. If only small aggregates form in solution, the enthalpy cannot compensate the increased entropy term, because of too many free intermolecular binding positions on the surface of the aggregates. The aggregates grow in size with increasing supersaturation, which is induced by higher precipitant or protein concentrations. As the surface to volume ratio decreases the enthalpy rises. When a critical aggregate size is reached (ΔG_c), ΔG can be reduced and the nuclei are stable. Higher protein or precipitant concentrations result in a lower energy barrier. If the energy barrier is not overcome, the solution remains in a metastable state.

In contrast to this homogeneous crystallization, heterogeneous crystallization can be enabled with seeding particles or application of energy to reduce the natural energy barrier ΔG_c and increase the probability of crystallization.^{35,36} The following growth of the crystal out of the nucleus, takes place due to a protein concentration gradient from the solution to the lower concentrated boundary layer of the crystal. For non-diffusion limited crystallization, the growth rate can be accelerated by convective mass transport.³⁵

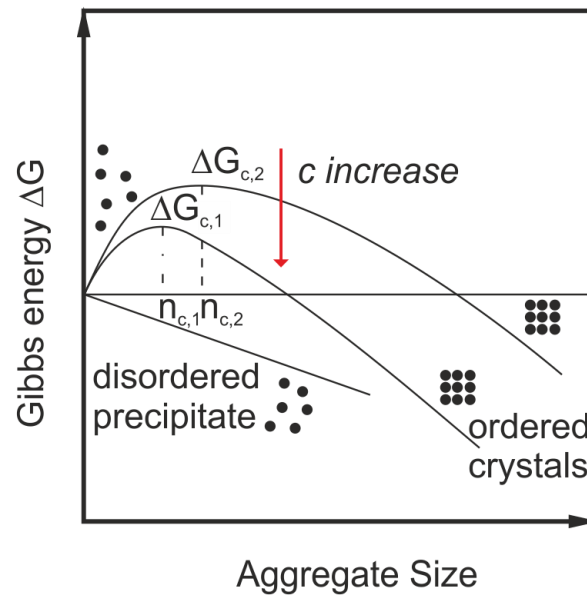


Figure 1.1: Free energy of aggregates in dependency of aggregate size³⁵

In the case of precipitation the energy barrier ΔG is so small, that the instantaneous aggregation to very small and disordered aggregates already reduces the energy. A further reduce in energy is possible due to inter particular transition like Ostwald ripening. Thereby crystals can also grow out of precipitate.³⁷ The crystallization and precipitation is terminated when the saturation and thereby the equilibrium is reached.³⁵

1.4.2 Liquid-liquid separation

The liquid-liquid phase separation (LLPS) is the separation of protein solutions in a protein dense and protein poor phase. It is the result of short range and strong anisotropic interactions between the molecules. This behavior can be described by the Gibbs energy of the solution ΔG . In figure 1.2 the Gibbs enthalpy is plotted over the volume concentration in dependency of the temperature. For high temperatures, the Gibbs energy has only one minimum. Below a critical temperature T_c the developing shows two local minima. This developing can be transferred to the plot of the temperature over the volume concentration. The points with the same slope build the binodal and the inflection point represents the spinodal. For temperatures above the T_c and above the binodal separation of protein solutions into two phases is not possible. For $T < T_c$ the separation range can be metastable for concentrations between the binodal and the spinodal or instable in the range between the spinodal line. The critical point is the point in which the binodal and the spinodal have the same value.

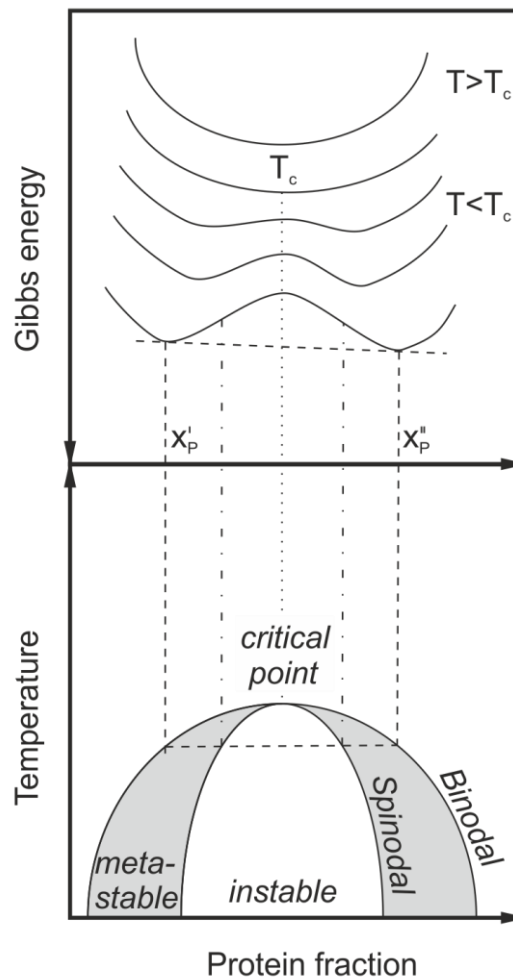


Figure 1.2: Origin of liquid-liquid phase separation (LLPS)¹⁴

1.4.3 Phase diagrams

The protein phase behavior is amongst others dependent on the in chapter 1.2.5 mentioned parameters. These dependencies can be best explained with phase diagrams. A common plot is the protein concentration as a function of the precipitant concentration with a distinction in different regions, which is exemplarily shown in figure 1.3. The solution is undersaturated for low precipitant and protein concentrations. The solubility line describes the transition to a saturated solution. The metastable region is divided into a region, where crystals can only grow when nuclei are present and the labile region in which the homogeneous nucleation occurs. In the precipitation range the supersaturation is so high, that the protein aggregates as amorphous precipitate. The boundaries between the different phases cannot be exactly determined, because systems are often also dependent on kinetic phenomena and can be kinetically hindered.^{35,38,39}

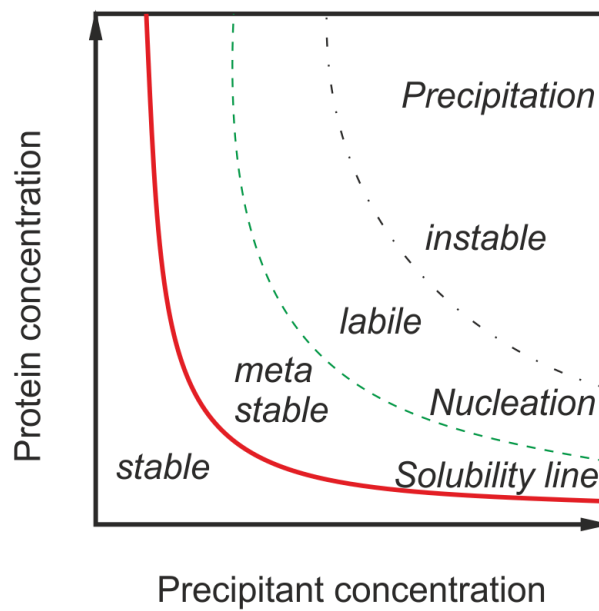


Figure 1.3: Protein phase diagram^{35,38,39}

However, for all proteins exist a liquid-liquid phase separation (LLPS) range.^{14,32} Therefore the phase diagram in figure 1.4 is expanded by this region. The x-axis describes the protein volume fraction as a measure of protein concentration, whereas the precipitant concentration is plotted on the y-axis. Moreover the y-axis is expanded to the temperature and the B_{22} . To plot the B_{22} has the advantage, that this parameter can be seen as universal. It combines in only one parameter influences such as temperature, the salt type and their concentration.³³ Again, the stable range of solved protein is at low protein and precipitant concentrations. The solubility line characterizes the saturated solution. Below this line, the solution is metastable. Crystallization can occur, when nuclei are in solution. The solution then separates in the solid part and the saturated solution.

Depending on whether the phase transition occurs in the liquid-solid region or in the LLPS range, crystals develop until the (liquid-solid) solubility line is reached or a separation in a protein solution of high protein concentration and a second with low protein concentration occurs, with its equilibrium on the binodal. The latter is instantaneously within the spinodal region. Again this equilibrium can be metastable as well and crystallization can happen out of this liquid-liquid separation. This can occur for LLPS conditions below the solubility line as shown in the phase diagram on the left side in figure 1.4 for all binodal points. When the solubility line crosses the binodal and spinodal, the LLPS is stable in the range above the solubility line (figure 1.4, right).

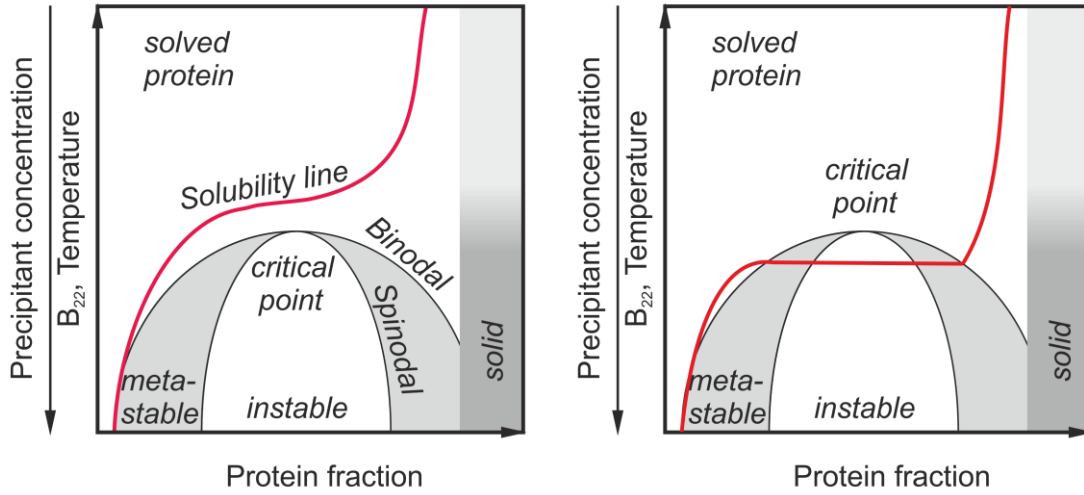


Figure 1.4: Schematic phase diagram of protein with metastable (left) and, stable LLPS (stable)(based on literature^{33,40-42})

1.4.4 Theoretical calculation of phase diagrams

Solubility line, binodal and spinodal of protein phase diagrams (figure 1.4) can be modeled with thermodynamic approaches.^{33,40,43,44} Haas et al.^{14,40,43} correlated experimental solubility data of varied pH, temperature, salt type and different salt concentrations with B_{22} -values by means of equation (1.7):

$$B_{22} = \frac{4}{M_w \rho_P} \left[1 - A \left\{ \left(\frac{\phi_s}{m} \right)^{-2/z} - 1 \right\} \right] \quad (1.7)$$

The parameter ρ_P is the protein density, ϕ_s is the volume fraction of the protein at saturation, z the coordination number of the protein crystals and $m = \Omega/\omega$ the number of water molecules, which have the same volume like one protein molecule. Ω is the volume of protein molecules, ω the molar volume of the water divided by the Avogadro number and A the single free adjustable parameter:

$$A = p(v^3 - 1) \quad (1.8)$$

This parameter A depends on the anisotropy p and the range of interaction v . The anisotropy is limited to $0 < p \leq 1$, whereby $p = 1$ describes isotropic interactions. The most common coordination numbers of protein crystals are $z = 4$ to $z = 6$.¹⁴ The solubility s is described by the transformation and multiplication with the density:

$$s = 10^3 \rho_P \phi_s \quad (1.9)$$

Except the B_{22} the other parameters are only little dependent on further solution conditions. Thus, the solubility line can be seen as universal. This is shown exemplarily by Haas and Drenth⁴⁰ for lysozyme with the parameters $M_W = 14000$ Da, $\rho_P = 1.36$ g cm⁻³, $z = 4$ and $A = 0.01$.

Moreover the whole Liquid-liquid phase separation (LLPS) can be calculated thermodynamically over the interaction parameter B_{22} .³³ In combination with the solubility line a universal phase diagram is obtained. The basis for the LLPS-calculation is the Gibbs energy per volume of a protein solution:^{33,43}

$$G_\lambda(\phi) = \frac{1}{\Omega} \left[\left(\frac{\phi^2}{\phi_c} \right) g_\lambda + k_B T \phi \ln \left(\frac{\phi}{m} \right) - k_B T \left\{ \frac{\phi - 6\phi^2 + 4\phi^3}{(1-\phi)^2} \right\} \right] \quad (1.10)$$

The volume fraction of the protein is described by ϕ , the volume fraction of the protein in the crystal by ϕ_c and the protein-protein interactions are described by the parameter g_λ :

$$g_\lambda = k_B T \phi_c (B_{22} M_w \rho - 4) \quad (1.11)$$

Thereby the corresponding phases in the LLPS at the binodal ϕ_α and ϕ_γ are calculated by:

$$G_\lambda(\phi_\gamma) - G_\lambda(\phi_\alpha) = \phi_\gamma \left(\frac{\partial G_\lambda}{\partial \phi} \right)_{\phi_\gamma} - \phi_\alpha \left(\frac{\partial G_\lambda}{\partial \phi} \right)_{\phi_\alpha} \quad (1.12)$$

and

$$\left(\frac{\partial G_\lambda}{\partial \phi} \right)_{\phi_\gamma} = \left(\frac{\partial G_\lambda}{\partial \phi} \right)_{\phi_\alpha} \quad (1.13)$$

The spinodal separation in ϕ_α^* and ϕ_γ^* is defined over the second deviation of the free energy:

$$\left(\frac{\partial^2 G_\lambda}{\partial \phi^2} \right)_{\phi_\gamma^*} = 0 \quad (1.14)$$

and

$$\left(\frac{\partial^2 G_\lambda}{\partial \phi^2} \right)_{\phi_\alpha^*} = 0 \quad (1.15)$$

1.5 Screening of protein crystallization conditions

Crystallization is a multivariate problem. Alone more than 400 different precipitants are provided in the Biological Macromolecule Crystallization Database.⁴⁵ Moreover the dependency on pH, protein and precipitant concentration expand the parameter space several fold to an infinite amount of screening conditions. Different screening strategies exist to reduce the number of experiments to a realizable size for the screening. The phase behavior, especially crystallization is then analyzed in dependency of varied parameters. Most screenings are based traditionally on empirical trial and error studies.^{46,47} An overview of different screening strategies in figure 1.5 is adopted from Rupp et al.⁴⁵

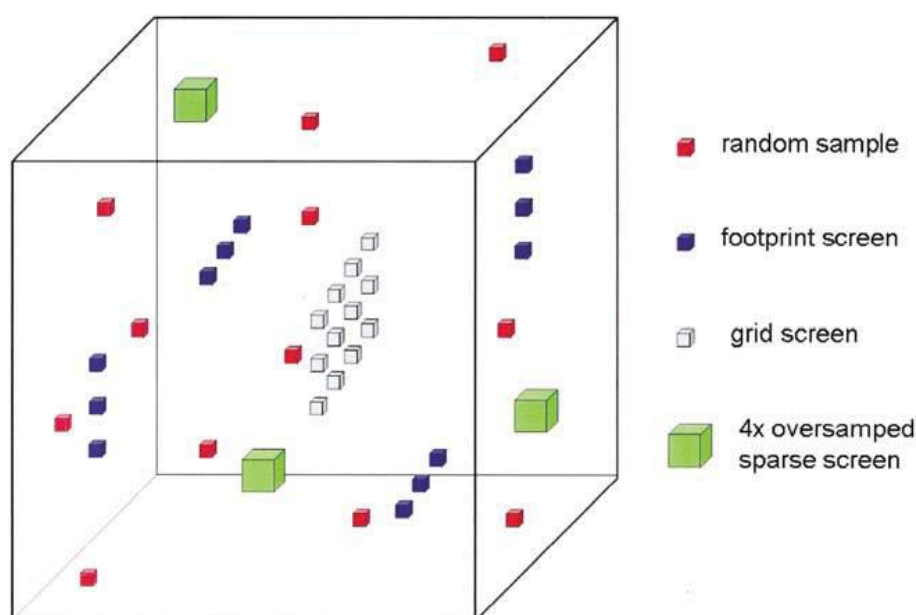


Figure 1.5: Screening strategies for protein phase behavior⁴⁵

In random samples the parameters are randomized chosen. Sparse matrix screens consist of a wide parameter space in which some discrete points are tested. With these conditions various pH-values, salts and precipitants can be screened.^{48,49} The first sparse matrix screens were developed by Jancarik and Kim.⁴⁹ Various modified screens can be purchased now from different companies (Hampton Research, Jena Bioscience), whereby preparation and implementation are simplified for high throughput. Other screening strategies are the footprint-screen where only one parameter is varied or a grid screen with the variation of two parameters.⁴⁵

With design of experiments, the screening conditions can also be adjusted. Thereby the parameters are varied systematically and different parameters are changed simultaneously. A regression analysis was applied successfully by Carter et al.⁵⁰

Other approaches are rational screenings. These screenings are based on the knowledge of the protein phase behavior. Examples are the implementation of the Hofmeister series on

crystallization of lysozyme,⁵¹ the correlation between osmotic second virial coefficient and protein phase behavior^{40,44,52} and considerations of different physical properties.⁵³

1.5.1 Empirical screening approaches

Besides the in chapter 1.2.5 mentioned influencing parameters, the phase behavior is also dependent on how the experiments are conducted. In literature^{39,54,55} different implementations to conduct crystallization experiments exist. They are summarized in the figure 1.6. The phase diagram with its different regions is adopted from figure 1.3.

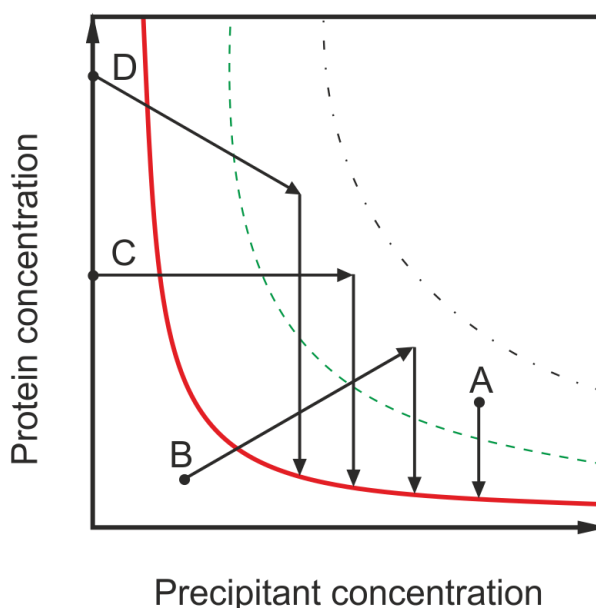


Figure 1.6: Experimental design for phase behavior screening; A: Batch; B: Vapor diffusion; C: Dialysis; D: Free-interface diffusion^{39,54,55}

In batch experiments (figure 1.6 A) is the protein stable in the starting buffer. By mixing the protein with the precipitant, the crystallization is induced. The evaporation is avoided by closing the reaction tube with a foil or an oil layer. Over the whole experimental time the conditions are not modified. One advantage is that the conditions can be defined accurately.

To conduct vapor diffusion experiments (figure 1.6 B) two different designs are generally used: Sitting drop or hanging drop. Both are based on the same mechanism. At the beginning, the protein solution is undersaturated in reaction tube or as a drop on a coverslip. In the reservoir the precipitant is located in a high concentration. These two solutions are connected over a gas phase, but completely sealed from the environment. A vapor pressure gradient is the result. The water diffuses out of the protein solution with the higher vapor pressure to the reservoir with the lower vapor pressure. The protein

concentration and the concentration of the non-volatile components increase with the duration of the experiment until the equilibrium is reached. Problems connected with this method are the uncontrolled change of conditions, like the reaction volume, the pH or the temperature.

The dialysis method also utilizes the diffusion effects (figure 1.6 C). However, the protein solution and the precipitant solution are separated by a semipermeable membrane. The precipitant can pass through the membrane, whereas the protein remains on the one side of the membrane. Since the protein reservoir is of a constant volume, only the precipitant concentration increases over the experiment.

The free-interface diffusion (FID) method is also based on diffusion (figure 1.6 D). Protein and precipitant mixtures are juxtaposed and the diffusion occurs from one solution into the other over capillaries. Thereby the resulting concentration gradient is time dependent.³⁹

1.5.2 Screening of thermodynamic properties

For the research on protein molecules the osmotic second virial coefficient (B_{22}) was first applied to measure interactions between molecules of the same kind. Meanwhile it is common either to attempt a prediction of protein phase behavior, in regard to crystallization or to increase the solubility of proteins. In 1994 George and Wilson⁵² found a small range of slight negative B_{22} -values, where the probability of crystal growth of various proteins is high. This range from $-8 \cdot 10^{-4} \text{ mol mL g}^{-2}$ to $-1 \cdot 10^{-4} \text{ mol mL g}^{-2}$ is called “crystallization slot”. Pjura et al. and Gabrielsen et al.^{56,57} confirmed this statement. They induced crystallization for bovine chymotrypsinogen A without any precipitant and a membrane protein after optimization of the conditions by means of a B_{22} -analysis. Moreover Haas et al. and Ruppert et al.^{40,44} explained theoretically the connection between B_{22} and solubility. The implementation of positive B_{22} -values in a rapid high solubility screening for lysozyme and an IgG1-antibody is shown in literature.^{58,59}

In recent years the interest on interactions between two different macromolecules arises. Relevant pairs are target protein-contaminant or protein-polymer. These interactions can be described by the osmotic second cross virial coefficient B_{23} . By means of this value the impact of interactions on phase behavior and its kinetics can be analyzed.

A strong correlation between phase behavior and B_{23} is expected by different authors.^{60–62} McCarty et al.⁶³ and Cheng et al.⁶² successfully applied the B_{23} on a separation problem with the model proteins lysozyme and ovalbumin. Further successful applications were the optimization of diafiltration sieving behavior of lysozyme-BSA mixtures⁶⁴ and the prediction of liquid-liquid equilibrium, as well as protein partition coefficients in aqueous two-phase system.⁶⁵ In a good first approximation Yousef et al.⁶⁶ modeled the osmotic

pressure of concentrated binary protein solutions with a free-solvent model by including interactions of protein to protein. The protein mixture of lysozyme and BSA was described with the modified Lennard-Jones potential (MLJ) by Choi et al.⁶⁰

By different measurement techniques like membrane osmometry, self-interaction chromatography or static light scattering, their determination is possible. The static light scattering and the self-interaction chromatography are described in more detail in the following subsections.

1.5.2.1 Static light scattering

With the static light scattering the so called “static” parameters of the protein can be determined. These are the radius of gyration, the molecular weight and the B_{22} . Therefore the solution of macromolecules is irradiated with polarized light of a distinct wave length. The incidence of the beam on a macromolecule results in scattering of parts of the beam. This intensity of the scattered light i_s is then measured under different detector angles θ proportional to the irradiated intensity I_0 :

$$\frac{i_s}{I_0} = \frac{16\pi^4 N}{\lambda^4} \cdot \frac{f}{d^2} \cdot \bar{\alpha}^2 \quad (1.16)$$

According to Rayleigh, this ratio is dependent on the wavelength λ of the irradiated light, the average polarizability of the macromolecules $\bar{\alpha}$, the distance between the detector and the molecule d , as well as the factor of polarization of the light f . The macromolecule-number density N is defined as:

$$N = \frac{cN_A}{M_w} \quad (1.17)$$

With the Lorentz-Lorenz-equation $\bar{\alpha}$ can be expressed as:

$$\bar{\alpha} = \frac{n_0 M_w}{2\pi N_A} \cdot \frac{dn}{dc} \quad (1.18)$$

Herein the macroscopic parameters are the refractive index increment dn/dc and the refractive index of the solvent n_0 . The Rayleigh ratio R_θ makes the static light scattering data instrumentation unspecific:

$$R_\theta = \frac{i_s(\theta)}{I_0} \cdot \frac{d^2}{f} = cM_w \frac{4\pi^2 n_0^2}{\lambda^4 N_A} \left(\frac{dn}{dc}\right)^2 \quad (1.19)$$

Optical parameters can be combined in the optical constant K :

$$K = \frac{4\pi^2 n_0^2}{N_A \lambda^4} \left(\frac{dn}{dc_P} \right)^2 \quad (1.20)$$

With the wavelength of the incident vertically polarized light in vacuum λ . Hence, from the equation (1.19) and (1.20) the simplified Rayleigh ratio Kc_P/R_θ is obtained for diluted and ideal solutions by:²⁴

$$\frac{Kc_P}{R_\theta} = \frac{1}{M_W} \quad (1.21)$$

For non-ideal and diluted solutions the equation is expanded by a virial expansion to:

$$\frac{Kc_P}{R_\theta} = \frac{1}{M_W} + 2B_{22}c_P + \dots \quad (1.22)$$

R_θ is for most proteins within the Rayleigh limit ($r < \lambda/20$). Therefore these proteins are isotropic light scattering molecules and the R_θ is proportional to scattered light intensity.

Whit two different macromolecules in solution the B_{ij} can be determined according to Comper and Laurent.⁶⁷

$$\begin{aligned} \frac{K^*}{R_\theta} = & \left(\sum_i^n M_i \left(\frac{dn}{dc} \right)_i^2 c_i \right)^{-1} \\ & + \frac{2 \sum_i^n \sum_j^n B_{ij} M_i M_j c_i c_j \left(\frac{dn}{dc} \right)_i \left(\frac{dn}{dc} \right)_j}{\left(\sum_i^n M_i \left(\frac{dn}{dc} \right)_i^2 c_i \right)^2} \end{aligned} \quad (1.23)$$

The modified optical constant K^* is:

$$K^* = \frac{4\pi^2 n_0^2}{N_A \lambda^4} \quad (1.24)$$

Therefore the osmotic second virial coefficients B_{ii} need to be obtained in separate experiments.

1.5.2.2 Self-interaction chromatography

Self-interaction-chromatography is a method to measure weak interactions of repulsive or attractive nature between protein molecules. Therefore the retention behavior of a protein sample is analyzed in two different columns and the results are compared. Both columns

are identical, only that one is modified with the protein of interest. The unmodified one is necessary to compensate for the size-exclusion effect of the column material. The direction of interaction between immobilized protein and the one in solution can be determined from the comparison of retention volume for both experiments. If the protein elutes earlier in the column with immobilized protein, interactions are repulsive. Higher retention volumes in the column with immobilized protein result from overall attraction.

In principle the distribution coefficient K_{SEC} for retention behavior of a protein sample in SEC is usually calculated with the following equation:

$$K_{SEC} = \frac{V_r - V_0}{V_i} = \frac{V_r - V_0}{V_t - V_0} \quad (1.25)$$

Where V_r is the average retention volume of the mobile protein, V_0 the interstitial or extra-particle column volume, V_t the total mobile phase volume and V_i the intraparticle pore volume, which is defined as the difference of V_t and V_0 ($V_i = V_t - V_0$).

If an immobilized column is used, the distribution coefficient $K_{overall}$ is then:

$$K_{overall} = K_{SEC} + K_{aff} K_{SEC} \quad (1.26)$$

K_{aff} describes the interaction which is evoked by weak interactions between the immobilized and the mobile protein molecules in the sample. The mathematical and thermodynamical basis is:

$$K_{aff} = \frac{q}{c_p} = \frac{\Delta V_{r,aff}}{m} = \frac{\int_{V_i} \left(\exp\left(\frac{-\Delta G(r, \Omega_1, \Omega_2)}{k T}\right) - 1 \right) dV_i}{V_i} \quad (1.27)$$

Where q is the amount of adsorbed protein per volume of resin, c_p the protein concentration of the mobile phase, m the amount of resin in terms of volume, $\Delta V_{r,aff}$ the change in retention volume caused by interaction and ΔG the free energy change. The latter is due to the motion of a single mobile phase molecule from the interstitial volume into the pore volume, where it interacts with one single immobilized protein molecule.

As Ahamed et al.⁶⁸ mentioned this equation is generally applicable for low protein load in the mobile phase, because the slope of the linear region of an adsorption isotherm is related to the potential of the mean force between molecules. With the assumption that the lower limit of the separation integral is set to 0 and by summing over all immobilized protein molecules the following equation results:⁶⁹

$$K_{aff} K_{SEC} = \frac{N \int_{\Omega_1} \int_{\Omega_2} \int_0^{\infty} (\exp(-W(r, \Omega_1, \Omega_2)/kT) - 1) r^2 dr d\Omega_2 d\Omega_1}{V_i} \quad (1.28)$$

Where N is the total number of immobilized protein molecules accessible for mobile protein molecules. According to literature^{17,68} the deviation due to the hard sphere contribution term is insignificant, and can therefore be neglected in the lower limit of the separation integral. The combination of equation (1.28) with equation (1.2) allows the calculation of the B_{22} in the following form:^{68,70}

$$B_{22} = \frac{N_A(K_{SEC} - K_{overall})V_i}{M_W^2 N} = \frac{(K_{SEC} - K_{overall})V_i}{m_P M_W} \quad (1.29)$$

Where $m_P = (M_W N)/N_A$ is the mass of immobilized protein.

Under the following assumptions the equation (1.29) is valid:⁶⁸⁻⁷¹

- The same adsorber material is used for the non-immobilized and immobilized column and the protein does not interact with adsorber material.
- The protein structure and the orientation of the immobilized protein are not affected by immobilization. Therefore the $\Delta G(r, \Omega_1, \Omega_2)$ in eq. (1.27) is equal to $\Delta W(r, \Omega_1, \Omega_2)$ in equation (1.29).
- The diameter of the pores has to be significantly bigger than the diameter of the protein.
- The interaction of one single mobile protein molecule occurs with only one single immobilized protein molecule at the same time.

2 Motivation and Research Proposal

The rapid growth of bio pharmaceuticals and therapeutics for example in the anti-cancer and autoimmune therapy illustrates the high potential of monoclonal antibody based products. The upstream processing of these molecules has been a major research area, while downstream processing is often neglected. Protein crystallization involves protein stabilization at high titer and is a promising alternative compared to chromatographic methods for purification and formulation in downstream processing.^{10,12,13,72} However only few applications of protein crystallization exist and antibody crystallization is even more challenging due to their large molecule size and therefore corresponding complexity.¹⁰ To make crystallization competitive to other downstream techniques it is essential to develop strategies for successful screening processes with less trial numbers as well as experimental time. At the end a fundamental understanding of protein phase behavior is required. This would not only increase the success of protein crystallization due to a fast process development and scale up but also enables a simplified optimization of other downstream processing steps.

As described in detail in chapter 1, an unlimited number of parameters like pH-values, precipitant types and concentrations influence the protein phase behavior in different manners. Appropriate crystallization conditions have to be found in the multivariate parameter space. Screenings for crystallization conditions are still challenging because they are often conducted in trial and error experiments.^{39,45} Thereby neither fundamental understanding of phase transitioning occurrence is gained nor is an allocation of responsible protein properties possible.⁴⁵ A typical screening set-up is illustrated in figure 2.1 at the top. Screening kits are composed of different kinds of precipitants at different pH-values and mixed together with the respective protein. Additionally, different buffer types are often used for protein and precipitants. After a distinct time period (the equilibration time) experiments are analyzed. Samples showing a promising result of protein phase behavior are further used for investigations. Protein and precipitant concentrations are varied in two dimensional phase diagrams, while other conditions and precipitants are neglected, although they might be more appropriate in another concentration range or at another pH-value.

One aim of this work was to develop a systematic and sophisticated screening method for protein phase behavior determination. By variation of different parameters more information can be obtained out of the conducted experiments. The influencing “parameters” of the sample conditions listed in figure 2.1 on the left can be easily determined experimentally or theoretically. “Characteristic” parameters on the right in

figure 2.1 like nucleation or crystallization kinetic, crystal size and solubility can be determined during the experiment. The result is a high amount of supplementary information about the protein phase behavior and influencing factors.

As illustrated in figure 2.1 below, protein phase behavior results from protein-protein interactions in solution. These interactions can be described with the osmotic second virial coefficient B_{22} . In literature different empirical and theoretical approaches exist for model proteins to correlate this parameter with protein phase behavior.^{43,52} However, it is unclear, how this information can be applied to characterize the phase behavior of monoclonal antibodies. Therefore, another aim was to characterize the protein-protein interactions via B_{22} and cross-interactions between protein and precipitant via osmotic second cross-virial coefficient B_{23} and to find correlations between B_{22} respectively B_{23} and antibody phase behavior. Screening procedures were refined to create deep insights as well as understanding of the phase behavior of antibodies. Another objective on this pathway was the identification of application limits for empirical and thermodynamic approaches to correlate the B_{22} to protein phase behavior. From the above, four different opportunity fields were identified and are subsequently outlined.

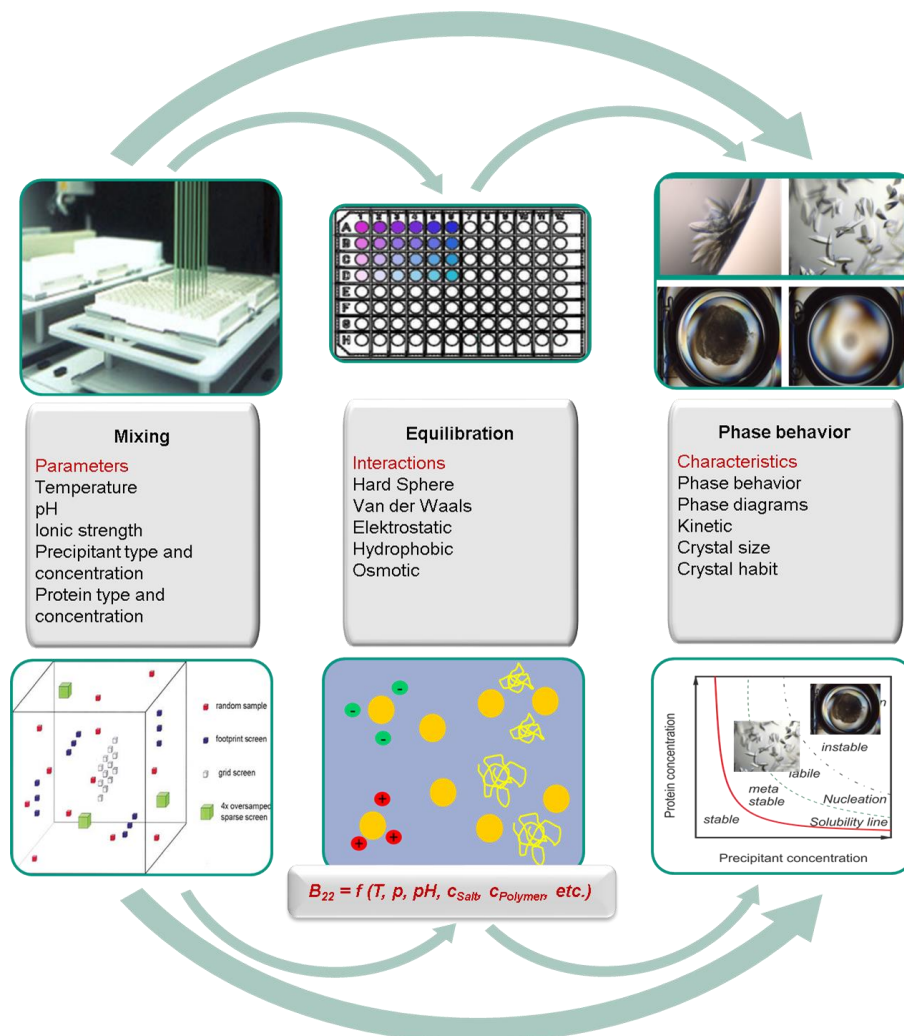


Figure 2.1: Schematic illustration of the research proposal

In **chapter 3: *Self-interaction Chromatography in Pre-packed Columns: A Critical Evaluation of SIC Methodology to Determine the Second Virial Coefficient*** the aim was to find an appropriate method to analyze the B_{22} using the model protein lysozyme. In literature various methods exist, which are based on different physical principles.^{68,73} Besides the static light scattering (SLS) as a traditional method, in particular the Self-Interaction-Chromatography (SIC) gained our interest due to its low protein consumption and less additional equipment. By the development and validation of a preparation process in pre-packed columns and characterization of protein load with a partial least squares regression the experimental effort could be successfully reduced. However, deviations between B_{22} -values from SIC experiments were found in literature⁶⁸ as well as between B_{22} -results of SLS and SIC. Reasons might be the invasive character of this method and the need to fulfill different related prerequisites. Hence, a detailed analysis of the influencing parameters was conducted with focus on the influence of protein binding on the adsorber on the later B_{22} -determination. In particular the influence of the amount of bound protein on the adsorber particle surface and the binding orientation were analyzed. Based on the results a method of choice was recommended.

Establishing a buffer system with a constant buffer capacity from pH 5 to 9 for crystallization screenings as conducted in **chapter 4: *Moving Through Three-dimensional Phase Diagrams of Monoclonal Antibodies*** offers some advantages compared to conventional crystallization condition screenings with screening kits.^{45,49} First, the amount of influencing parameters can be reduced, when protein and precipitant are prepared with the same buffer. Second, phase diagrams are one strategy to systematically analyze the influence of different parameters on protein phase behavior. Third, by developing a semi-automated platform the influence of fluid phase conditions and precipitants can be systematically investigated. The buffer system enabled one to analyze the precipitant and protein concentration as a function of pH over a broad pH-range in detailed three-dimensional phase diagrams. By using an automatic imaging system the characterization of phase behavior could be expanded to further parameters. Besides the phase behavior and the crystal form and size after a distinct time, the times at which first structures are visible in samples were determined as parameter for the nucleation and crystallization kinetic. The objective was the implementation of a systematic screening method with a buffer system and additional analytics. The screening was conducted with three different antibodies and various common used salts as precipitants. The empirical Hofmeister series describes the salting out strength of salts on proteins.^{74,75} Different modified series exist in literature depending on the protein and on its net charge.⁷⁶⁻⁷⁸ Since the antibodies are positively charged over a broad pH-range, some authors expect the reverse Hofmeister series.^{78,79} One goal was to analyze the feasibility of the Hofmeister series for antibodies and the pH-dependency of antibodies on the salting out effect.

Another objective was to gain theoretical understanding about ongoing processes in solution by combining the systematic approach of the buffer system with a thermodynamic analysis. Therefore the qualitative conclusions of chapter 4 were further analyzed by means of protein-protein interactions with the thermodynamic factor B_{22} in **chapter 5: *From Osmotic Second Virial Coefficient (B_{22}) to Phase Behavior of a Monoclonal Antibody***. According to studies with model proteins in literature,^{52,73} the crystallization probability of proteins is higher in a range of slight negative B_{22} -values, namely the crystallization slot. However, for large molecules like antibodies some authors^{80,81} recommend a smaller crystallization slot closer to zero, others⁴¹ could not find any correlation. The aim was to investigate whether empirical ranges in form of a crystallization slot allow a general description of phase behavior. It would be beneficial to have a universal phase diagram based on thermodynamic principles to control protein phase behavior. However, it is questionable if simple models can describe the compositions of the different aggregation states and the protein concentration dependency for a complex molecule like a monoclonal antibody or if kinetic phenomena and the complexity of the molecule have to be taken into account. Therefore, experimental strategies were developed to characterize the compositions of different aggregation states and to compare these data to theoretically modeled ones. The aim was to outline which simplifications of thermodynamic principles including the B_{22} are applicable to describe phase behavior of complex large molecules such as monoclonal antibodies and to point out the limits of this thermodynamic factor.

According to Finet et al.⁸² PEG has a high potential to induce crystallization for large proteins. Moreover the strength of interaction can be adjusted over the molecular weight. Another aim was to answer questions like how the antibody phase behavior is influenced by PEG, which role play the PEG molecular weight and the pH and how the phase behavior differs from that with salts in **chapter 6: *Influence of Macromolecular Precipitants on Phase Behavior of Monoclonal Antibodies***. It was attempted to gain additional fundamental understanding with the new approach of analyzing cross interactions between protein and PEG with the measured osmotic second cross virial coefficient (B_{23}). Another goal was to analyze how and if the use of B_{22} and B_{23} lead to a predictive description of protein phase behavior for systems consisting of monoclonal antibodies and PEG as precipitant.

The findings of the above named questions and tasks are presented and discussed in four research papers in the following chapters.

3 Self-interaction Chromatography in Pre-packed Columns: A Critical Evaluation of SIC Methodology to Determine the Second Virial Coefficient

Natalie Rakel, Kristina Schleining, Florian Dismer, Juergen Hubbuch

Section IV: Biomolecular Separation Engineering, Institute of Engineering in Life Sciences, Karlsruhe Institute of Technology, Engler-Bunte-Ring 1, 76131 Karlsruhe, Germany

Published in the Journal of Chromatography A, 2013;1293:75-84

Corresponding author:

Juergen Hubbuch

Karlsruhe Institute of Technology

Institute of Engineering in Life Sciences

Section IV: Biomolecular Separation Engineering

Engler-Bunte-Ring 1, 76131 Karlsruhe, Germany

Phone: +49-721-608-42557, fax: +49-721-608-46240

E-mail: juergen.hubbuch@kit.edu.

Keywords: Self-interaction chromatography; Static light scattering; Protein interactions; Phase behavior

Abstract

The characterization of protein-protein interactions is commonly conducted via self-interaction chromatography to describe magnitude and direction of the interactions with the resulting osmotic second virial coefficient (B_{22}). However, the method is invasive and protein immobilization on the adsorber surface can influence the results obtained. In order to replace batch immobilization procedures followed by a column packing, direct on-column preparation was optimized in terms of protein immobilization under a continuous flow. Surface load was measured applying a novel method based on partial least squares analysis of spectral scans to reduce analytical error when determining the amount of immobilized protein. Subsequently influencing parameters such as the effects of absolute surface load, injected protein concentration and distribution of protein orientation were analyzed and system performance evaluated. The results disprove the consistency of the SIC method regarding the non-random orientation of proteins on adsorber particles. Thus the determined B_{22} -values differ quantitatively from those determined with static light scattering. Furthermore, variations in immobilization conditions influence the results obtained. These results make clear that SIC does not fulfill the theoretical framework of B_{22} -analysis. It is rather a qualitative measure of protein-protein interactions in the respective system used for experimentation.

3.1 Introduction

Phase behavior of proteins is currently one of the key parameters determining protein purification but even more formulation strategies. Ever higher product titer, the search for alternative processing steps in the mAb industry as well as the drive toward highly concentrated formulations make it mandatory to get a deeper understanding into protein phase behavior, solubility issues and rheological parameters of solutions of high protein concentrations.

A widely used predictive method to describe phase behavior of proteins in solution is the application of the osmotic second virial coefficient (B_{22}). It is a promising fundamental thermodynamic approach to evaluate buffer conditions in terms of protein stability and phase behavior [1–3]. With this approach interactions between molecules of the same type in a diluted solution are characterized. The magnitude and sign of the B_{22} -value indicates whether attraction or repulsion dominates. While a negative value corresponds to attraction, repulsion results in a positive B_{22} . This can be applied to estimate the phase behavior of concentrated protein solutions. George and Wilson [4] postulated that in the so called “crystallization slot”, a small range of slight negative B_{22} -values, the probability of crystal growth of various proteins is high. Pjura et al. [5] optimized crystallization conditions by choosing liquid phase compositions with B_{22} within this crystallization slot and could crystallize bovine chymotrypsinogen A without any precipitant. Even the crystal structure of a membrane protein could be determined after optimization with B_{22} -screening via X-ray diffraction by Gabrielsen et al. [6]. On the other hand the screening for positive B_{22} -values could be used for a rapid determination of high solubility formulation conditions [1]. Le Brun et al. [7] for example could increase the stability of an IgG1 antibody in solution with a B_{22} -buffer screening. A theoretical explanation for the connection between B_{22} and solubility is published by Haas et al. and Ruppert et al. [8,9].

To determine the B_{22} different colloidal measurement techniques are described in literature such as membrane osmometry [5,10], sedimentation equilibrium measurements [11], self-interaction chromatography (SIC) [6,11–13] and static light scattering (SLS) [14–16]. Because of the low protein and time consumption SIC is the most commonly applied technique in literature and most of the mentioned studies were conducted with this technique. The self-interaction of different kinds of proteins such as membrane proteins [6], antibodies [17,18] or the model proteins [3,19,20] were analyzed either to increase the solubility or to find crystallization conditions. Based on these results García et al. [21] and Deshpande et al. [22] further reduced the required volume by applying the SIC on microchips. Therefore the SIC is object of a thorough investigation in terms of immobilization technique and comparability of the results to static light scattering

experiments. SIC is based on the comparison of protein retention behavior in a column with immobilized protein of the same kind to its behavior in an unmodified column. Weak interactions between free protein in the mobile phase and immobilized protein result in a shift in retention volume revealing the nature of their interaction. But covalent immobilization itself is an invasive methodology changing protein properties by eliminating surface charges while leaving only certain parts of the protein accessible to the solvent [23]. The question however arises in how far the immobilization procedure influences the results of a B_{22} measurement? As B_{22} is considered a physical characteristic of protein and buffer systems used, the analytical technique as such should not influence the outcome of analysis. Potential sources of error such as the kind of adsorber material [20], the immobilization degree [3,24] or the injected protein concentration [3,20] have been identified. However the influence of the buffer conditions during immobilization on B_{22} -values and the distribution of protein orientation in the adsorber particles have so far not been addressed.

To shed some light into this, we followed a new approach for preparing a SIC set-up that is based on the treatment of activated adsorber particles in pre-packed columns under continuous flow conditions. This includes immobilization of proteins and blocking of remaining active groups on the adsorber particle surface. The uniformity of protein distribution after immobilization on the adsorber particle surface and along the column was monitored via confocal laser scanning microscopy (CLSM). The overall immobilization degree was determined from the mass balance of remaining protein in the coupling buffer [13,20]. Since a part of the reactive compound on the adsorber particle surface is released during immobilization reaction that shows UV absorption at 280 nm, the time consuming bicinchoninic acid (BCA) assay is mostly used for analytics [1,7,13,20]. In this paper we used an alternative approach that allowed direct quantification of protein in the coupling buffer using its unique absorption spectrum by applying partial least squares (PLS) regression [25].

Following a reproducible and well characterized preparation of a SIC analytical set-up, the following parameters were systematically investigated regarding to their effect on the B_{22} : the injected protein concentration, the adsorber particle surface load and the buffer conditions during the immobilization procedure. Finally, the obtained SIC B_{22} -values were compared to SLS-data.

3.2 Theory

3.2.1 Osmotic second virial coefficient (B_{22})

The osmotic second virial coefficient (B_{22}) describes magnitude and direction of non-ideality of the osmotic pressure π in a dilute solution. It is part of the virial expansion of the osmotic pressure π :

$$\pi = RTc_P \left(\frac{1}{M_W} + B_{22}c_P + \dots \right) \quad (3.1)$$

Parameters are the universal gas constant R , the temperature T , the protein concentration c_P and the molecular weight of the protein M_W . The reasons for the non-ideality are weak interactions between two molecules of the same kind in a dilute solution. These interactions are based on excluded volume, electrostatic interaction, osmotic potential, hydrophobic and short range interactions (van der Waals, solvation, hydrogen bonding) [26–28]. Interactions between proteins can be described via the potential of mean force $W(r, \Omega_1, \Omega_2)$, which is correlated to the B_{22} [20,29,30]:

$$B_{22} = -\frac{N_A}{M_W^2} \int_{\Omega_1} \int_{\Omega_2} \int_0^\infty \left[\exp\left(\frac{-W(r, \Omega_1, \Omega_2)}{k T}\right) - 1 \right] r^2 dr d\Omega_2 d\Omega_1 \quad (3.2)$$

Where k is the Boltzmann constant, N_A is the Avogadro constant, r the center-to-center-distance of two protein molecules in solution and Ω_1, Ω_2 the rotation angles defining the orientation of both molecules toward each other. According to equation (3.2) the B_{22} contains information about apparent intermolecular forces. Repulsive interactions between molecules result in positive, attractive ones in negative B_{22} -values.

The potential of mean force $W(r, \Omega_1, \Omega_2)$ is defined as the work required to bring two indefinitely separated protein molecules to a finite separation r averaged over all possible configurations of the solvent molecule, assumes that the potential of mean force is spherically symmetrical and only accounts for a two body protein-protein interaction [24].

For a chromatographic system where one of the interaction partners is immobilized this relationship does not apply and several studies have correlated the distribution factor K_D to the potential of mean force between the mobile molecule and the stationary phase [3,20,24]. Different approaches in the respective correlations accounted for the experimental differences. Tessier et al. [3] added a separate excluded volume contribution to reach their final B_{22} -value. Teske et al. [24] argued this to be redundant as they measured a retention volume in excess of that for a protein-free stationary phase. Ahamed

et al. [20] followed the approach of Teske et al. [24], however, relating the B_{22} to distribution coefficients to K_{SEC} and $K_{overall}$ allowing more flexibility in the experimental set-up. However when comparing data obtaining when measuring B_{22} in free solution addressing equation (3.2) with the chromatographic determination of the B_{22} in SIC several prerequisites are set [3,12,20,24]:

- Adsorber material: usage of inert adsorber material with no interaction of the protein and the adsorber material. A pore diameter which is significantly larger is size than the protein diameter.
- Immobilized protein: random orientation of the immobilized protein and structure conservation. Therefore the free energy change of bringing a protein molecule from the interstitial volume into the pore volume so that it interacts with a single immobilized protein molecule is equal to the potential mean force between two protein molecules free in solution.
- Interaction: one single free protein molecule interacts with one single immobilized protein molecule and does not interact with other free protein molecules. Teske et al. [24] accounted for multipoint interactions indicating, however, that this would lead to deviations between B_{22} measured in free solution and B_{22app} measured in SIC.

If these prerequisites are met the degree of interaction between immobilized protein and the one in solution can be determined by evaluating the effect of protein interaction on retention behavior according to equation (3.3) [20,24]:

$$B_{22} = \frac{N_A(K_{SEC} - K_{overall})V_i}{M_W^2 N} = \frac{(K_{SEC} - K_{overall})V_i}{m_P M_W} \quad (3.3)$$

Where N is the total number of immobilized protein molecules accessible for mobile protein molecules, K_{SEC} the distribution coefficient for retention behavior of a protein sample based on pure diffusive behavior, $K_{overall}$ is the distribution coefficient of the quantitative affinity chromatography with weak interactions, $V_i = V_t - V_0$ the intraparticle pore volume, with V_t the total accessible volume and V_0 the interstitial or extra-particle column volume and $m_P = (M_W N)/N_A$ the mass of immobilized protein.

One important line of argumentation which is in most studies left as an un-proven assumption can be found in the random orientation of the molecule after the immobilization. This however is a major – also theoretical - prerequisite when attempting to correlate SIC to the B_{22} measured in free solution.

3.3 Materials and Methods

3.3.1 Materials and Apparatus

Lysozyme from chicken egg white (monomer molecular weight 14.3 kDa, isoelectric point pI 10.7 [31], lyophilized, product no. L6876) was purchased from Sigma-Aldrich Inc. Sodium chloride (product no. 567440), sodium hydrogen phosphate dihydrate (product no. 137036), sodium dihydrogen phosphate dodecahydrate (product no. 1.06573), ethanolamine (product no. 100844), sodium hydroxide (product no. 567530), sodium acetate trihydrate (product no. 106265), hydrochloric acid (product no. 100317) and acetone (product no. 100014) were bought from Merck KGaA. In addition, acetic acid (Carl Roth GmbH+Co. KG, product no. 3738), N-hydroxysuccinimide (Thermo Scientific, product no. 24500) and Cy5 NHS mono ester (Amersham Biosciences, product no. PA15101) were used. All prepared buffers and protein samples were filtrated with a 0.2 μm cellulose membrane to avoid contamination and dust particles in the solutions.

3.3.2 Preparation of SIC- and SEC-Columns

For the immobilization procedure, pre-packed 1 mL HiTrap™ N-hydroxysuccinimide (NHS)-activated Sepharose™ High Performance (HP)-columns (GE Healthcare, product no. 17-0716-01) were used. The immobilization reaction is based on a covalent amide coupling between NHS-activated groups on the surface of adsorber particles and primary amino groups of proteins [32]. As shown in figure 3.1 the continuous flow is adjusted by a peristaltic pump to 1 mL/min and the temperature was set to 4°C. The full procedure consisted of a pre-wash-, coupling-, wash- and blocking step. The pre-wash step of the chromatographic resin was performed with 15 mL of pre-wash-buffer (1 mM HCl). The coupling solution consisted of 10 mL protein solution at a concentration of 1 - 7 mg/mL protein in coupling buffer (0.1 M sodium phosphate, 0.5 M sodium chloride, pH 6.2 - 8) [13,20]. The coupling solution was circulated for 4 h [32]. Subsequent to the immobilization procedure, the coupling solution with remaining protein was collected followed by a column wash with 20 mL of coupling buffer. The protein concentrations of both solutions – coupling solution and wash solution – were used to determine the overall surface load. In a final blocking step, remaining active NHS-groups at the adsorber particle surface were blocked, as the column was flushed in a cycle for 12 h at 4°C with blocking buffer (1 M ethanolamine, 0.5 M NaCl, 0.1 M sodium phosphate, pH 6.0).

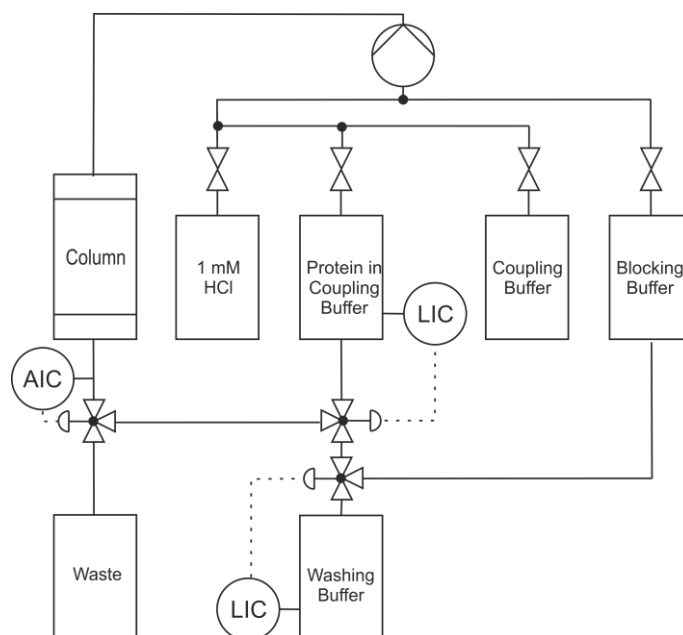


Figure 3.1: Flow sheet for the immobilization of protein in pre-packed SIC-columns; control units AIC (analysis indicator controlling) and LIC (level indicator controlling)

To monitor the immobilization reaction, an online UV/vis-spectroscopic detector was used. For the validation of the procedure, immobilization reaction experiments were carried out with the same assembly, but with an additional refractometer as well as dynamic and static light scattering detectors connected in series after the column. Since the released NHS showed absorption at 280 nm blurring the signal of lysozyme at that wavelength, these detectors helped to determine small changes in the solution composition of protein and NHS.

Unmodified columns acting as blank reference, were prepared according to the blocking procedure described above. All columns in use were stored at 4°C in 10 mM sodium phosphate (pH 7).

3.3.3 Determination of uniform protein distribution in adsorber particles

Uniformity of protein coupling in the adsorber particles after immobilization was analyzed using confocal laser scanning microscopy (CLSM). Labeling of bound lysozyme on primary amino groups of lysine residues with fluorescent dye Cy 5 was performed batch wise in coupling buffer at a constant dye to protein ratio of 20 µg Cy 5 per mg immobilized lysozyme [33]. After 30 min incubation time particles were repeatedly washed by discarding the supernatant after centrifugation (13,000 rpm for 5 min) and adding fresh coupling buffer until the supernatant remained colorless.

Microscopic analysis using confocal laser-scanning microscopy (LSM 510 META, Carl Zeiss AG, Jena, Germany; software LSM 510 Version 3.2 SP2) was carried out with a constant gain at an excitation wavelength of 630 nm and emission was measured with a longpass filter above 650 nm [34]. 30 μ l of labeled and suspended adsorber particles were pipetted into an optically transparent micro well plate (Whatman Ltd, product no. 7706-2370). To check for homogeneous protein distribution throughout the complete column, samples (50 mg adsorber material) were taken from the top, the middle and the bottom of three different columns. For 162 particles the midpoint was determined and the fluorescence intensity profiles in x-y as well as in x-z direction were analyzed. To determine the intensity over the radius of a particle an averaging procedure was conducted [35]. For one cross-section the intensity signal for five different lines across the midpoint were first averaged separately and then evaluated. For detailed information see Hubbuch and Kula. [34] and Schröder et al. [35].

3.3.4 Determination of surface load

Surface load was determined by measuring unbound protein in coupling and wash solution followed by mass balancing. Protein concentration was determined by two procedures. Procedure 1: protein and released NHS-groups were separated with PD-10 desalting columns (GE Healthcare, product no. 17-0851-01) followed by concentration measurement at UV 280 nm. Procedure 2: protein concentration was determined directly from the absorption spectra of the mixture of NHS and lysozyme by applying partial-least-squares (PLS) regression as published by Hansen et al. [25].

The calibration and validation of the model with the MATLAB based PLS toolbox (Eigenvector Research, Wenatchee, WA, USA) was based on a three level full factorial design (MODDE, Umetrics, Umeå, Sweden) in the concentration range of 0 - 0.8 mg/mL lysozyme and 0 - 0.025 mg/mL NHS. For every coupling pH three sample sets were prepared independently and analyzed with a separate calibration model. Absorption spectra recorded ranged from 250 nm to 330 nm and were measured in multi full area 96-well plates with 200 μ l (Greiner Bio-One Ltd., product no. 655801, Tecan infinite[®]M200, Tecan Group Ltd., Crailsheim, Germany). Two latent variables were defined and mean centered data were used.

3.3.5 Self-interaction-chromatography

The degree of interaction between immobilized protein and the one in solution is determined by evaluating the effect of protein interaction on retention behavior according to equation (3.3) [20,24].

All chromatographic measurements were conducted with an FPLC-System ÄKTA™purifier with the auto sampler A-905 (GE Healthcare, Uppsala, Sweden, software Unicorn 5.2). The flow rate was set to 1 mL/min [20]. Prior to running experiments the whole system was equilibrated with buffer according to the conditions (buffer type, pH and ionic strength) used in the respective experiment until UV and conductivity signal were constant. 50 µl of lysozyme solution with a concentration of 2 mg/mL were injected. Measurements were done in triplicates for varying sodium chloride (NaCl)-concentrations from 0.1 M to 1 M in three different buffers: 10 mM sodium phosphate (NaPi, pH 7.6), 20 mM sodium phosphate (NaPi, pH 7.6) and 20 mM sodium acetate (NaOAc, pH 4.5)-buffer. According to equation (3.3) the retention volumes V_t and V_0 were determined by injections of salt and Blue Dextran. The reproducibility of data and stability of the columns were measured by repeating the measurements over a period of four weeks.

3.3.6 Determination of isoform distribution

The covalent attachment of the NHS-activated fluorescent dye Cy 5 to lysine residues follows the same reaction type as the immobilization reaction on the adsorber particle and was thus used to study the reactivity of the six lysine residues. The mono-labeled isoforms in the final mixture were quantified by the published protocol to separate lysozyme-Cy 5 isoforms from Teske et al. [36] and Dismer and Hubbuch [33]. The conditions for the reaction in solution and the analytics with a RESOURCE™ Column (GE Healthcare, product no. 17-1178-01) were adopted from Dismer and Hubbuch [33] and conducted with lysozyme without adsorber particles in solution.

3.3.7 Static light scattering

Static light scattering is a non-invasive method to determine the interactions between molecules due to the change in the averaged intensity of scattered light. For protein solutions scattering is a function of protein concentration and detection angle. So called “static” parameters of protein molecules such as molecular weight M_W and osmotic second virial coefficient B_{22} can be obtained due to the concentration dependency of the scattered light [37].

For B_{22} -determination, scattered light intensities were measured with an automated-batch composition gradient multi-angle light scattering system (CG-MALS). This is a combination of a pump system with degasser including three 0.1 µm inline-filters, light scattering detector and refractometer operated in series (Calypso, DAWN®HELEOS™ 8+, Optilab® reX, Wyatt Technology Corp., Santa Barbara, CA, USA, Software CALYPSO Version 1.2.8.5, ASTRA Version 5.3.4.20). The desired salt concentration and the protein concentration gradient were set using three pumps (flow rate 0.6 mL/min). During analysis

the flow was stopped at each concentration step for the delay time of at minimum 60 sec. For different protein concentrations the particular light scattering signals were measured at seven angles to determine the B_{22} . The background scattering of pure solvent was subtracted. By applying the adjusted refractive index increment dn/dc_P of 0.185 mL/g [38–40] the protein concentration was determined with the refractometer. The B_{22} was determined with the Zimm-Formalism [30,37]. To validate each measurement the resulting molecular weight M_W was compared to the literature value of 14.3 kDa. An additional dynamic light scattering detector in the system was used to indicate aggregation in solution. The calibration for the SLS instrument to determine absolute R_θ was done with toluene, which has an established Rayleigh ratio R_{90} at an angle of 90° of $1.406 \cdot 10^{-5} \text{ cm}^{-1}$ at a wavelength λ of 633 nm [16,41].

3.4 Results and Discussion

Traditionally immobilization reaction of protein on different kinds of adsorber materials for preparation of SIC-Columns is conducted batch wise prior to column packing [3,7,20]. The use of Sepharose (CNBr-activated Sepharose™ 4B and NHS-activated Sepharose™ 4 Fast Flow (FF)) [12,20] is as common as the use of Toyopearl AF-Formyl-650 [42,43]. The surface of adsorber particles is activated by cyanogen bromide (CNBr) [3,12] or N-hydroxysuccinimide (NHS) [20,42,43]. Common for these chromatographic adsorber materials is the sufficient size of pore structure in relation to protein dimensions. Ahamed et al. [20] worked with Sepharose™ 4 Fast Flow (FF) particles and showed already the feasibility of NHS-activated sepharose adsorber particles. In this work the preparation of SIC-columns was carried out directly in pre-packed NHS-activated Sepharose™ HP-columns. Both materials, Sepharose™ FF and Sepharose™ HP are based on a highly cross-linked agarose matrix with differences in the degree of cross-linking of 4 % compared to 6 % respectively, the length of the spacer arm with 14-, respectively 10-atoms, the adsorber particle size of 90 μm compared to 34 μm and the substitution value of 18 μmol NHS/mL medium to 10 μmol NHS/mL medium.

3.4.1 Homogeneity of immobilized lysozyme in the column

While the commonly used batch coupling procedures rely on a perfectly mixed system and a restricted influence of mass transfer limitations, coupling procedures under a continuous flow in a packed column might be hampered by a non-uniform protein distribution over one particle and along the column. To counteract this, cooled ambient conditions of 4°C over a period of 4 h were used during coupling reaction to slow down the reaction. The protein distribution after immobilization of the adsorber particles was analyzed using a confocal laser-scanning microscope as described above. For all 162 analyzed adsorber

particles the fluorescent intensity profile was measured. The fluorescence intensity correlates to the amount of coupled protein when neglecting attenuation effects. Intensity profiles measured along the x-axis in the x-y plane going through the center of a particle for one column are shown in figure 3.2. Mean intensities for particles from top, middle and bottom position of the column are plotted with their absolute standard deviation (in the range of 0.2 - 0.8) over the normalized particle diameter $d/d_{max, particle}$. Normalization is required due to varying particle sizes. The normalized diameter data points were averaged into 0.1 ranges. The intensity profile showed a plateau in normalized diameter range of 0.2 - 0.8 with an intensity mean value I of 104.9 ± 7.8 AU. Toward the particle outer range the intensity decreased. The reason for this is that the adsorber particles were not exactly spherical and the edges were included in the calculation of the normalized diameter when the averaging procedure was conducted.

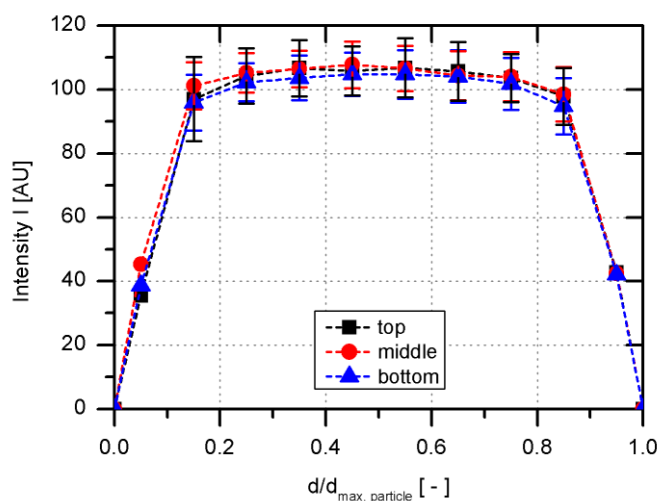


Figure 3.2: Mean intensity profile over the normalized particle diameter along the column

The homogeneous lysozyme distribution is thus given both, within the single particles as well as along the column length. The mean standard deviation of the intensity (1.2 AU) over the column length is not significant as it is lower than the mean standard deviation over all measured positions. In comparison the finding of Teske et al. [24], where a decrease of fluorescence intensity was observed toward the inner core of the adsorbent particle, can clearly be attributed to non-labeled protein occupying the adsorbent sites at the inner part [34,36].

3.4.2 Surface coverage of immobilized protein

The determination of B_{22} -values in SIC is clearly influenced by the surface load of the adsorbent both in terms of experimental performance but also fulfilling the prerequisites set by the theoretical framework. Prior to answering the theoretical and experimental findings there is a clear need for a more accurate measurement of the actual surface load.

In literature [1,7,13,20] the concentration is often determined with the bicinchoninic acid (BCA) assay with a maximal error of 20 %. This is far off of what should be expected from an analytical tool. Furthermore this to the given experimental errors over the whole procedure of SIC this might explain the deviations already seen in previous studies [20,24]. In this work the remaining protein concentration after immobilization was analyzed using two alternative procedures. Procedure 1 – use of desalting PD 10-columns prior to UV 280 nm measurements – reduced the maximal error to 5 % compared to the 20 % error given by the BCA assay [20]. Even more accurate results combined with less time effort could be reached by Procedure 2 – the PLS regression. After the calibration of the respective model, the surface load could be determined within one minute per sample by measuring the spectra from 250 nm to 330 nm in 1 nm steps. The maximal error for known lysozyme concentrations was below 4 %.

In addition the amount of coupled protein is not controlled as a function of time as found in Ahamed et al. [20] but simply a function of volume and protein concentration in the coupling buffer. The immobilization reaction was analyzed by online measurements with different detectors in series and in general 3 h of incubation were found to be sufficient to reach equilibrium in all experimental runs. These results are in agreement with Brinkley [32], who determined a reaction time of 1 - 2 h for a complete coupling reaction. Summarizing, the new procedure for preparing a SIC set-up provides a homogeneous protein distribution, a rapid and reliable determination of the surface load (4 % error) and a good control over the immobilization procedure.

3.4.3 B_{22} -determination using the prepared SIC-columns

In figure 3.3 B_{22} -values extracted from earlier SIC studies [20,24] and values obtained with the current set-up (coupling pH 8, surface load 20 mg protein/mL column volume) are plotted as a function of sodium chloride (NaCl) concentration from 0.1 M to 1 M in 20 mM sodium acetate (NaOAc) as well as 10 mM and 20 mM sodium phosphate (NaPi)-buffer. For all three buffers the B_{22} -values are decreasing with increasing salt concentration.

The negative slope is less pronounced for the NaPi-buffers (10 mM and 20 mM) because of the lower pH-value of NaOAc. Low salt concentrations promote repulsive interaction due to the high net charge (pI of lysozyme is 10.7) and electrostatic repulsion in NaOAc-buffer. Higher salt concentrations on the other hand increase the shielding effect and the hydrophobic interactions. Thus, the dehydration of the polar surface of the protein is enhanced and the attractive interaction increased. The influence of the different buffer capacities for the NaPi-buffer is negligible.

The determined B_{22} -results for NaOAc-buffer show the same trend as literature data, but the absolute values deviate from each other, particularly at NaCl concentrations below 0.4 M. For example the B_{22} -values at a NaCl concentration of 0.3 M of this work and from Ahamed et al. [20] are both positive whereas Teske et al. [24] determined a negative value. The B_{22} -values of about 0.7 M NaCl are similar. At a NaCl concentration of 1 M the B_{22} -values from this work are the lowest. For 10 mM NaPi-buffer the data obtained by Ahamed et al. [20] are comparable to those determined in this work, although slight deviations are visible in the mid salt concentration range from 0.4 M to 0.8 M. Teske et al. [24] determined B_{22} -values for the 20 mM NaPi-buffer, which deviate to lower B_{22} -values over the whole measured range. Besides the differences due to the SIC, the slight lower pH of 7 can be an explanation for the deviation. However, a deviation to higher B_{22} -values would have been expected with a lower pH due to the higher net charge of the protein and the higher repulsive interactions between the molecules.

On the one hand trends are in agreement, but on the other maximal deviations of up to $-5 \cdot 10^{-4} \text{ mol mL g}^{-2}$ for the NaOAc-buffer were detected. Such deviations can result in a wrong interpretation of interactions due to opposite algebraic sign.

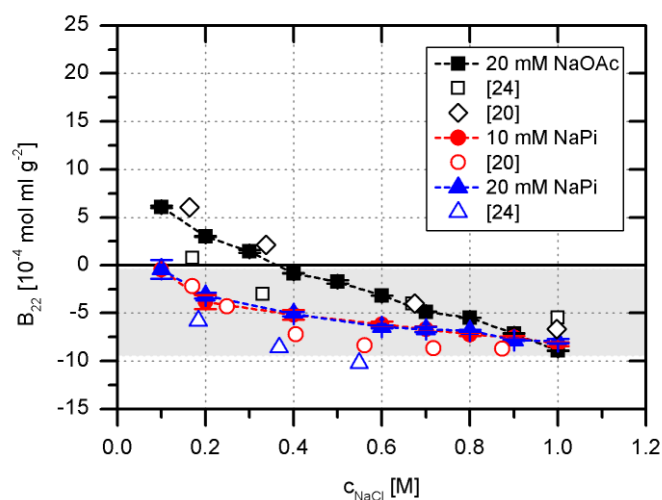


Figure 3.3: B_{22} -values for lysozyme over varying NaCl concentration in 20 mM NaOAc-buffer pH 4.5, 10 mM NaPi-buffer pH 7.6 and 20 mM NaPi-buffer pH 7.6; literature data: 20 mM NaOAc pH 4.5, 20 mM NaPi pH 7.0 [24]; 10 mM NaOAc pH 4.5, 10 mM NaPi-buffer pH 7.6 [20]; in gray crystallization slot [4]

To study the reproducibility of the experiments and the column stability, retention volume measurements of protein samples were conducted over a period of four weeks. The results were reproducible and lysozyme eluted in symmetrical peaks. The column could be used as long as no microbiological degradation occurred, which deteriorates the packing integrity of the column [20].

3.4.4 Protein-protein interactions in the mobile phase

SIC-measurements are based on the assumption that only one immobilized protein molecule interacts with one single molecule of the mobile phase at the same time and that protein-protein interactions in the mobile phase are negligible. The latter is generally reached by injecting only low amounts of protein in the mobile phase. As there is conflicting information in literature [3,12,20,24] regarding the influence of mobile phase protein concentration we thoroughly analyzed the influence of mobile phase concentrations used in this work. Within a range of 1 - 5 mg/mL no significant deviations in the retention volume were observed. At this low concentration protein-protein interactions in the mobile phase do not seem to play a significant role. This finding is comparable to Ahamed et al. [20] who also found negligible influence in the range of 1 - 5 mg/mL. As a result all experiments in this work were conducted with a constant injection volume of 50 μ L column volume and protein concentration of 2 mg/mL.

3.4.5 Multi-body interactions – Surface coverage of immobilized protein

The surface load or better protein density on the adsorbent surface determines the probability that the prerequisite of the theoretical framework of two-body interactions has to be discarded in favor to a situation of multi-body interactions. Teske et al. [24] did account for this in their theoretical framework, however, stating that this will lead to a clear deviation between B_{22} measured in free solution and SIC analysis. For the comparability to other publications and different adsorber materials the surface load is converted into percent surface coverage θ . The calculation is conducted according to Ahamed et al. [20], assuming an equal accessible surface area per volume of packed column (equal phase ratio) for Sepharose™ HP and Sepharose™ FF of approximately $42.5 \text{ m}^2 \text{ mL}^{-1}$ and a radius of the lysozyme molecule of 1.56 nm. A surface load of 15 mg/mL then correspond to a surface coverage of 11.25 %.

The influence of surface coverage θ on B_{22} -values determined in this work is plotted three-dimensional in figure 3.4 for the three different buffers 20 mM NaOAc pH 4.5, 10 mM NaPi pH 7.6 and 20 mM NaPi pH 7.6 in dependency on NaCl-concentration (a)-(c). Additionally the influence of the surface coverage is plotted for 20 mM NaOAc-buffer for the three different salt concentrations 0.4, 0.7 and 0.9 M NaCl and for 10 mM NaPi pH 7.6 and 20 mM NaPi pH 7.6 with a NaCl concentration of 0.9 M for demonstration purposes (d). For surface coverage lower than 1 % the B_{22} was determined with a positive value except for 10 mM NaPi-buffer at 0.9 M NaCl, but decreases sharply with increasing surface coverage. For lower surface coverage of less than 4 % it became evident that the error in determining B_{22} -values increased significantly. This behavior is connected to the

very weak or negligible interactions at a low surface coverage, which are unsatisfactory detectable. Differences in the retention volumes were too small, so that the influence of the experimental error increased significantly. Comparable deviations are described by Tessier et al. [3], who explained these deviations with non-specific interactions with the base matrix using low NaCl concentrations. This however might not be the case in the current data set as we detected positive B_{22} for low surface coverage with NaCl concentrations as high as 1 M. This finding rules out non-specific electrostatic interactions. The rather high positive values of the B_{22} for low surface coverage are due to the denominator term in equation (3.3) where the surface load comes into play. For low surface coverage and retention difference which is close to the detection error this leads to the observed picture. The lower retention volumes for low surface coverage θ and high NaCl concentrations when compared to the reference column with no immobilized protein could be mainly due to the inherent lower distribution coefficient $K_{overall}$ for retention behavior of a protein sample when pores are reduced in size due to immobilized or adsorbed protein [44]. At higher surface coverage ranging from ranging from 11.25 % to 22 % the B_{22} was found to be nearly independent of the surface coverage for all NaCl concentrations investigated. This range of surface coverage with a constant B_{22} -value corresponds to a surface load of 15 - 30 mg/mL.

Teske et al. [24] calculated a ‘high estimate’ of surface load q in the order of surface coverage $\theta \sim 14$ % for the lower limit when multi-body interaction should occur. Different values for the surface coverage found in literature range from 9 % [3], 14 - 17 % [24], 15 % [20] and 33 % [3]. In the work of Tessier et al. [3] the lower surface coverage of only 9 % was characterized by high non-specific electrostatic interactions at low ionic strength developing into negligible interactions at high ionic strength. Using the high surface coverage of 33 % repulsive interactions at low ionic strength and strongly attractive interactions at high ionic strength were found. The latter agrees with findings of this work where at higher surface coverage an increase in attractive interactions is found with increasing surface coverage. When comparing our findings with data computed by Teske et al. [24] a clear difference is detected. In our study, the surface coverage between 11.25 % and 22 % does not influence the B_{22} -value obtained for a given concentration of NaCl. In contrast to this Teske et al. [24] computed a direct influence of surface coverage on B_{22} with a higher surface coverage leading to lower B_{22} -values in the range from 8.5 % to 33 %. This difference might be explained that in our case we did reach a constant interaction scenario – be it two-body or multi-body interactions – while the computation of Teske et al. [24] simulates a change in surface properties influencing the retention behavior.

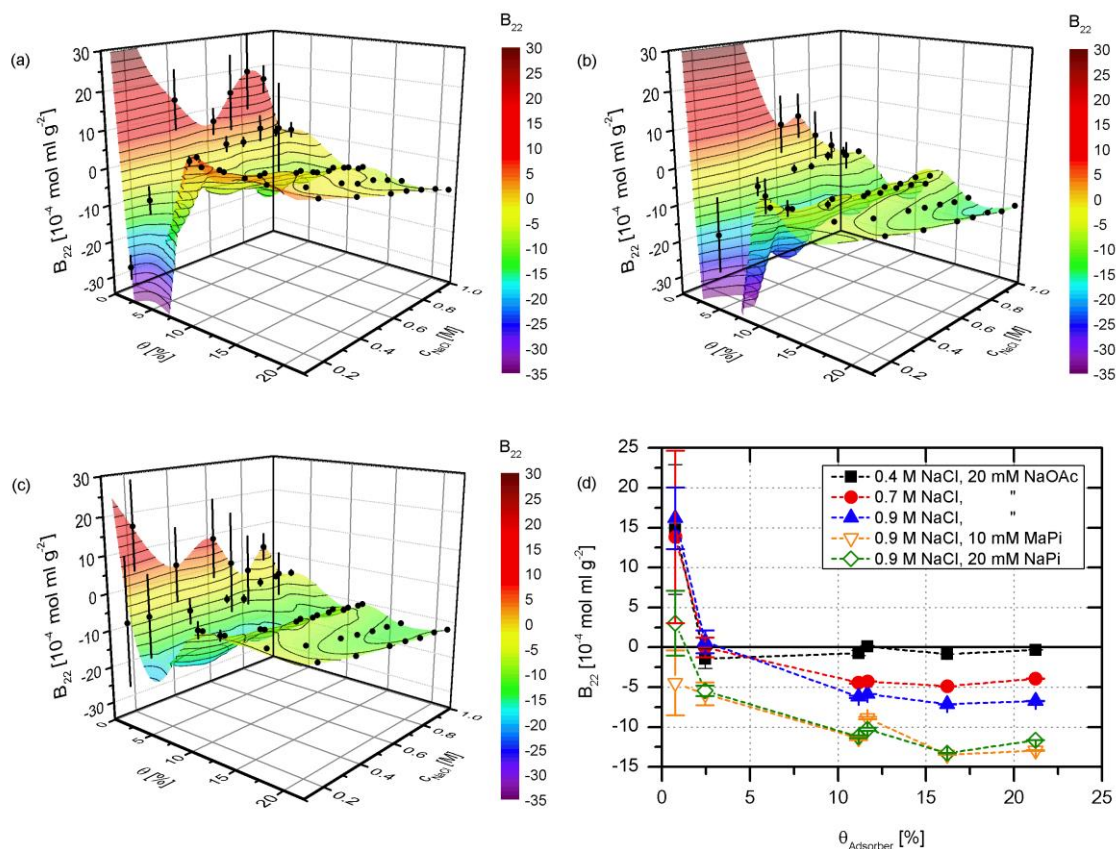


Figure 3.4: (a-c) B_{22} as a function of surface coverage and NaCl concentration in 20 mM NaOAc, 10 mM NaPi and 20 mM NaPi-buffer; (d) B_{22} for lysozyme over surface coverage of adsorber particles at 0.4, 0.7 and 0.9 M NaCl in 20 mM NaOAc-buffer pH 4.5 and 0.9 M NaCl in 10 and 20 mM NaPi-buffer pH 7.6

3.4.6 Influence of protein orientation on B_{22} -determination

According to the theoretical framework behind SIC protein-protein interactions between immobilized proteins and those in the mobile phase need to resemble those interactions found in free solution. This is only given when the structure of the immobilized species remains unchanged upon immobilization and a random orientation of the immobilized species to mimic the orientation independent interactions in free solution.

Several researchers have assumed such a random orientation throughout the development of SIC [12,13,20,24,45]. However this situation has never been experimentally proven to be valid. In contrast to this it was shown both experimentally and theoretically – based on molecular dynamic simulations – that binding of lysozyme on a cation exchanger is characterized by distinct orientations depending on the molecular structure of the protein [33]. Furthermore, the argumentation toward a random immobilization procedure mostly follows the reasoning that the lysine residues on the surface are more or less symmetrically distributed over the protein surface without recognizing the difference in reactivity of these potential binding sites.

In order to get an insight into the different reactivities of the potential binding sites – lysine residues – we analyzed the reactivity in coupling buffer of different pH-values when covalently attaching a Cy 5 dye [34] mimicking the reaction of protein with NHS-activated adsorber material. The reactivity of the six lysine residues was then studied by quantifying the mono-labeled isoforms in the final mixture after 30 min. Resulting isoforms were separated via ion-exchange chromatography and the absorption spectra at 280 nm and 650 nm were analyzed. The peaks can be assigned to variants of different labeled lysine residues [33]. Since the reaction of NHS esters with amines has an optimum pH of about 8.2 [32], the height of all isoform peaks decreased with decreasing pH and the non-labeled lysozyme peak increased. Therefore the relative peak areas of the mono-labeled lysozyme isoforms were compared with regard to relative reactivity of every single lysine residue in dependency to the pH. The relative isoform distribution of mono-labeled lysozyme is plotted as labeling efficiency for every of the six lysine residues in figure 3.5.

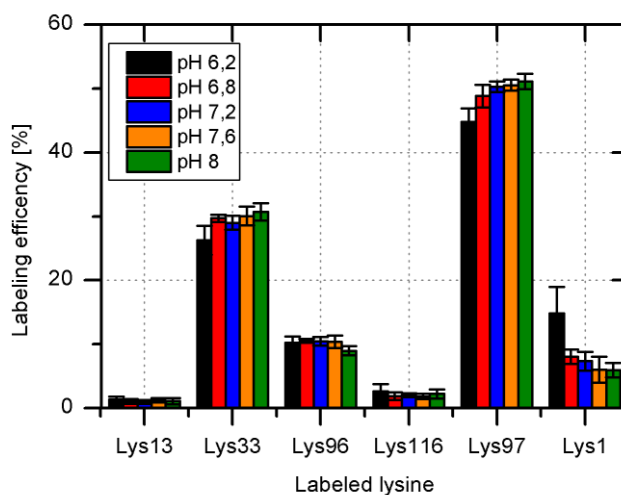


Figure 3.5: Relative isoform distribution of Cy 5 mono-labeled lysozyme at 280 nm and different pH

A clear picture arises from this study assuming that an approximately equal reactivity would be needed for a random distribution. The binding sites lys 96/lys 97 show the highest value with an approximate reactivity of 60 % over all lysines. The second place is taken by the binding site at lys 33 with a labeling efficiency of approximately 30 %. Together this accounts for the overall labeling efficiency of 90 %. It is thus foreseeable that – given that a correlation between binding orientation and site reactivity exists – the majority of immobilized protein is immobilized through either of these sites due to the different reactivity [46,47]. The ratio of these binding sites will be dependent on the reactivity described above and the orientation upon reaching the adsorbent surface prior to the immobilization reaction.

From figure 3.5 one might assume that the orientation of immobilized lysozyme remains largely constant over the investigated pH-range from pH 6 - pH 8. To elucidate this, the

five coupling conditions with different pH-values from 6.2 to 8 were compared in terms of B_{22} -values obtained by SIC using these columns. Besides the coupling pH, all other coupling buffer parameters were kept constant during the preparation of SIC-columns, as well as the surface load of around 20 mg/mL.

B_{22} -values obtained in the three different buffers (20 mM NaOAc, 10 mM NaPi and 20 mM NaPi) in dependency of the coupling pH are plotted in figure 3.6 (a-c) at different NaCl concentrations. Moreover, the dependency of B_{22} -values on coupling conditions is exemplary plotted for three NaCl concentrations in 20 mM NaPi-buffer pH 7.6. For these constant experimental conditions, but varying pH during the immobilization procedure the B_{22} obtained in 20 mM NaPi- buffer decreases with increasing coupling pH until a coupling pH 7.6 with a slight increase for the highest coupling pH 8. The maximal deviation of $8 \cdot 10^{-4} \text{ mol mL g}^{-2}$ in B_{22} -values for lysozyme among the three NaCl concentrations tested occurred between pH 6.2 and 7.6.

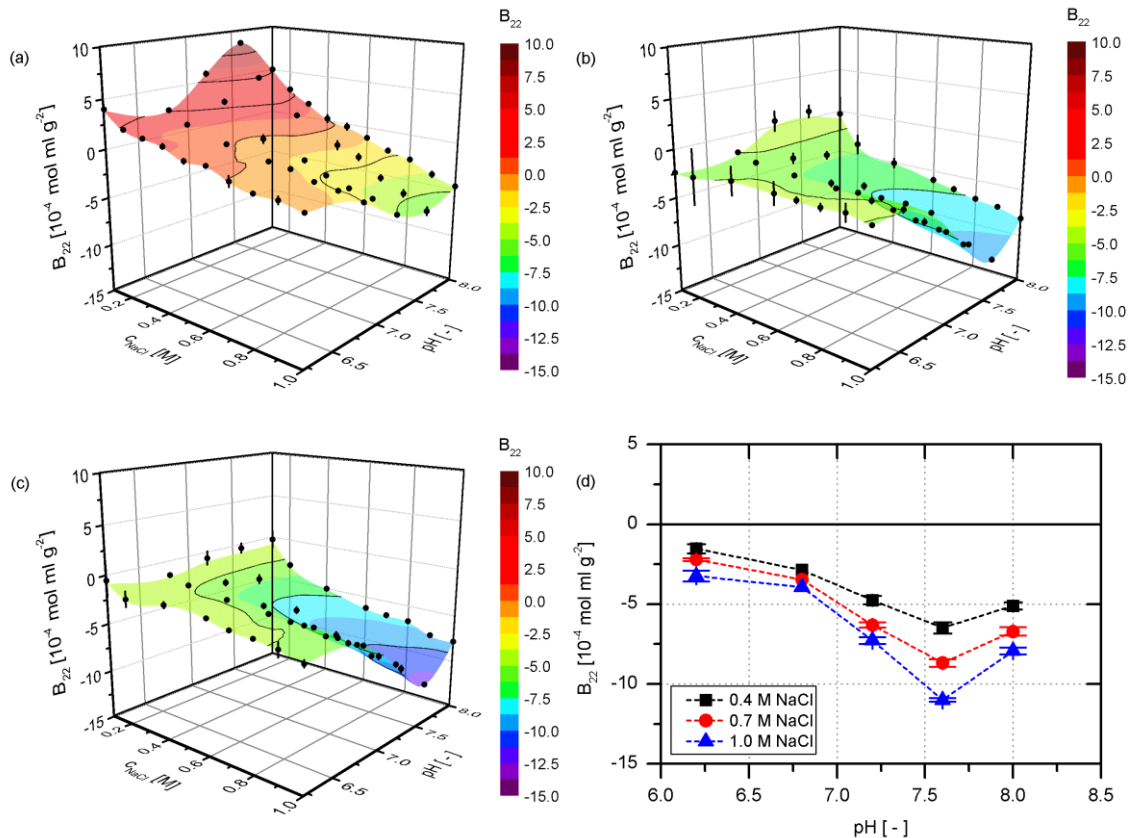


Figure 3.6: (a-c) B_{22} as function of NaCl concentration and immobilization pH during column preparation for 20 mM NaOAc, 10 M NaPi and 20 mM NaPi-buffer; (d) Influence of immobilization pH on B_{22} for different NaCl concentrations in 20 mM NaPi-buffer pH 7

This clearly confirms that the coupling conditions influence B_{22} -values obtained by SIC. These deviations could be a result of an irreversible structural alteration, a reversible structural transformation or a variation in the preferred binding site due to the different pH during coupling reaction. The change in coupling conditions should not influence the

stability of the protein. Thus, the treatment for protein during the immobilization reaction was conducted with a low salt concentration in a gentle pH-range between 6 and 8. The solubility of lysozyme is sufficient and the structure of the molecule should be only little affected by the coupling reaction. A comparison with figure 3.5 however does also not lead to a clear correlation. The process behind these findings is could not have been elucidated yet and is subject to further research.

3.4.7 B_{22} -determination comparing SIC and SLS

The above clearly indicates that comparing literature data on SIC obtained with different adsorber, coupling conditions, surface coverage and experimental conditions will not lead to a greater insight. Ahamed et al. [20] further presented a wealth of data comparing 14 B_{22} -curves over increasing NaCl concentration determined by six different experimental techniques. A rather strong scatter of data can be observed. We thus decided to make a direct comparison between SIC and SLS for our system.

The results of SIC data (surface load 20 mg/mL, coupling pH 7.6) were plotted in figure 3.7 with corresponding B_{22} -values obtained by SLS. The B_{22} -values for the two techniques are decreasing with increasing salt concentration. For all data, the B_{22} -values are positive in the range of 0.1 - 0.2 M NaCl. Higher salt concentrations up to 1 M led to negative and constantly decreasing B_{22} -values. The clear differences between the two approaches are found in the respective intersections with the x-axis between 0.2 M and 0.5 M and connected to this the overall more negative value for B_{22} in the attractive region for data obtained with SLS when compared to the SIC data.

At 0.7 M the absolute B_{22} -values determined by SIC and SLS differs by $-6 \cdot 10^{-4} \text{ mol mL g}^{-2}$. In NaPi-buffers (10 mM and 20 mM) comparable deviations between SIC and SLS were determined in an equal range (data not shown) [20]. Reasons for the differences between SIC and SLS can be the result of thermodynamic conventions of the methods [48], but these should have only a small effect on the B_{22} -values [49]. Ahamed et al. [20] specifies the inherent error limit with $-2 \cdot 10^{-4} \text{ mol mL g}^{-2}$ for SLS-measurements and $-1 \cdot 10^{-4} \text{ mol mL g}^{-2}$ for SIC-experiments. However, the SIC-results exceed this error depending on which immobilization conditions are used (see Section 4.6). This might be a result of the restricted orientation of potential protein-protein interactions in SIC. In contrast to the SIC, the SLS data of this work and from literature show an absolute mean deviation from the arithmetic average of $1.8 \cdot 10^{-4} \text{ mol mL g}^{-2}$ at the respective NaCl concentration. Since different buffer capacities, pH-values and lysozyme manufacturer were used, the variation of determined B_{22} -values between the literature data and those obtained in this work are in a reliable and reproducible range. Hence, non-invasive methods are preferred to determine B_{22} -values. When using SIC due to its low protein

consumption, one should be aware of deviations caused by a non-randomized immobilized adsorber particle surface. Other authors try to reduce the protein consumption by optimizing non-invasive measurement techniques. One example is an online method for SLS-measurements with a dual detection cell [50,51] to measure the B_{22} out of one peak.

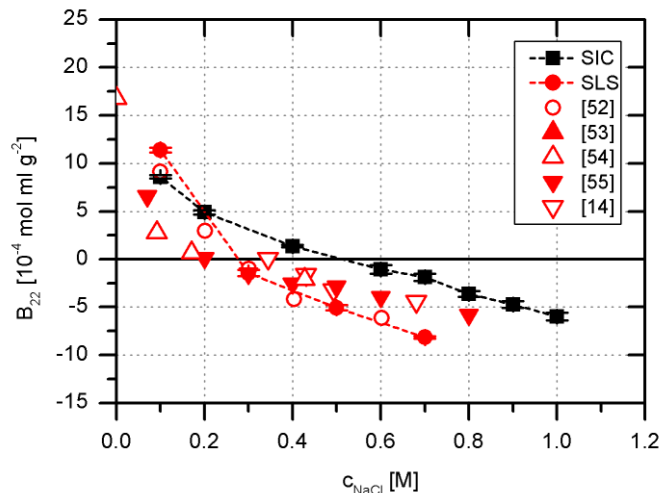


Figure 3.7: Mean B_{22} -values and the absolute standard deviation for lysozyme in 20 mM NaOAc-buffer pH 4.5 and varying NaCl concentration: SIC, SLS and SLS-literature data: 25 mM NaOAc pH 4.7 [52], NaOAc pH 4.5 [53], 50 mM NaOAc pH 4.7 [54], 50 mM NaOAc pH 4.6 [55], 100 mM NaOAc pH 4.2 [14]

3.5 Conclusions

The preparation of self-interaction chromatography-columns was simplified by immobilizing the protein directly in pre-packed and NHS-activated columns and optimized by surface load determination with the PLS regression-method. By doing so, a tool for SIC experimentation could be established expressing a high degree of experimental reproducibility and applicability. The novel method for determination of achieved immobilized protein density is novel and superior to existing techniques for protein determination.

A major prerequisite of applying SIC to measure a thermodynamically sound B_{22} -value lies in the random immobilization of protein onto the chromatographic column. The orientation of immobilized protein strongly depends on the pattern and reactivity of – mainly – lysine on the surface. It has clearly been shown that for lysozyme a preferential orientation of immobilized protein is obtained as a function of immobilization conditions. This finding will probably apply for the majority of proteins.

Thus, the prerequisite of a randomized binding orientation on the adsorber is not valid and the knowledge of the structural arrangement must be taken into account while working along the SIC methodology. In conclusion the use of SIC to determine thermodynamically

accurate B_{22} -values or even simple protein-protein interactions comparable to studies in free solution is highly questionable. In some cases SIC might still be useful to elucidate qualitative trends, but quantitative data need to be validated by other techniques.

3.6 References

- [1] D.H. Johnson, A. Parupudi, W.W. Wilson, L.J. DeLucas, *Pharm. Res.* 26 (2009) 296–305.
- [2] U. Odenthal, S. Haehn, P. Tunggal, B. Merkl, D. Schomburg, C. Frie, M. Paulsson, N. Smyth, *J. Biol. Chem.* 279 (2004) 44504–44512.
- [3] P.M. Tessier, A.M. Lenhoff, S.I. Sandler, *Biophys. J.* 82 (2002) 1620–1631.
- [4] A. George, W.W. Wilson, *Acta Crystallogr. Sect. D: Biol. Crystallogr.* 50 (1994) 361–365.
- [5] P.E. Pjura, A.M. Lenhoff, S.A. Leonard, A.G. Gittis, *J. Mol. Biol.* 300 (2000) 235–239.
- [6] M. Gabrielsen, L.A. Nagy, L.J. DeLucas, R.J. Cogdell, *Acta Crystallogr. Sect. D: Biol. Crystallogr.* 66 (2010) 44–50.
- [7] V. Le Brun, W. Friess, S. Bassarab, S. Mühlau, P. Garidel, *Eur. J. Pharm. Biopharm.* 75 (2010) 16–25.
- [8] S. Ruppert, S.I. Sandler, A.M. Lenhoff, *Biotechnol. Progr.* 17 (2001) 182–187.
- [9] C. Haas, J. Drenth, W.W. Wilson, *J. Phys. Chem. B.* 103 (1999) 2808–2811.
- [10] C.A. Haynes, K. Tamura, H.R. Korfer, H.W. Blanch, J.M. Prausnitz, *J. Phys. Chem.* 96 (1992) 905–912.
- [11] J. Behlke, O. Ristau, *Biophys. Chem.* 76 (1999) 13–23.
- [12] S.Y. Patro, T.M. Przybycien, *Biotechnol. Bioeng.* 52 (1996) 193–203.
- [13] P.M. Tessier, S.D. Vandrey, B.W. Berger, R. Pazhianur, S.I. Sandler, A.M. Lenhoff, *Acta Crystallogr. Sect. D: Biol. Crystallogr.* 58 (2002) 1531–1535.
- [14] B. Guo, *J. Cryst. Growth.* 196 (1999) 424–433.
- [15] O.D. Velev, Y.H. Pan, E.W. Kaler, A.M. Lenhoff, *Cryst. Growth Des.* 5 (2005) 351–359.
- [16] W.W. Wilson, *J. Struct. Biol.* 142 (2003) 56–65.

- [17] T. Ahamed, B.N.A. Esteban, M. Ottens, G. Van Dedem, L. Van der Wielen, M.A.T. Bisschops, A. Lee, C. Pham, J. Thömmes, *Biophys. J.* 93 (2007) 610–619.
- [18] R.A. Lewus, P.A. Darcy, A.M. Lenhoff, S.I. Sandler, *Biotechnol. Progr.* 27 (2011) 280–289.
- [19] A.C. Dumetz, A.M. Snellinger-O'Brien, E.W. Kaler, A.M. Lenhoff, *Protein Sci.* 16 (2007) 1867–1877.
- [20] T. Ahamed, M. Ottens, G. Van Dedem, L. Van der Wielen, *J. Chromatogr. A* 1089 (2005) 111–124.
- [21] C.D. García, D.G.J. Hadley, W.W. Wilson, C.S. Henry, *Biotechnol. Progr.* 19 (2003) 1006–1010.
- [22] K. Deshpande, T. Ahamed, L. Van der Wielen, J.H.T. Horst, P.J. Jansens, M. Ottens, *Lab Chip.* 9 (2009) 600–605.
- [23] Z. Grabarek, J. Gergely, *Anal. Biochem.* 185(1990) 131–135.
- [24] C.A. Teske, H.W. Blanch, J.M. Prausnitz, *J. Phys. Chem. B.* 108 (2004) 7437–7444.
- [25] S.K. Hansen, E. Skibsted, A. Staby, J. Hubbuch, *Biotechnol. Bioeng.* 108 (2011) 2661–2669.
- [26] C.J. van Oss, *Colloids Surf. B: Biointerfaces* 5 (1995) 91–110.
- [27] D. Leckband, J. Israelachvili, *Q. Rev. Biophys.* 34 (2001) 105.
- [28] B.L. Neal, A.M. Lenhoff, *AIChE J.* 41 (1995) 1010–1014.
- [29] Y. Moon, *Fluid Phase Equilib.* 168 (2000) 229–239.
- [30] B.H. Zimm, *J. Chem. Phys.* 14(1946) 164.
- [31] Y. Mine, *Trends Food Sci. Technol.* 6 (1995) 225–232.
- [32] M. Brinkley, *Bioconjugate Chem.* 3 (1992) 2–13.
- [33] F. Dismer, J. Hubbuch, *J. Chromatogr. A* 1149 (2007) 312–320.
- [34] J. Hubbuch, M.R. Kula, *Bioprocess Biosyst. Eng.* 31 (2008) 241–259.
- [35] M. Schröder, E. von Lieres, J. Hubbuch, *J. Phys. Chem. B.* 110 (2006) 1429–1436.
- [36] C.A. Teske, R. Simon, A. Niebisch, J. Hubbuch, *Biotechnol. Bioeng.* 98 (2007) 193–200.
- [37] B.H. Zimm, *J. Chem. Phys.* 16 (1948) 1093.
- [38] V. Ball, J.J. Ramsden, *Biopolymers.* 46 (1998) 489–492.

- [39] J.A. De Feijter, J. Benjamins, F.A. Veer, *Biopolymers*. 17 (1978) 1759–1772.
- [40] A.S. Parmar, M. Muschol, *Biophys. J.* 97 (2009) 590–598.
- [41] D.F. Rosenbaum, C.F. Zukoski, *J. Cryst. Growth*. 169 (1996) 752–758.
- [42] A.C. Dumetz, A.M. Chockla, E.W. Kaler, A.M. Lenhoff, *Biochim. Biophys. Acta* 1784 (2008) 600–610.
- [43] B.W. Berger, C.M. Gendron, C.R. Robinson, E.W. Kaler, A.M. Lenhoff, *Acta Crystallogr. Sect. D: Biol. Crystallogr.* 61 (2005) 724–730.
- [44] J. Hubbuch, T. Linden, E. Knieps, J. Thömmes, M.R. Kula, *J. Chromatogr. A* 1021 (2003) 105–115.
- [45] V. Le Brun, W. Friess, T. Schultz-Fademrecht, S. Muehlau, P. Garidel, *Biotechnol. J.* 4 (2009) 1305–1319.
- [46] K. Wadu-Mesthrige, N.A. Amro, G.-Y. Liu, *Scanning* 22 (2006) 380–388.
- [47] P.M. Tessier, S.I. Sandler, *Protein Sci.* 13 (2004) 1379–1390.
- [48] H. Cabezas, J.P. O’Connell, *Ind. Eng. Chem. Res.* 32 (1993) 2892–2904.
- [49] C.J. Coen, H.W. Blanch, J.M. Prausnitz, *AIChE J.* 41 (1995) 996–1004.
- [50] H. Bajaj, V.K. Sharma, D.S. Kalonia, *Pharm. Res.* 24 (2007) 2071–2083.
- [51] H. Bajaj, V.K. Sharma, D.S. Kalonia, *Biophys. J.* 87 (2004) 4048–4055.
- [52] R. Piazza, M. Pierno, *J. Phys. Condens Matter*. 12 (2000) A443–A449.
- [53] R.A. Curtis, J. Ulrich, A. Montaser, J.M. Prausnitz, H.W. Blanch, *Biotechnol. Bioeng.* 79 (2002) 367–380.
- [54] M. Muschol, F. Rosenberger, *J. Chem. Phys.* 103 (1995) 10424.
- [55] D.F. Rosenbaum, A.M. Kulkarni, S. Ramakrishnan, C.F. Zukoski, *J. Chem. Phys.* 111(1999) 9882.

4 Moving Through Three-dimensional Phase Diagrams of Monoclonal Antibodies

Natalie Rakel, Miriam Baum, Juergen Hubbuch

Section IV: Biomolecular Separation Engineering, Institute of Engineering in Life Sciences, Karlsruhe Institute of Technology, Engler-Bunte-Ring 1, 76131 Karlsruhe, Germany

Published in Biotechnology Progress, 2014, 30(5), 1103-13

Corresponding author:

Juergen Hubbuch,
Karlsruhe Institute of Technology
Institute of Engineering in Life Sciences
Section IV: Biomolecular Separation Engineering
Engler-Bunte-Ring 1, 76131 Karlsruhe, Germany
Phone: +49-721-608-42557, fax: +49-721-608-46240,
E-mail: juergen.hubbuch@kit.edu

Keywords: Protein phase behavior; phase diagram; monoclonal antibody; crystallization; high throughput screening

Abstract

Protein phase behavior characterization is a multivariate problem due to the high amount of influencing parameters and the diversity of the proteins. Single influences on the protein are not understood and fundamental knowledge remains to be obtained. For this purpose, a systematic screening method was developed to characterize the influence of fluid phase conditions on the phase behavior of proteins in three-dimensional phase diagrams. This approach was applied to three monoclonal antibodies to investigate influences of pH, protein and salt concentrations, with five different salts being tested. Although differences exist between the antibodies, this extensive study confirmed the general applicability of the Hofmeister series over the broad parameter range analyzed. The influence of the different salts on the aggregation (crystallization and precipitation) probability was described qualitatively using this Hofmeister series, with a differentiation between crystallization and precipitation being impossible, however.

4.1 Introduction

One of the fastest growing and most important product classes in biological pharmaceuticals and therapeutics is the group of monoclonal antibodies (mAb). They are applied mainly for cancer and autoimmune therapy, such as for the treatment of leukemia or rheumatism. While substantial progress was made in designing specific antibodies, the challenging recovery and purification processes still are the most cost-intensive tasks. This is mainly due to the application of a Protein A-step [1,2]. The FDA product quality standards are high, because thousands of patients need a weekly sterile dose of a few grams for intravenous administration over long terms [3]. Even though current platform processes are highly optimized in terms of yield and achieved purity, they lack performance when it comes to processing high titers and when long-term stability of the molecule becomes a critical issue. In this context crystallization of antibodies is a promising strategy to generate highly concentrated and stable products [2,4–6].

Crystallization is a selective step in the protein purification process and combines purification and simplification of the formulation in a single step only. Its advantages are a high purity and concentration as well as increased stability in the crystalline form. On the industrial scale, crystallization is applied for few proteins, like insulin only [6]. One reason is the time-consuming and cost-intensive screening of protein crystallization conditions. Moreover, screening success is not guaranteed, since the protein phase behavior in the solution is influenced by many chemical and physical parameters, such as the salt content, buffer capacity, pH value, type of precipitant, and temperature [7,8]. Antibody crystallization is even more challenging due to their large size and high degree of segmental flexibility as well as the extensive and potentially variable glycosylation pattern [2]. Hence, only few complete intact antibodies have been crystallized so far [9,10]. Most crystals were obtained from antibody fragments. In some cases, deletion of regions of the antibody has been inevitable for a successful crystallization [11,12].

One approach to enhancing the understanding of protein crystallization and facilitating condition screening consists in the generation of phase diagrams. Derived systematic correlations can foster future screenings. The knowledge can be transferred to different process steps, such as purification, formulation, storage, and delivery [10]. Moreover, crystallization conditions can be used to generate crystals for 3D structure determination, the ultimate objective being to increase biological understanding of the protein structure, their reaction mechanisms as well as their function [11,13]. Even diseases caused by a phase transition of proteins, like cataracts [14] or neurodegenerative diseases [15] can be better understood. Furthermore, the transferability to proteins of comparable properties can be investigated [10,16]. Despite these opportunities, crystallization condition screenings

are conducted mainly with commercially available kits in trial-and-error-experiments. This does not provide for any further understanding [7]. Automatic platforms are needed for use as screening tools in systematic investigations of the influence of the fluid phase conditions, salts, and excipients.

In the course of the project reported here we established such a screening tool for the systematic evaluation of mAb phase behavior. This tool consists of fully automated robotic stations. The influence of different salts, pH values as well as protein and salt concentrations were analyzed. To create a comprehensive database, three-dimensional (3D) phase diagrams were generated for three different antibodies and the respective salt as a function of their concentrations and the pH. A newly established buffer system was introduced to eliminate possible influences due to changing buffer components [17]. This system ensures a constant buffer capacity over a pH range of four orders of magnitude (5 - 9) and allows for a systematic evaluation of parameters like the pH value and salt concentrations. The antibody phase behavior depending on those parameters was then analyzed optically and apparent crystallization, precipitation, liquid-liquid phase separation, and gelation were distinguished. In addition, the time until the first visible structures were obtained and the crystal size after 40 days were determined for all three mAbs.

4.2 Materials and Methods

4.2.1 Materials

Protein A-purified monoclonal antibodies mAb04c (type IgG4, pI 8.3-8.8), mAb02a (type IgG1, pI 8.3-8.9), and mAb05a (type IgG1, pI 8.2-8.5) in solution were kindly provided by Boehringer Ingelheim Pharma GmbH & Co. KG (Biberach, Germany). Prior to the experiments, a buffer exchange was performed in a Vivaspin 20, Vivaspin 2 or Vivaspin 500 (30 kDa Cutoff PES-membrane; VS2022, VS0222 and VS0122; Sartorius Stedim Biotech, Göttingen, Germany) at 8,000 g and 20°C. The protein concentration was adjusted to the desired value.

The chemicals of acetic acid, sodium chloride (NaCl), sodium hydroxide (NaOH), MES, lithium sulfate (Li_2SO_4), and ammonium chloride (NH_4Cl) were obtained from Merck KGaA (Darmstadt, Germany), whereas MOPSO, CHES, and ammonium sulfate ($(\text{NH}_4)_2\text{SO}_4$) were obtained from Applichem GmbH (Darmstadt, Germany). HEPPSO was supplied by molekula Germany (Taufkirchen, Germany) and sodium sulfate (Na_2SO_4) by Sigma-Aldrich (St. Louis, MO, USA).

All buffers and protein samples were freshly prepared and filtered with a 0.2 μm cellulose membrane to prevent contaminations and dust particles in the respective solutions.

4.2.2 Buffer system preparation and pH characterization

The buffer system established is comparable to buffers used in pH-gradient-based ion-exchange chromatography [18]. This multi-component buffer with its monoprotic acid components listed in table 4.1 is characterized by a constant buffer capacity over a pH range from 5 to 9. The overall titration curve is the summation of the overlapping titration curves of every single component having a different pKa value [19]. The buffer capacity is constant over the pH range described, since the resulting titration curve is almost linear. Thus, the pH can be adjusted by varying the buffer ratios of pH 5 and 9 buffer.

A two-fold concentrated buffer system was produced and split into two equal aliquots after dissolution [20]. Each aliquot was diluted with deionized water and titrated with 4 M NaOH to pH 5 or 9, resulting in a buffer capacity of 10 mM for each buffer. These buffers served as salt-free buffers (see table 4.1).

Table 4.1: *pH Buffer System Composition (10 mM) with the Corresponding pKa value [21] and Molarity*

| Buffer component | pKa-value [-] | Molarity [mM] |
|------------------|-----------------|---------------|
| MES | 6.10 | 10.05 |
| Acetic acid | 4.76 | 16.6 |
| MOPSO | 6.90 | 8.9 |
| HEPPSO | 8.04 | 12.3 |
| CHES | 9.30 | 14.4 |

As precipitants, the salts of ammonium sulfate (3 M), lithium sulfate (2.5 M), sodium sulfate (1 M), ammonium chloride (3 M), and sodium chloride (3 M) were used. If not stated otherwise, the maximal concentration listed in the brackets was utilized for the salt buffer. The precipitant had been added to the buffer system before the pH value (HI-3220, HANNA instruments US, Woonsocket, RI, USA) and volume were adjusted.

Table 4.2: Screening Experiment Number, including Precipitation Buffer Composition Expressed by the Salt Ratio and pH Ratio

| No | Precipitant | r_{Salt} [-] | r_{pH} [-] |
|----|---|--|-----------------------|
| 1 | (NH ₄) ₂ SO ₄ , Na ₂ SO ₄ , NH ₄ Cl, NaCl | 0.25, 0.5, 0.75, 1 | 0, 0.25, 0.5, 0.75, 1 |
| | Li ₂ SO ₄ | | 0, 0.25, 0.5, 0.75 |
| | (NH ₄) ₂ SO ₄ | 0.33, 0.42, 0.58, 0.67, 0.75, 0.83 | |
| 2 | Li ₂ SO ₄ | 0.3, 0.4, 0.5, 0.6, 0.7, 0.8 | 0.25, 0.5, 0.75, 1 |
| | Na ₂ SO ₄ | 0.05, 0.1, 0.2, 0.3, 0.8, 0.9 | |
| | NaCl | 0.03, 0.1, 0.17, 0.23, 0.67, 0.83 | |
| | (NH ₄) ₂ SO ₄ | 0.033, 0.066, 0.1, 0.133, 0.267, 0.2, 0.233, 0.267, 0.3, 0.33, 0.367, 0.4 | |
| 3 | Li ₂ SO ₄ | 0.08, 0.16, 0.24, 0.32, 0.4, 0.48, 0.56, 0.64, 0.72, 0.8, 0.88, 0.96 | 0.75 |
| | Na ₂ SO ₄ | 0.3, 0.4, 0.5, 0.6, 0.7, 0.8 | 0.25, 0.5, 0.75, 1 |
| | NH ₄ Cl (max. 5 M) | 0.1, 0.6, 0.7, 0.8, 0.9, 1 | |
| | NaCl (max. 5 M) | 0.05, 0.2, 0.6, 0.7, 0.9, 1 | |

The precipitation buffer was prepared on a robotic platform (Freedom EVO100, Tecan Group., Männedorf, Switzerland) in the 2 mL scale with 96-deep well plates (Nalgene Nunc, Rochester, NY, USA, product no. 260252). The respective salt buffer with its maximal salt concentration $c_{Salt,max}$ at pH 5 and 9 was diluted with the buffer system at pH 5 and 9 (salt-free buffer) to obtain c_{Salt} . The used salt ratio r_{Salt} was then defined by:

$$r_{Salt} = \frac{c_{Salt}}{c_{Salt,max}} \quad (4.1)$$

Moreover, the pH was adjusted by varying the ratio of pH 5 to 9 buffer.

$$r_{pH} = \frac{V_{pH\ 9}}{V_{pH\ 5} + V_{pH\ 9}} \quad (4.2)$$

Each r_{Salt} in table 4.2 was combined with all r_{pH} -values, adding up to 288 precipitation buffer conditions. However, different salt concentrations can shift the pH after mixing and influence the buffer. Consequently, the pH was determined for every single precipitation buffer composition at room temperature (HI-110 with HI-1330B electrode, HANNA instruments US, Woonsocket, RI, USA). In addition, pH or salt gradient measurements were conducted for all five salts using an FPLC-System ÄKTA™purifier equipped with a pH and conductivity meter (GE Healthcare, Uppsala, Sweden, software Unicorn 5.2) in which either the salt concentration was kept constant at zero or the maximal salt

concentration or the r_{pH} was maintained at 0 or 1. The pH and the conductivity were measured online under a flow rate of 0.1 mL/min and a gradient length of 10 mL.

The resulting surface plots of the pH measured as a function of the ratio and the salt concentration for sodium chloride as well as ammonium chloride are shown in figure 4.1. Sodium chloride only shows a small deviation from the linearity, whereas ammonium chloride leads to apparently higher pH values. This offset results from a $(\text{NH}_4)^+$ pKa value of 9.21 [22], with the effect on the measured pH being more pronounced at higher salt concentrations. This behavior was comparable in all buffers containing $(\text{NH}_4)^+$.

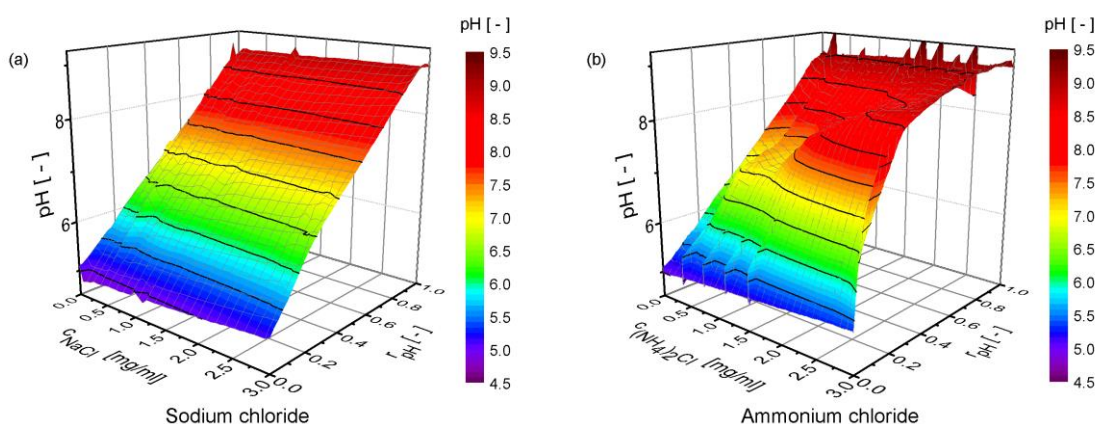


Figure 4.1: Influence of sodium (a) and ammonium chloride (b) on pH adjustment for the buffer-system

4.2.3 Screening buffer preparation

To determine the 3D phase diagrams of the three antibodies, the different precipitation buffers of table 4.2 were used in combination with the three antibodies and protein concentrations listed in table 4.3. The conditions were divided into three screening experiments. Every mentioned protein concentration c_P was mixed with all precipitation conditions of the same screening experiment number. All three antibodies were used for the screening experiments 1 and 2, while screening experiment 3 was conducted with mAb04c only. The first experiment was a screening over the whole pH and salt concentration range. In the second screening experiment the focus was placed on conditions under which phase transition occurred. In the third screening experiment, mAb04c was further analyzed in terms of crystallization at $r_{pH} = 0.75$ and $r_{pH} = 1$ for lithium sulfate and ammonium sulfate, respectively, as well as over a broader salt and protein concentration range for ammonium and sodium chloride. These combinations resulted in a total of 2,784 different screening conditions.

The original buffer of the antibody was replaced by the described buffer systems with pH 5 and 9. Sample formulation for different screening buffer compositions took place on a

robotic platform (Freedom EVO100, Tecan Group, Männedorf, Switzerland). The antibody was diluted and mixed with the buffer system (pH 5 and 9) on the 100 μL scale (1.5 mL Safe-Lock tubes™, Eppendorf AG, Hamburg, Germany, product no. 0030 120.086) to obtain the starting buffer with different pH ratios r_{pH} and protein concentrations c_P (see table 4.3). Nearly 10 μL of the starting buffer were pipetted into microbatch plates (MRC Under Oil 96 Well Crystallization Plate, Swissci AG, Neuheim, Switzerland) and 10 μL precipitation buffer (see table 4.2) were added. The plates were sealed with Crystal Clear Sealing Tape (Hampton Research, Aliso Viejo, CA, USA, product no. HR4-506) to completely prevent evaporation during the experiments. The alternative method with an oil drop on the surface was dismissed, as the oil/buffer interface influences the phase behavior due to heterogeneous nucleation at the boundary surface, as was mentioned by D’Arcy et al. [23]. The complete preparation of a plate takes about 10 min.

Table 4.3: Screening Experiment Number, Including the Used Protein, Salts, and Protein Concentrations of Starting Buffers

| No | Protein | Salt | c_P [mg/mL] |
|----|------------------------|--|------------------------------|
| 1 | mAb04c, mAb05a, mAb02a | Na_2SO_4 , $(\text{NH}_4)_2\text{SO}_4$, Li_2SO_4 , NH_4Cl , NaCl | 2.5, 5, 7.5, 10 |
| 2 | mAb04c, mAb05a, mAb02a | $(\text{NH}_4)_2\text{SO}_4$, NaCl , Na_2SO_4 , Li_2SO_4 | 6, 9, 15, 20 |
| 3 | mAb04c | $(\text{NH}_4)_2\text{SO}_4$ | 4, 6, 8, 10, 12, 15, 18, 20 |
| | | Li_2SO_4 | 4, 7, 10, 12, 14, 16, 18, 20 |
| | | Na_2SO_4 | 5, 10, 15, 20 |
| | | NH_4Cl , NaCl | 15, 20, 25, 30 |

With a minimum of six salt-free starting and precipitation buffers at two pH-values (5 and 9) (table 4.4), a complete 3D phase diagram was obtained for one salt and protein under varying screening conditions. On this basis, the phase behavior could be analyzed over a broad range of known pH values and compositions. For every additional salt, only two more buffers (salt buffer: pH 5 and 9) were necessary.

Table 4.4: Nomenclature of the Different Buffers

| Buffer name | Description |
|----------------------|---|
| Salt-free buffer | Buffer system without added salt |
| Salt buffer | Buffer system with maximal added salt concentration |
| Precipitation buffer | Buffer system with one added salt |
| Starting buffer | Buffer system with added protein |
| Screening buffer | Buffer system with added protein and salt |

4.2.4 Antibody phase behavior analysis

Nonagitated, diffusion-driven systems represent an intermediate screening step on the way towards stirred batch crystallization. For this reason, the protein phase behavior was analyzed in microbatch plates for a period of 40 days in distinct time intervals (day 1: 2 h, days 2-4: 4 h, days 4-8: 6 h, days 9-40: 24 h). The imaging system Rock Imager 54 (Formulatrix, Waltham, MA, USA, Software Rock Maker) was used to take XY images. The images recorded at different time intervals revealed a delayed formation of first visible structures or transformations. This delay then served as a parameter for kinetic analysis. The polarizability and fluorescence intensity after excitation in the UV range are measures of the birefringence and protein concentration gradients in the solution. The samples were analyzed after 40 days to specify the quality of the aggregates and to find out whether the crystal was built from protein. According to Bergfors [24] the phase behavior can be classified as follows:

1. Clear,
2. light precipitate,
3. heavy precipitate,
4. liquid-liquid phase separation,
5. gelation,
6. microcrystals smaller than 20 μm ,
7. crystals (needles).

Structures, smaller than the microscopic resolution limit of 3 μm , were classified as precipitate. Liquid-liquid phase separation in the form of droplets in solution was not observed in any of the analyzed samples after 40 days. In this context, aggregation is used as the hypernym of crystallization and precipitation. As an approximation of the crystal size (l), an average of the longest side of 5-10 distinct crystals was determined visually and manually during crystallization. Use of an automated imaging system facilitated the handling of the high amount of images.

4.3 Results

4.3.1 Influence of sulfate salts on mAb04c phase behavior: Ammonium, lithium, and sodium sulfate

Because the five salts are composed of three different cations and two anions, the phase behavior was first analyzed as a function of the anion and second as a function of the cation for all three antibodies. The resulting phase diagrams for mAb04c with the ammonium, lithium, and sodium sulfate are plotted in figure 4.2. The phase behavior of

mAb04c is divided into three different states: Dissolved, crystallized or precipitated. No gelation occurs.

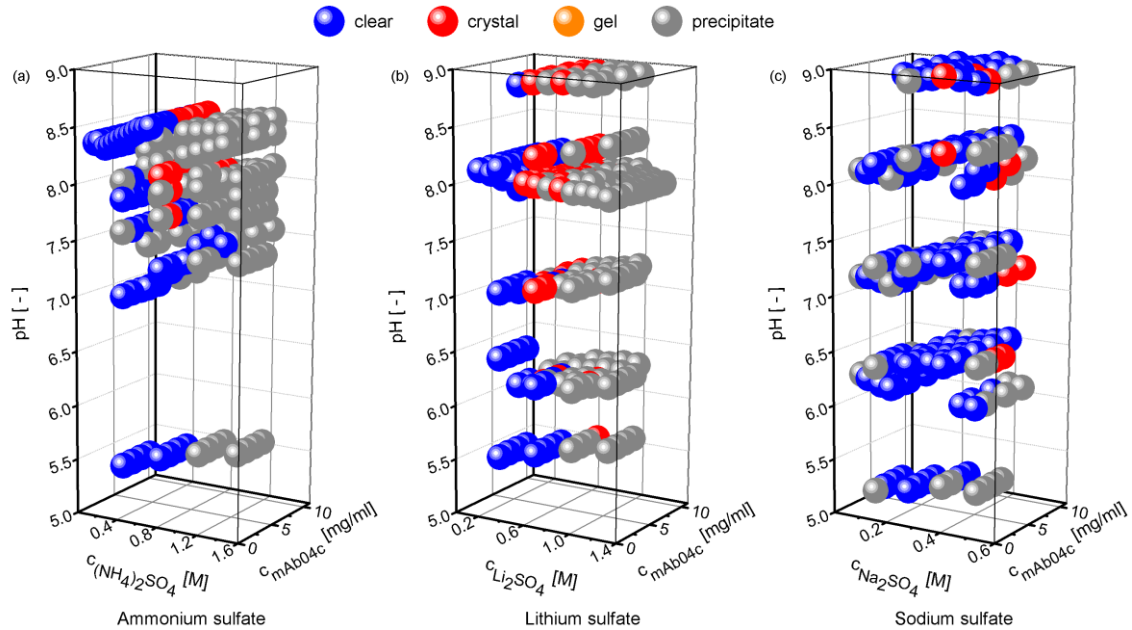


Figure 4.2: Phase diagrams of mAb04c with ammonium (a), lithium (b), and sodium sulfate (c) as a function of the pH

As shown in figure 4.2 (a), no crystallization occurs in the tested protein concentration range for mAb04c and pH values below 7.5 for ammonium sulfate. With increasing pH value, the crystallization probability is increasing and the protein and salt concentration range in which mAb04c crystallizes is broader. At $\text{pH } 8 \pm 0.2$, some crystal needles form at low protein (1-3.75 mg/mL) and salt concentrations of 0.75 M. Around the pI of mAb04c at $\text{pH } 8.5 \pm 0.2$, the probability of crystallization increases. For salt concentrations in the range of 0.5 - 0.75 M and protein concentrations from 5 - 10 mg/mL, samples show needle crystallization. Precipitation is dependent on the ammonium sulfate concentration at the respective pH.

When applying lithium sulfate (figure 4.2 b), crystallization occurs at various salt concentrations, especially above pH 7. At pH 8, the phase behavior is slightly dependent on the protein concentration, but strongly influenced by the salt concentration in the analyzed range. The solution stays clear for salt concentrations below 0.3 M. With lithium sulfate concentrations between 0.4 and 0.7 M, mAb04c crystallizes. Above this salt concentration, the precipitation range starts. At a constant protein concentration of 10 mg/mL or salt concentration of 0.4 M, crystals are obtained over a broad pH range (7 - 9).

The combination of mAb04c and sodium sulfate presented in figure 4.2 (c) results mainly in light precipitation. Crystallization occurs under few conditions. At salt concentrations of 0.4 - 0.5 M and protein concentrations higher than 4 mg/mL, crystals grow in the pH range

of 6.5 - 9. At 0.5 M sodium sulfate, all analyzed samples show aggregation (precipitation or crystallization). In addition, light precipitation is visible at low salt concentrations. Compared to salt concentrations below 0.1 M, precipitation starts at higher protein concentrations in the salt concentration range between 0.1 and 0.4 M. Hence, an increasing sodium sulfate concentration leads to a salting-in behavior.

4.3.2 Influence of sulfate salts on mAb05a and mAb02a phase behavior: Ammonium, lithium, and sodium sulfate

The mAb05c antibody showed no crystallization in the analyzed pH and concentration ranges for the three different sulfate salts. However, gelation was observed under various conditions at the transition line from a clear solution to precipitation. The phase diagrams for ammonium, lithium, and sodium sulfate are plotted in figure 4.3.

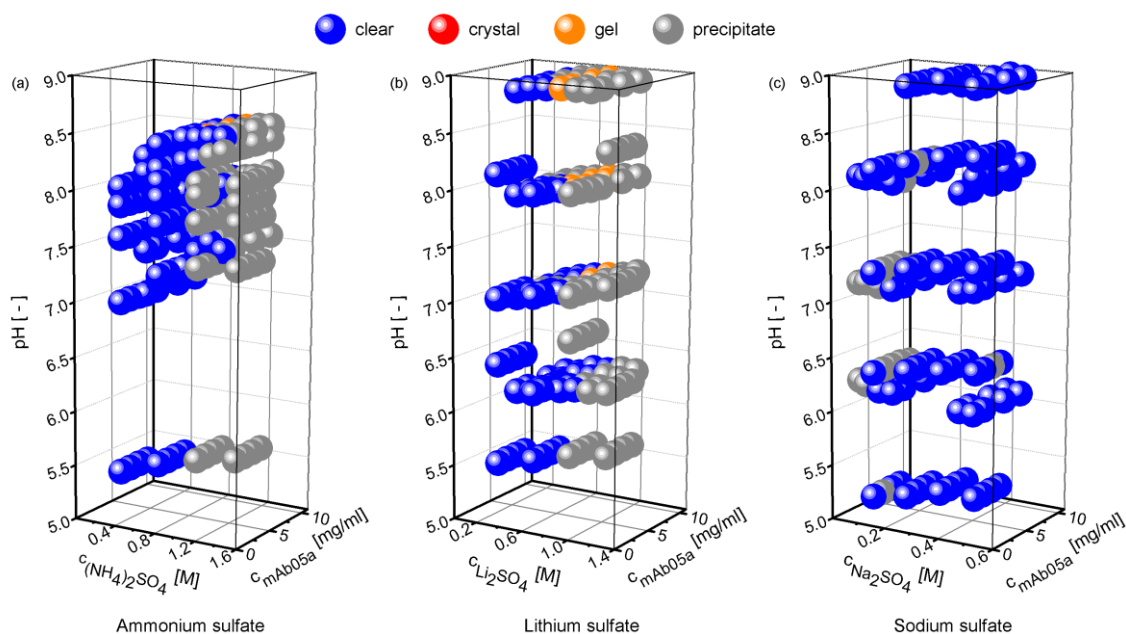


Figure 4.3: Phase diagrams of mAb05a with ammonium (a), lithium (b), and sodium sulfate (c) as a function of the pH

For mAb05a in the presence of ammonium sulfate, phase transition occurred at salt concentrations of 0.8 M. The protein gelled at a pH of 8.5 ± 0.2 near the pI of the antibody and at 0.875 - 1.1 M ammonium sulfate only. In figure 4.3 (b) the phase diagram for mAb05a in combination with lithium sulfate is plotted. The protein precipitates above 0.6 M and gels in the salt and protein concentration range of 0.75 - 0.875 M with 3-10 mg/mL protein at a pH from 7 to 9. The gelation as well as the precipitation is dependent on the pH and protein concentration. As shown in figure 4.3 (c), sodium sulfate induces a salting-in behavior of mAb05a at low sodium sulfate concentrations below 0.3 M in the pH range of 5 - 8. The higher the pH is, the higher is the salt concentration required for precipitation. Generally, ammonium sulfate tends to gel in a smaller pH range,

compared to lithium sulfate. The ranges are comparable to that of mAb04c crystallization. The salting-in behavior of mAb04c with sodium sulfate in the solution is also detected for mAb05a.

mAb02a shows less phase transitions for the three sulfate salts than mAb05a and mAb04c, (figure 4.4). mAb02a precipitates above ammonium sulfate concentrations of 1.2 M and above 1 M lithium sulfate concentration. Gelation occurs at an ammonium sulfate concentration of 1.25 M and pH 8.5 as well as at lithium sulfate concentrations of 1.25 M in the pH range of 7 to 9. In the presence of sodium sulfate, the salting-in behavior is comparable to that of mAb05a and mAb04c.

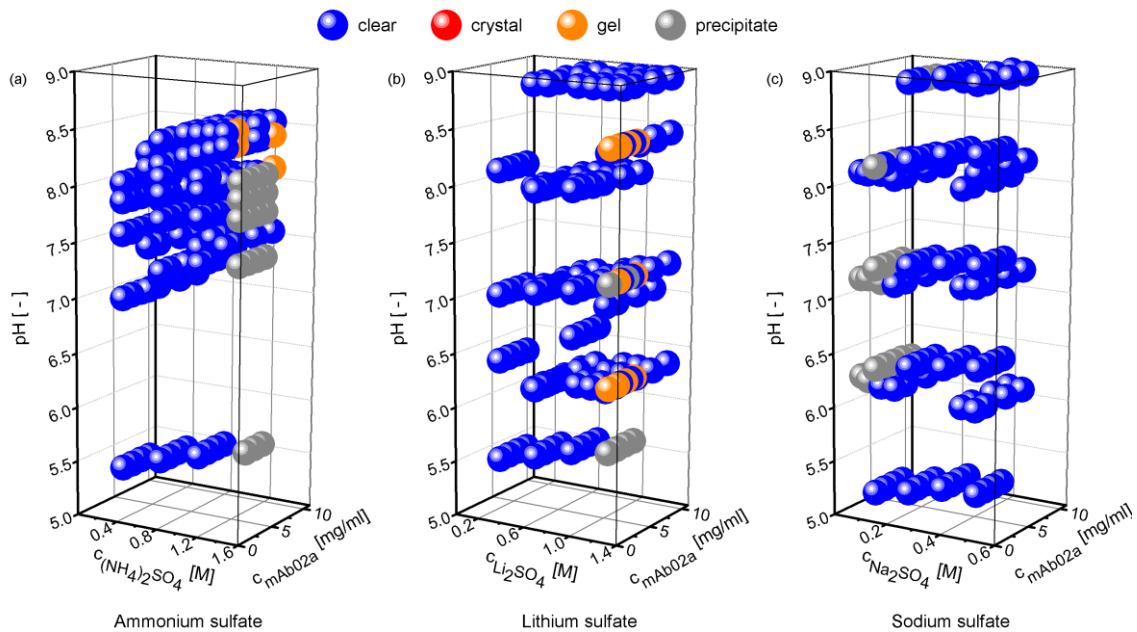


Figure 4.4: Phase diagrams of mAb02a with ammonium (a), lithium (b), and sodium sulfate (c) as a function of the pH

4.3.3 Influence of chloride salts on mAb04c, mAb05a and mAb02a phase behavior: Ammonium and sodium chloride

The systems containing chloride salts analyzed were ammonium chloride and sodium chloride. mAb04c and mAb05a did not show any phase transition with ammonium chloride in solution, whereas light precipitation of mAb02a occurred in the small pH range of 7 - 8 below ammonium chloride concentrations of 0.375 M. The phase diagrams for the three antibodies and sodium chloride are plotted in figure 4.5. For mAb04c and sodium chloride, only light precipitation occurs in the pH range from 6 to 9 for protein concentrations of up to 15 mg/mL and salt concentrations below 0.15 M. For sodium chloride and mAb05a as well as for mAb02a, light precipitation is induced at higher salt concentrations of about 0.375-1 M. Above this salt concentration, the solution stays clear for all antibodies.

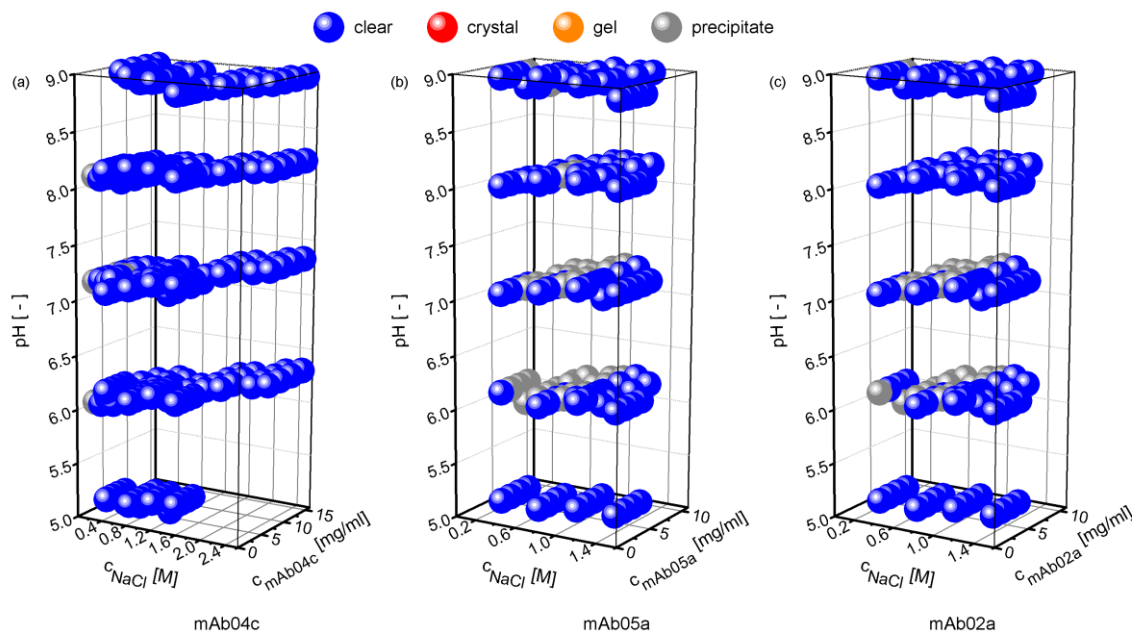


Figure 4.5: Phase diagrams of mAb04c (a), mAb05a (b), and mAb02a (c) with sodium chloride as a function of the pH

4.3.4 Time-dependent analysis of the phase behavior

The time span between the start of the experiment and first visible structures due to phase transition was analyzed when determining the phase behavior. The solution became cloudy and white-gray aggregates were built. In none of the systems were droplets visible over the experiment duration at the resolution limit. This behavior differs from that observed for antibodies by Jion et al. [25] and Lewus et al. [10] Ahamed et al. [26], by contrast, observed precipitation comparable to our findings for the antibody IDEC-152. However, we do not share his opinion that a precipitating sample can be described as an LLPS according to Cheng et al. [27]. Cheng et al. [27] only describe the supernatant of a precipitating sample in the equilibrium state, which is qualitatively consistent with the low-concentration branch of the metastable liquid-liquid phase boundary. The precipitate is defined as a frustrated liquid-liquid phase separation, which is kinetically trapped and, hence, not consistent with the dense phase of the LLPS.

In this work, it is therefore distinguished between precipitation (white-gray aggregates) and LLPS. Depending on the conditions, crystals developed from these aggregates. All antibodies showed a predominantly instantaneous and strong precipitation in ammonium sulfate. In the case of mAb04c in ammonium sulfate, only the crystallized samples showed a time delay. The highest probability and the broadest region of crystallization were reached for mAb04c with lithium sulfate. Sodium sulfate led to a late phase transition compared to ammonium sulfate or lithium sulfate. The higher the salt concentration is, the faster is the phase transition. The longest time span until a phase transition was measured in sodium chloride. Exceptions with no phase transition after 40 days are mAb04c and

mAb05a with ammonium chloride. These results are summarized in figure 4.6 exemplarily for the combination of mAb04c and the sulfate salts of ammonium, lithium, and sodium sulfate at pH 8.0 – 8.3. The color as well as the size of the symbols represent the time of first visible structures.

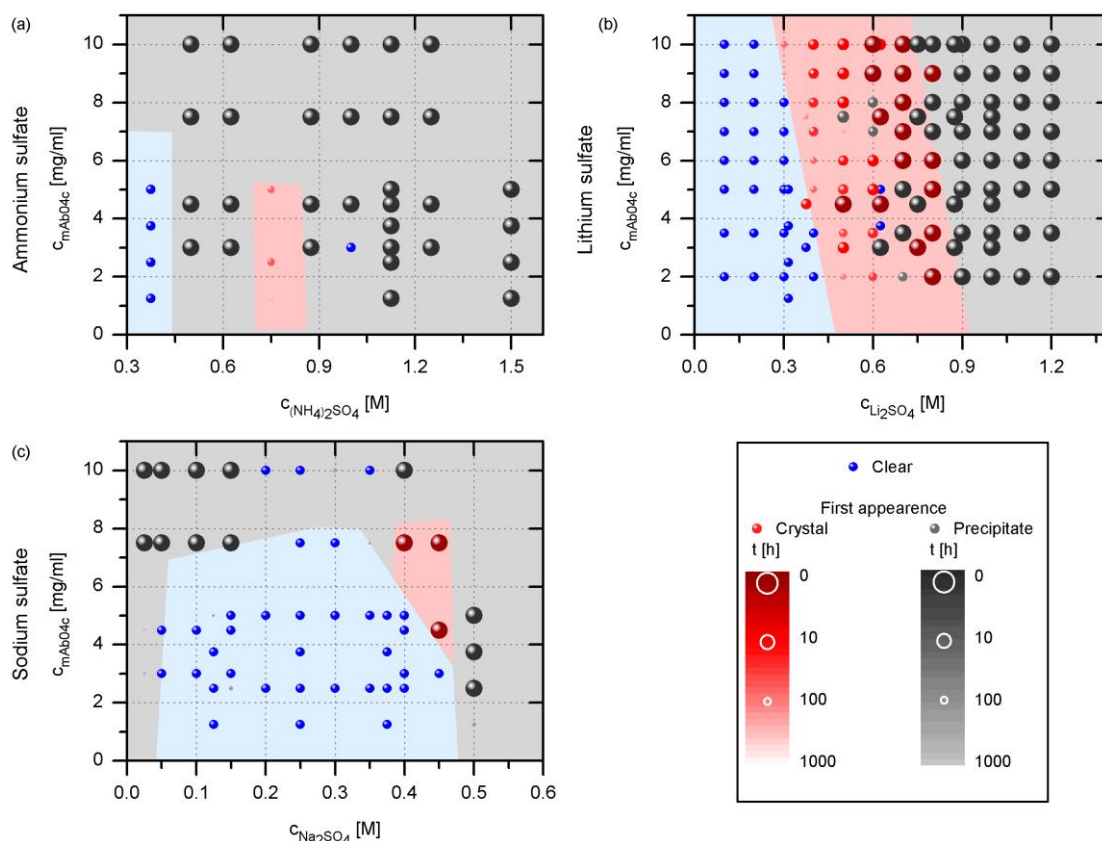


Figure 4.6: Phase transition of mAb04c at pH 8.0 - 8.3 for ammonium, lithium, and sodium sulfate. Color and size represent the time of first visible structures

4.3.5 Size of crystals

mAb04c was the only antibody in this screening revealing crystallization results over a broad pH and salt concentration range. With lithium sulfate, a detailed and systematic phase diagram was obtained, in which a discrete partitioning between a clear stable solution and aggregation (crystallization and precipitation) could be achieved. For a constant protein concentration of 9 mg/mL and varying salt concentrations between 0.3 and 0.8 M, results are presented in figure 4.7. From 0.3 to 0.4 M the needle-shaped crystals increase in quantity and size up to 400 μm . Further increase in the salt concentration up to 0.5 and 0.6 M leads to a decreasing size down to 100 μm , while the quantity is increased. At 0.7 M, only precipitate or microcrystals smaller than 10 μm are built. At a salt concentration of 0.8 M, the microcrystals aggregated, leading to spherical particles in the form of sea urchin-like structures of 50 μm in diameter (figure 4.7) comparable to those mentioned in literature [28,29]. For decreasing protein concentrations, the number of

crystals was reduced, while the sizes of the crystals were comparable. Irrespective of the tested protein concentrations, particle sizes for lithium sulfate are summarized as mean values in figure 4.8 (b).

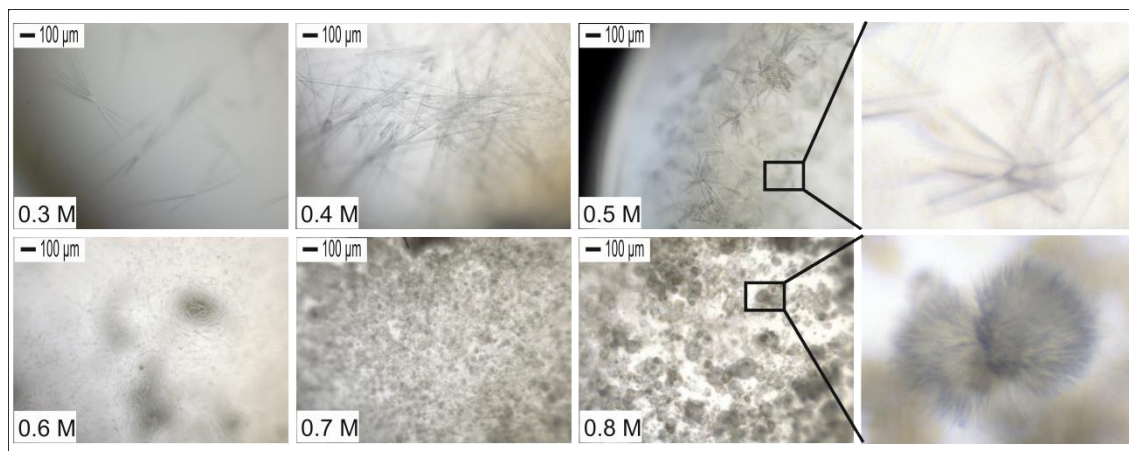


Figure 4.7: Phase behavior of mAb04c with lithium sulfate at $c_{mAb04c} = 9 \text{ mg/mL}$ and $c_{\text{lithium sulfate}} = 0.3 - 0.8 \text{ M}$; 0.5 and 0.8 M images are zoomed

Screening conditions of mAb04c with ammonium sulfate as well as with sodium sulfate produce crystals in a small range near the apparent shift from the clear solution to the precipitate, as illustrated by figure 4.2. The resulting mean particle sizes are summarized for ammonium sulfate and sodium sulfate in figure 4.8 (a, c). No systematic relationship between the crystal size and salt concentration can be found for these two salts. The biggest sizes of crystals are obtained for ammonium sulfate near the pI at pH 8.2. For sodium sulfate, two local maxima exist around pH 7 and 9 with particle sizes smaller than $100 \mu\text{m}$.

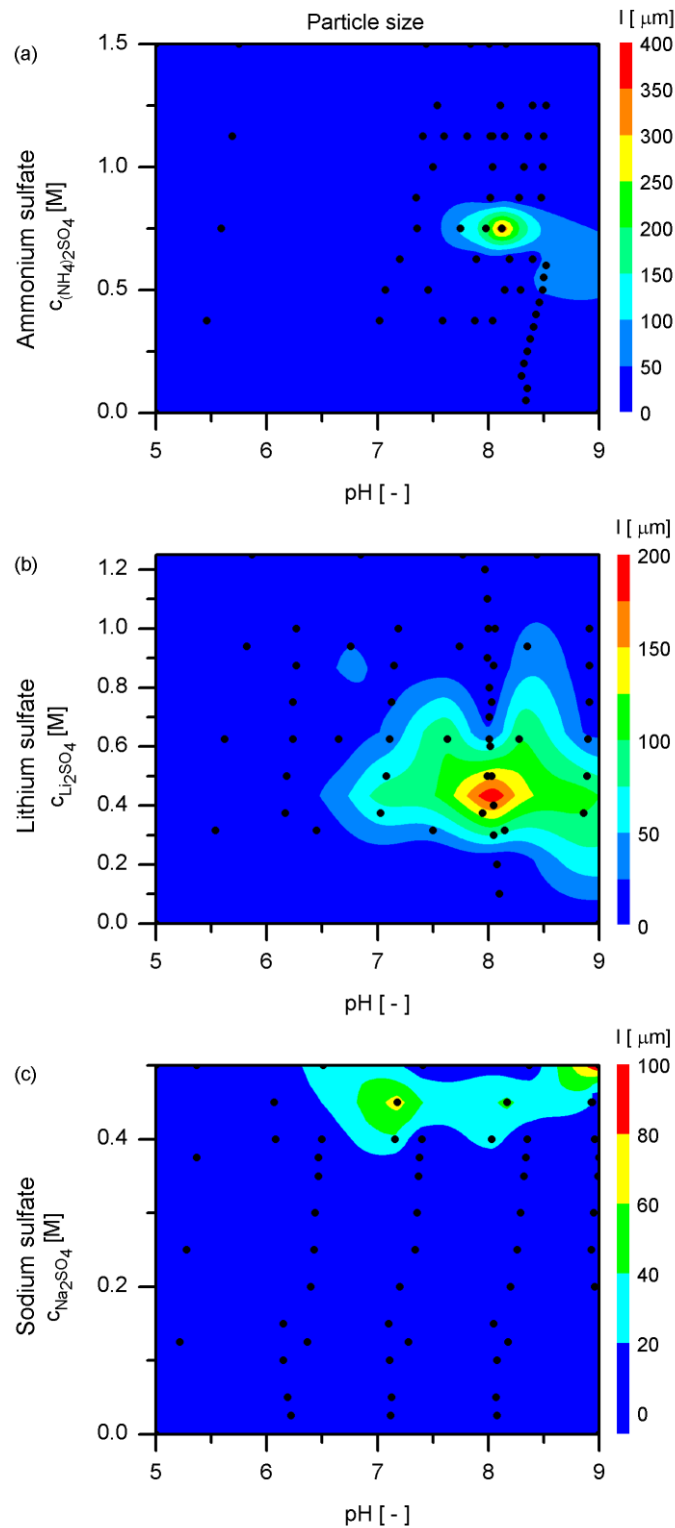


Figure 4.8: Length of the mAb04c crystals obtained in ammonium sulfate, lithium sulfate, and sodium sulfate

4.4 Discussion

An automated platform process and a novel buffer system of constant composition were developed to systematically screen the phase behavior of proteins. The main advantage of the buffer system consists in its constant buffer capacity (10 mM) and component

composition over the pH range from 5 to 9. Only the NaOH content changes with the pH. Various salts can be used as precipitant. With the help of a robotic platform, 3D phase diagrams were obtained as a function of the pH and salt and protein concentrations. Screening with one protein and salt type required a minimum of six buffers. For every additional salt, only two more salt buffers were needed. The ratios of the different buffers were adjustable at will to screen interesting conditions in detail. Using a microbatch approach, the conditions set did not change during the experiment. Moreover, the experimental approach could be applied easily to different proteins. Having characterized the phase behavior over time with an imaging system, additional information is obtained about the pathway of phase transition and its kinetics. Additional automated image evaluation with software like ImageJ can further reduce the analysis expenditure of the images. In this way, a method to systematically determine the influence of the fluid phase conditions was successfully established.

Because the protein phase behavior is poorly understood, theoretical considerations cannot replace such a screening [30]. Other experimental techniques, such as the screening for B_{22} values, might help to increase the crystallization probability. However, the experimental effort as well as the protein and time consumed for B_{22} determination under one condition is quite high, as shown by the theoretical considerations of Ahamed et al. [31]. Moreover, theoretical models cannot replace phase behavior experiments, because quantitative predictions are not possible [10].

4.4.1 Phase behavior of the three antibodies

Interactions of protein molecules are complex due to their individual structure and size [32,33]. According to van Oss et al. [34], the interactions among antibodies seem to be more hydrophobic compared to other proteins. Nevertheless, a more detailed understanding of the phase behavior and in particular of the salt influences on protein phase behavior is lacking [7,33,35]. For this reason, the established screening procedure was applied to three different antibodies in combination with five different salts.

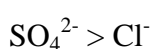
In none of the analyzed systems, was a liquid-liquid phase separation (LLPS) visible in the form of droplets in the resolution range. However, a high amount of aggregates formed first, which correspond to high local protein concentrations. Nuclei built and the aggregates fed the growth of the crystals. According to Ng et al. [36] and Streets et al. [37], this behavior is crystal growth by Ostwald ripening. Over a period of a few days, the aggregates almost dissolved. This is a sign of dominant short-range interactions in these systems and the phase behavior deviates from the classical nucleation theory [38,39]. The number of crystallization nuclei is a function of supersaturation. As shown in figure 4.7, the size of the crystals for mAb04c and lithium sulfate increased under conditions closer to

the metastable region. With increasing supersaturation, the amount of crystals increased, while the size decreased from 400 to 10 μm . The time of their appearance decreased from several hours to instantaneous aggregation. The crystallization probability of mAb04c with ammonium sulfate and sodium sulfate in the screening experiments was smaller under the tested conditions compared to that of lithium sulfate. On the other hand, most systems, especially with mAb05a and mAb02a, showed a direct transition from the clear solution to precipitation with increasing salt concentration. These systems have a too small metastable region compared to the mAb04c and sulfate systems. The kinetics may be too slow to obtain crystals within 40 days or nuclei cannot grow to crystals above the solubility line due to inhibited orientation of the molecules towards each other. The latter is also considered for the samples of mAb05a and mAb02a showing gelation, a state in which a further orientation of the molecules is kinetically hindered and dynamically arrested [10]. In contrast to an LLPS, this state is a non-equilibrium state and according to Evans et al. [40], nucleation is improbable.

For the sulfate salts, it was shown that a pH value close to the pI of the protein induced more effective aggregation and the desired crystallization, respectively. This is in agreement with Chernov et al. [41] and Collins et al. [42]. The broadness of the pH range in which the crystallization occurred is dependent on the cation (figure 4.2).

4.4.2 Influence of the different anions

The influence of salts on the protein behavior in solution is often described by the Hofmeister series [35,43-45]. In 1888, Hofmeister stated a stronger impact of anions on the protein phase behavior, which has been an often shared opinion in literature until today [42,46-48]. Accordingly, all three antibodies showed no or only slow and light precipitation in the presence of the Cl^- anion. This anion is located at the borderline between chaotropic to kosmotropic. Moreover, the antibodies were stabilized in solution at high salt concentrations. With the kosmotropic SO_4^{2-} anion, the aggregation in solution was more pronounced over a broad salt concentration range and often instantaneous. The salting-out effect increased with increasing salt concentration. In addition, a more differentiated phase behavior with crystallization and precipitation as well as gelation was obtained for all antibodies. The anions were ordered according to Hofmeister from kosmotropic to chaotropic salts [41,42,46,49]:



Antibody aggregation followed the Hofmeister series independently of the pH. However, the antibodies were positively charged for a pH below their pI of 8.2 - 8.8. Consequently, the reverse Hofmeister effect was expected in literature [42,44]. Other authors [44,47,50]

affirm a reverse Hofmeister series for salt concentrations lower than 200 - 300 mM monovalent salt only. In this concentration range light precipitation of the antibody was observed for sodium sulfate and sodium chloride systems only. mAb04c was crystallized effectively with the kosmotropic anion SO_4^{2-} and none of the antibodies crystallized reproducibly with the more chaotropic anion Cl^- , as had been proposed by Collins et al. [42,51] for basic proteins.

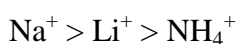
4.4.3 Influence of different cations

Although anions are dominant in inducing aggregation, the differences in anions are not sufficient to describe the overall phase behavior observed, since the aggregation probability differs with the cation as well [10,42,52]. Hofmeister already published a series for cations, but in literature this series is modified depending on the investigated protein [10,41,53]. Consequently, the series is more ambiguous than that of the anions [10,33].

Working with the same sulfate anion, the aggregation probability of Na^+ was already high at salt concentrations of 0.05 M for mAb04c, mAb05a as well as for mAb02a and tested protein concentrations of up to 10 mg/mL (figure 4.2 and figure 4.3). Heavy precipitate was observed at 0.5 M for mAb04c. On the other hand, mAb04c in Li^+ (0.3 M) or NH_4^+ (0.6 M) required higher concentrations for aggregation and the heavy precipitation occurred in comparable concentration ranges. mAb05a and mAb02a showed comparable trends (figure 4.3). Nevertheless, the strength of aggregation followed an opposite trend. The probability of crystallization was higher for mAb04c with lithium sulfate than with ammonium sulfate (figure 4.2). The pH and salt concentration range in which crystallization occurred were broader for lithium and sodium sulfate than for ammonium sulfate. mAb05a gelled with lithium sulfate from pH 7 to 9, while ammonium sulfate induced gelation only close to pH 8.5. Moreover, the aggregation was mainly direct for ammonium sulfate and the time of first visible structures increased from lithium sulfate to sodium sulfate (figure 4.6) for all antibodies.

For the Cl^- anion, no aggregation of mAb04c and mAb05a and only light precipitation of mAb02a in the pH range of 7.5 - 8 were observed in combination with NH_4^+ . With sodium chloride, all antibodies showed light precipitation, while the salt concentration range of mAb04c was significantly smaller than for mAb05a and mAb02a.

Based on an overall analysis of the results, the cations were sorted according to Baldwin et al. and Curtis et al. [35,54] The suggested order is:



Then, the investigated phase behavior of all three antibodies with the five salts can be correlated to the following Hofmeister series:



Although the antibodies are mainly positively charged in the pH range analyzed, the direct Hofmeister series is obtained. Because salt concentrations higher than 200 - 300 mM monovalent salt induce aggregation, these findings are in agreement with Zhang et al. [47] and Schwierz et al. [50]. A special behavior was induced by the Na^+ cation. At low salt concentrations, light precipitation was observed for sodium sulfate and sodium chloride. In combination with sodium sulfate, all three antibodies showed a salting-in effect above 0.125 M sodium sulfate (figure 4.2 f and figure 4.3 e, f). An equivalent effect was found for mAb04c with sodium chloride in the same salt concentration range (figure 4.5 a). For mAb02a and mAb05a, the range of light precipitation was shifted towards higher sodium chloride concentrations up to 1 M (figure 4.5 b).

4.5 Conclusions

A systematic approach to describing protein phase behavior was established. For this purpose, a buffer system with a constant buffer capacity over the broad pH range (5 - 9) was implemented to exclude influences from varying buffers. By applying the process on a robotic platform in a microbatch format, it is possible to generate an extensive database of known conditions in 3D phase diagrams. The analysis of the phase behavior with an imaging system allows the description of the phase behavior after a certain time, but also for the determination of the pathway and the kinetics of phase transition. Thus, detailed information about the phase behavior of proteins is gained in only one screening.

Using this approach, the phase behavior of three antibodies was analyzed systematically in 3D phase diagrams as a function of the pH and varying salt and protein concentrations for five different salts. Overall, the anions have a stronger influence on the phase behavior, with their impacts differing for all three antibodies. Because the influence of the cation on the phase behavior of the three antibodies is more ambiguous, a universal series in terms of a Hofmeister series can be determined at least partly in order to describe the precipitating effects of the salts. Protein crystallization and the pH influence on aggregation cannot be described by this series for the three antibodies. Although the theoretical explanation cannot be resolved, this series and the study of crystallization probability as well as of the pH influence help to understand the phase behavior of the antibodies. These data may serve as basis for further investigations. A detailed analysis of thermodynamic effects or

structural differences of antibodies would be advantageous and could foster fundamental understanding.

4.6 Acknowledgements

The authors are grateful for support by the BMBF (Federal Ministry of Education and Research), grant no. 0315338B and Boehringer Ingelheim Pharma GmbH & Co. KG, Biberach, Germany. They thank Frieder Kröner for his help concerning the buffer system composition.

4.7 Literature Cited

- [1] Roque ACA, Lowe CR, Taipa MA. Antibodies and genetically engineered related molecules: production and purification. *Biotechnol Prog.* 2004;20:639–654.
- [2] Low D, O’Leary R, Pujar NS. Future of antibody purification. *J Chromatogr B Analyt Technol Biomed Life Sci.* 2007;848:48–63.
- [3] Mather JP. Engineered antibody therapeutics. *Adv Drug Deliv Rev.* 2006;58:631–632.
- [4] Schmidt S, Havekost D, Kaiser K, Kauling J, Henzler HJ. Kristallisation für die Aufarbeitung von Proteinen. *Chem Ing Tech.* 2004;76:819–822.
- [5] Salinas BA, Sathish HA, Bishop SM, Harn N, Carpenter JF, Randolph TW. Understanding and modulating opalescence and viscosity in a monoclonal antibody formulation. *J Pharm Sci.* 2010;99:82–93.
- [6] Lightfoot EN, Moscariello JS. Bioseparations. *Biotechnol Bioeng.* 2004;87:259–273.
- [7] Rupp B. Maximum-likelihood crystallization. *J Struct Biol.* 2003;142:162–169.
- [8] Chayen NE, Saridakis E. Protein crystallization: from purified protein to diffraction-quality crystal. *Nat Methods.* 2008;5:147–153.
- [9] Zang Y, Kammerer B, Eisenkolb M, Lohr K, Kiefer H. Towards protein crystallization as a process step in downstream processing of therapeutic antibodies: screening and optimization at microbatch scale. *PLoS One.* 2011;6:e25282.
- [10] Lewus RA, Darcy PA, Lenhoff AM, Sandler SI. Interactions and phase behavior of a monoclonal antibody. *Biotechnol Prog.* 2010;27:280–289.
- [11] Stura EA, Feinstein A, Wilson IA. Crystallization and preliminary crystallographic data for an antiprogestone monoclonal antibody Fab’ and steroid-Fab’ complexes. *J Mol Biol.* 1987;193:229–231.

- [12] Wun KS, Miles LA, Crespi GAN, Wycherley K, Ascher DB, Barnham KJ, Cappai R, Beyreuther K, Masters CL, Parker MW, McKinstry WJ. Crystallization and preliminary X-ray diffraction analysis of the Fab fragment of WO2, an antibody specific for the Aβ peptides associated with Alzheimer's disease. *Acta Crystallogr Sect F Struct Biol Cryst Commun.* 2008;64(Part 5):438–441.
- [13] Gabrielsen M, Nagy LA, DeLucas LJ, Cogdell RJ. Self-interaction chromatography as a tool for optimizing conditions for membrane protein crystallization. *Acta Crystallogr D Biol Crystallogr.* 2010;66(Part 1):44–50.
- [14] Benedek GB. Cataract as a protein condensation disease: the Proctor Lecture. *Invest Ophthalmol Vis Sci.* 1997;38:1911–1921.
- [15] Lashuel HA, Hartley D, Petre BM, Walz T, Lansbury PT. Neurodegenerative disease: amyloid pores from pathogenic mutations. *Nature.* 2002;418:291.
- [16] McPherson A. A comparison of salts for the crystallization of macromolecules. *Protein Sci.* 2001;10:418–422.
- [17] Ries-Kautt MM, Ducruix AF. Relative effectiveness of various ions on the solubility and crystal growth of lysozyme. *J Biol Chem.* 1989;264:745–748.
- [18] Kröner F, Hubbuch J. Systematic generation of buffer systems for pH gradient ion exchange chromatography and their application. *J Chromatogr A.* 2013;1285:78–87.
- [19] Celentano FC, Gianazza E, Dossi G, Righetti PG. Buffer systems and pH gradient simulation. *Chemom Intell Lab Syst.* 1987;1:349–358.
- [20] Rea JC, Moreno GT, Lou Y, Farnan D. Validation of a pH gradient-based ion-exchange chromatography method for high-resolution monoclonal antibody charge variant separations. *J Pharm Biomed Anal.* 2011;54:317–323.
- [21] Haynes WM, editor. *CRC Handbook of Chemistry and Physics* 91st ed. London. Taylor & Francis Ltd.; 2010.
- [22] Farquhar GD, Firth PM, Wetselaar R, Weir B. On the gaseous exchange of ammonia between leaves and the environment: Determination of the ammonia compensation point. *Plant Physiol.* 1980;66:710–714.
- [23] D'Arcy A, Mac Sweeney A, Stihle M, Haber A. The advantages of using a modified microbatch method for rapid screening of protein crystallization conditions. *Acta Crystallogr Sect D Biol Crystallogr.* 2003;59:396–399.
- [24] Bergfors T, editor. *Protein Crystallization*, 2nd ed. La Jolla: International University Line; 2009.
- [25] Jion AI, Goh L, Oh SKW. Crystallization of IgG1 by mapping its liquid-liquid phase separation curves. *Biotechnol Bioeng.* 2006;95:911–918.
- [26] Ahamed T, Esteban BNA, Ottens M, et al. Phase behavior of an intact monoclonal antibody. *Biophys J.* 2007;93:610–619.

- [27] Cheng YC, Lobo RF, Sandler SI, Lenhoff AM. Kinetics and equilibria of lysozyme precipitation and crystallization in concentrated ammonium sulfate solutions. *Biotechnol Bioeng*. 2006;94:177–188.
- [28] Pusey ML, Paley MS, Turner MB, Rogers RD. Protein crystallization using room temperature ionic liquids. *Cryst Growth Des*. 2007;7:787–793.
- [29] Muschol M, Rosenberger F. Liquid–liquid phase separation in supersaturated lysozyme solutions and associated precipitate formation/crystallization. *J Chem Phys*. 1997;107:1953.
- [30] Finet S, Vivarès D, Bonneté F, Tardieu A. Controlling biomolecular crystallization by understanding the distinct effects of PEGs and salts on solubility. *Methods Enzymol*. 2003;368:105–129.
- [31] Ahamed T, Ottens M, Van Dedem G, Van der Wielen LAM. Design of self-interaction chromatography as an analytical tool for predicting protein phase behavior. *J Chromatogr A*. 2005;1089:111–124.
- [32] Leckband D, Israelachvili J. Intermolecular forces in biology. *Q Rev Biophys*. 2001;34:105.
- [33] McPherson A. Introduction to protein crystallization. *Methods*. 2004;34:254–265.
- [34] Van Oss CJ. Hydrophobicity of biosurfaces - origin, quantitative determination and interaction energies. *Colloids Surf B Biointerfaces*. 1995;5:91–110.
- [35] Baldwin RL. How Hofmeister ion interactions affect protein stability. *Biophys J*. 1996;71:2056–2063.
- [36] Ng JD, Lorber B, Witz J, Théobald-Dietrich A, Kern D, Giegé R. The crystallization of biological macromolecules from precipitates: evidence for Ostwald ripening. *J Cryst Growth*. 1996;168:50–62.
- [37] Streets AM, Quake SR. Ostwald ripening of clusters during protein crystallization. *Phys Rev Lett*. 2010;104:1–4.
- [38] Haas C, Drenth J. The interface between a protein crystal and an aqueous solution and its effects on nucleation and crystal growth. *J Phys Chem B*. 2000;104:368–377.
- [39] Ten Wolde PR, Frenkel D. Homogeneous nucleation and the Ostwald step rule. *Phys Chem Chem Phys*. 1999;1:2191–2196.
- [40] Evans RML, Poon WCK, Cates ME. Role of metastable states in phase ordering dynamics. *Europhys Lett*. 1997;38:595–600.
- [41] Chernov A. Protein crystals and their growth. *J Struct Biol*. 2003;142:3–21.
- [42] Collins KD. Ions from the Hofmeister series and osmolytes: effects on proteins in solution and in the crystallization process. *Methods*. 2004;34:300–311.

- [43] Lyklema J. Simple Hofmeister series. *Chem Phys Lett.* 2009;467:217–222.
- [44] Bostrom M, Tavares FW, Finet S, Skouri-Panet F, Tardieu A, Ninham BW. Why forces between proteins follow different Hofmeister series for pH above and below pI. *Biophys Chem.* 2005;117:217–224.
- [45] Piazza R, Pierno M. Protein interactions near crystallization: a microscopic approach to the Hofmeister series. *J Phys Condens Matter.* 2000;12:A443–A449.
- [46] Nucci NV, Vanderkooi JM. Effects of salts of the Hofmeister series on the hydrogen bond network of water. *J Mol Liq.* 2008;143:160–170.
- [47] Zhang Y, Cremer PS. Chemistry of Hofmeister anions and osmolytes. *Annu Rev Phys Chem.* 2010;61:63–83.
- [48] Manning MC, Chou DK, Murphy BM, Payne RW, Katayama DS. Stability of protein pharmaceuticals: an update. *Pharm Res.* 2010;27:544–575.
- [49] Cacace MG, Landau EM, Ramsden JJ. The Hofmeister series: salt and solvent effects on interfacial phenomena. *Q Rev Biophys.* 1997;30:241–277.
- [50] Schwierz N, Horinek D, Netz RR. Reversed anionic Hofmeister series: the interplay of surface charge and surface polarity. *Langmuir.* 2010;26:7370–7379.
- [51] Collins KD. Charge density-dependent strength of hydration and biological structure. *Biophys J.* 1997;72:65–76.
- [52] Bénas P, Legrand L, Riès-Kautt M. Strong and specific effects of cations on lysozyme chloride solubility. *Acta Crystallogr Sect D Biol Crystallogr.* 2002;58:1582–1587.
- [53] Dumetz AC, Snellinger-O'Brien AM, Kaler EW, Lenhoff AM. Patterns of protein–protein interactions in salt solutions and implications for protein crystallization. *Protein Sci.* 2007;16:1867–1877.
- [54] Curtis RA, Ulrich J, Montaser A, Prausnitz JM, Blanch HW. Protein-protein interactions in concentrated electrolyte solutions. *Biotechnol Bioeng.* 2002;79:367–380.

5 From Osmotic Second Virial Coefficient (B_{22}) to Phase Behavior of a Monoclonal Antibody

Natalie Rakel^{1,2}, Katharina Christin Bauer¹, Lara Galm¹, Juergen Hubbuch¹

¹Section IV: Biomolecular Separation Engineering, Institute of Engineering in Life Sciences, Karlsruhe Institute of Technology, Engler-Bunte-Ring 1, 76131 Karlsruhe, Germany

²Roche Diagnostics GmbH, 68305 Mannheim, Germany

Published in Biotechnology Progress, 2015, 31(2), 438-451

Corresponding author:

Juergen Hubbuch

Karlsruhe Institute of Technology

Institute of Engineering in Life Sciences

Section IV: Biomolecular Separation Engineering

Engler-Bunte-Ring 1, 76131 Karlsruhe, Germany

Phone: +49-721-608-42557, fax: +49-721-608-46240

E-mail: juergen.hubbuch@kit.edu.

Keywords: Protein interactions; Phase behavior; Phase diagram; Monoclonal Antibody; Static light scattering

Abstract

Antibodies are complex macromolecules and their phase behavior as well as interactions within different solvents and precipitants are still not understood. To shed some light into the processes on a molecular dimension the occurring self-interactions between antibody molecules were analyzed by means of the osmotic second virial coefficient (B_{22}). The determined B_{22} follows qualitatively the phenomenological Hofmeister series describing the aggregation probability of antibodies for the various solvent compositions. However, a direct correlation between crystallization probability and B_{22} in form of a crystallization slot does not seem to be feasible for antibodies since the phase behavior is strongly dependent on their anisotropy. Kinetic parameters have to be taken into account due to the molecular size and complexity of the molecules. This is confirmed by a comparison of experimental data with a theoretical phase diagram. On the other hand the solubility is thermodynamically driven and therefore the B_{22} could be used to establish a universal solubility line for the monoclonal antibody mAb04c and different solvent composition by using thermodynamic models.

5.1 Introduction

Active proteins are complex molecules due to their sequence variability and individual structure. This said, the highly conserved structure of monoclonal antibodies led to a production platform approach based on cultivation, harvest and purification steps centered around Protein A chromatography as a high affinity chromatographic operation [1]. Nevertheless production process buffer conditions, additives and contaminant compositions may change frequently due to different process steps. Thus, conditions need to be selected in terms of preserving protein stability and activity [2]. An overview of agents that may enhance solubility is listed by Bondos et al. [3]. Examples for potential crystallization agents are published by Rupp [4]. However, the complex influence of physical process parameters like pH, conductivity, temperature, type and concentration of buffer, salt, additives and contaminants as well as physical characteristics of the protein, such as hydrophobicity on protein phase behavior and solubility are still not understood [5]. For salts the Hofmeister series is a good approximation toward their ability to induce aggregation probability of proteins, however this series or its numerous variations is neither sufficient to describe at which concentration the aggregation might occur, nor to take structural specifics of proteins into account [6,7].

Given that molecular understanding is far from being established as today's molecular modeling tools cannot handle the above mentioned complexity, thermodynamic approaches arising from physical chemistry and simplifying the complexity of the system at hand are the only toolbox currently available. One promising approach might be the correlation between protein phase behavior and the nature of protein-protein interactions. Hard sphere, van der Waals, electrostatic, hydrophobic and osmotic forces contribute to the protein interactions. These interactions are traditionally characterized in a diluted solution and quantified via the osmotic second virial coefficient (B_{22}) [8]–[10]. The B_{22} -value represents the magnitude and direction of the non-ideality of the osmotic pressure π in a diluted protein solution. It is part of the virial expansion of the osmotic pressure π :

$$\pi = RTc_P \left(\frac{1}{M_W} + B_{22}c_P + \dots \right) \quad (5.1)$$

The parameters are the universal gas constant R , the temperature T , the protein concentration c_P and the molecular weight of the protein M_W . The parameter B_{22} describes the nature of interactions between two proteins in their environment. Positive B_{22} -values represent repulsion whereas negative values describe attraction.

Positive B_{22} -values are thus the aim when formulations of higher protein solubility and stability need to be found. Examples are given in the literature for lysozyme [11] and an IgG1-antibody [12]. For negative B_{22} -values and thus attracting conditions George and Wilson [13] reported an empirical correlation between the probability of protein crystallization and slightly negative B_{22} -values. Within the so called “crystallization slot” $-8 \cdot 10^{-4} < B_{22}/(\text{mol mL g}^{-2}) < -1 \cdot 10^{-4}$ model proteins such as lysozyme, bovine serum albumin (BSA), Ovalbumin and Ribonuclease A crystallized due to slight attraction [13,14]. Using this approach bovine chymotrypsinogen A could be crystallized with sodium chloride by varying the ionic strength and the pH within the crystallization slot [15], crystals of membrane protein were obtained by analyzing the changes in B_{22} -values for different amphiphiles and additives [16] or the antibody IDEC-152 was enhanced to build crystals by investigating the influence of pH and precipitant on B_{22} [17]. Although all of the above proteins including the antibody IDEC-152 showed a higher crystallization probability in this crystallization slot, some authors [18,19] recommend a modified crystallization slot for larger protein molecules with a molecular weight above approximately 100 kDa which covers the size range of antibodies. Vivarès and Bonneté [18] showed this for Urateoxidase (128 kDa) as well as Ebel [19] for malate dehydrogenase (130 kDa). Haas and Drenth [20] postulated that for protein molecules in the range of 140 kDa the modified crystallization slot ranges from $-0.9 \cdot 10^{-4} < B_{22}/(\text{mol mL g}^{-2}) < -0.35 \cdot 10^{-4}$, whereas for proteins with a molecular weight of 14 kDa the crystallization slot ranges from -9 to $-3.5 \cdot 10^{-4} \text{ mol mL g}^{-2}$.

The thermodynamic background of the B_{22} and its connection to the phase behavior in protein solutions is provided in detail by Elcock [21], Neal [22,23] and Ruppert [24]. Moreover, a correlation between the B_{22} and the solubility s defined as the protein concentration in a saturated solution is published by Haas et al. [20,25,26] with the Haas-Drenth-Wilson (HDW)-model in equation (5.2):

$$B_{22} = \frac{4}{M_w \rho_P} \left[1 - A \left\{ \left(\frac{s}{10^3 \rho_P m} \right)^{-2/z} - 1 \right\} \right] \quad (5.2)$$

The parameter ρ_P is the protein density, z the coordination number of the protein crystals and $m = \Omega/\omega$ the number of water molecules, which have the equivalent volume as one protein molecule. Ω is the volume of one protein molecule and ω the molar volume of water V_W divided by the Avogadro number N_A . A is a single free adjustable parameter:

$$A = p(v^3 - 1) \quad (5.3)$$

The parameter A itself depends on the degree of anisotropy p and the range of interaction v . The anisotropy p ranges from 0 to 1, whereby $p = 1$ describes isotropic interactions. For

protein crystals coordination numbers of $z = 4 - 6$ are frequently obtained in experiments [26]. Haas et al. [25] based their model on the assumption, that variations of crystallization conditions, like solvent, temperature and pH only have little effect on the product of anisotropy and range of interactions between protein molecules $p(v^3 - 1)$ and therefore on A .

Another model has been established by Ruppert et al. [24]. The Ruppert-Sandler-Lenhoff (RSL)-model is derived from the equality of the protein fugacities in the liquid and solid equilibrium phases using the infinite dilution as standard state for the liquid phase. It is defined as follows:

$$B_{22} = \frac{1}{2M_W s} \cdot \left[A_C - (1 - K) \cdot \ln \left(\frac{V_W}{M_W} \cdot s \right) \right] - \frac{V_P}{M_W^2} - \frac{dn/dc_P}{n_0 M_W} \quad (5.4)$$

$V_P = \Omega \cdot N_A$ is the partial molar volume of the protein at infinite dilution in the aqueous solution, dn/dc_P describes the refractive index increment, n_0 the refractive index and A_C plus K are adjustable parameters.

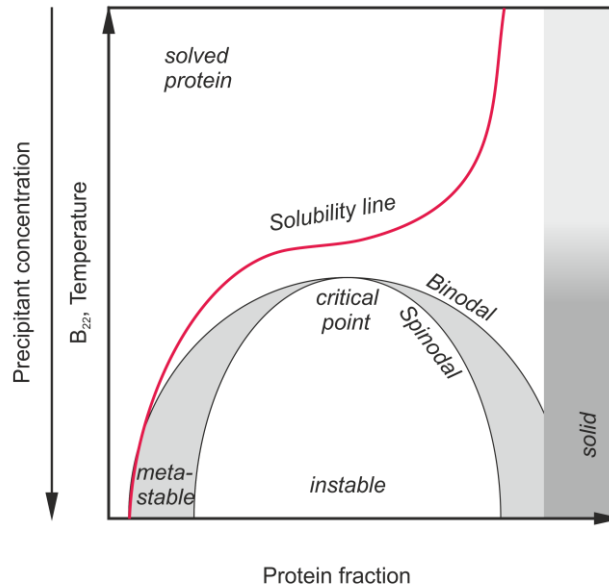


Figure 5.1: Schematic phase diagram of proteins on the basis of Haas et al. [20], Ahamed et al. [27], and Lewus et al. [17]

Regarding a schematic and simplistic phase diagram as plotted in figure 5.1 on the basis of Haas et al. [20], Ahamed et al. [27] and Lewus et al. [17] the solubility line separates the undersaturated from the supersaturated region. Above the solubility line - undersaturated region - the protein solution is stable with respect to phase changes. Between solubility line and binodal, a phase transition (liquid-solid) may occur with its one state on the solubility line being in equilibrium with the solid state - gray gradient on the right hand side of figure

5.1- as found in classical nucleation theory [28]. Crystals develop from solution in this two-state region. The binodal represents the coexistence curve at which two liquid phases, a protein rich and lean phase, can coexist. Between binodal and spinodal (light grey zone) conditions are metastable. Within the spinodal region the system is instable and such a system leads to an instantaneously spinodal decomposition into the two phases with its local equilibria on the binodal. The resulting LLPS is in this case metastable and crystallization might happen out of the protein rich phase. A combination of experimentally obtained solubility data, binodal data and thermodynamic approaches listed above allows the establishment of such a phase diagram as shown previously for few model proteins [20,24,25] and a monoclonal antibody (IDEC-152) [17,27].

The basis to model such a phase diagram is the Gibbs energy per unit volume of a protein solution [20,27]:

$$G_\lambda(\phi_P) = \frac{1}{\Omega} \left[\left(\frac{\phi_P^2}{\phi_c} \right) g_\lambda + k_B T \phi_P \ln \left(\frac{\phi_P}{m} \right) - k_B T \left\{ \frac{\phi_P - 6\phi_P^2 + 4\phi_P^3}{(1 - \phi_P)^2} \right\} \right] \quad (5.5)$$

The volume fraction of the protein is described by ϕ_P , the volume fraction of the protein in the crystal by ϕ_c and the protein-protein interactions are described by the parameter g_λ :

$$g_\lambda = k_B T \phi_c (B_{22} M_w \rho_P - 4) \quad (5.6)$$

The corresponding protein lean and protein rich phases in the LLPS at the binodal ϕ_α and ϕ_γ are calculated by:

$$G_\lambda(\phi_\gamma) - G_\lambda(\phi_\alpha) = \phi_\gamma \left(\frac{\partial G_\lambda}{\partial \phi_P} \right)_{\phi_\gamma} - \phi_\alpha \left(\frac{\partial G_\lambda}{\partial \phi_P} \right)_{\phi_\alpha} \quad (5.7)$$

and

$$\left(\frac{\partial G_\lambda}{\partial \phi_P} \right)_{\phi_\gamma} = \left(\frac{\partial G_\lambda}{\partial \phi_P} \right)_{\phi_\alpha} \quad (5.8)$$

The spinodal separation in ϕ_α^* and ϕ_γ^* is defined over the second deviation of the free energy:

$$\left(\frac{\partial^2 G_\lambda}{\partial \phi_P^2} \right)_{\phi_\gamma^*} = 0 \quad (5.9)$$

and

$$\left(\frac{\partial^2 G_\lambda}{\partial \phi_P^2}\right)_{\phi_\alpha^*} = 0 \quad (5.10)$$

The question arises if these simplifications of thermodynamic principles including the B_{22} are applicable to describe phase behavior of complex and large molecules such as monoclonal antibodies and whether empirical ranges for example in form of a crystallization slot allow a general description of phase behavior of antibodies.

At first sight monoclonal antibodies seem to be a perfect candidate system for a general application of crystallization given the high degree of homology found for this molecule class. However, reports from the literature and industry show that this is not the case [29] In general every mAb shows structural differences in the variable Fab region determining the specific affinity of each antibody. When examining the constant region Fc of the IgG subclasses, we find a homology of around 95%. However, there are more pronounced differences when comparing the different subclasses. Major structural differences in the Fc region leading to differences in the surface pattern but most important leading to the flexibility of the respective IgG subclass found in the hinge region. This is due to a changing number of residues and inter-chain disulfide bonds. The flexibility of the hinge region mainly serves the ability to interact with differently spaced epitopes but will thus also determine antibody–antibody interactions. In the present manuscript, we compare the behavior and interaction parameters of three antibodies belonging to two IgG subclasses, namely IgG1 and IgG4. Comparing IgG1 and IgG4 we find a difference in the hinge amino acids number 15 and 12 respectively giving rise to a higher flexibility between the Fab arms as well as between Fc and Fab for IgG1 [30].

A first focus was laid to evaluate if clear differences between the three mAbs and two subclasses could be identified in terms of interaction parameters. We systematically analyze the phase behavior of three antibodies under different fluid phase conditions with respect to the self-interaction of the protein molecules. The self-interaction in form of the B_{22} was experimentally determined using static light scattering (SLS). The use of a buffer system enabled us to analyze the influence of three different salt types with varying concentration in a pH-range from pH 5 - 9. This was followed by a more detailed investigation of mAb04c belonging to the subclass IgG4. The results are compared with two dimensional phase diagrams from microbatch experiments to evaluate the transferability of B_{22} -values on the macroscopic phase behavior [6] as well as the applicability of the crystallization slot. The correlation of the already established Hofmeister Series for the three antibodies [6]



and the B_{22} was investigated by means of ammonium sulfate, lithium sulfate and sodium chloride. Additional experimental solubility data are used to model the universal solubility line with the thermodynamic approaches of equation (5.2) and (5.4). Finally, a comparison of an experimentally determined phase diagram with the thermodynamic model according to (5.5)-(5.10) is presented for the system of the antibody mAb04c with lithium sulfate.

5.2 Material and Methods

5.2.1 Chemicals

Protein A-purified monoclonal antibodies mAb04c (type IgG4, pI 8.3-8.8), mAb05a (type IgG1, pI 8.2-8.5) and mAb02a (type IgG1, pI 8.3-8.9) in solution were kindly provided by Boehringer Ingelheim Pharma GmbH & Co. KG, Biberach, Germany. The provided antibody solution was processed with Vivaspin 20, Vivaspin 2 or Vivaspin 500 (30 kDa Cutoff PES-membrane, VS2022, VS0222 and VS0122, Sartorius Stedim Biotech, Göttingen, Germany) several times at 8,000 g and 20°C to achieve full buffer exchange. The protein concentration was then adjusted to the desired value using UV-absorption measurements at 280 nm (Tecan infinite[®] M200, Tecan Group, Crailsheim, Germany).

The chemicals acetic acid, sodium hydroxide (NaOH), MES, lithium sulfate (Li_2SO_4) and sodium chloride (NaCl) were obtained from Merck KGaA (Darmstadt, Germany), MOPSO, CHES and ammonium sulfate ($(\text{NH}_4)_2\text{SO}_4$) from Applichem GmbH (Darmstadt, Germany), HEPPSO from molekula Germany Ltd. (Taufkirchen, Germany) and sodium sulfate from Fluka[™] (Sigma-Aldrich GmbH, St. Louis, MO, USA).

The buffer system with a constant buffer capacity of 10 mM in the pH-range of 5 - 9 applied in this study contains five monoprotic acid-components: 10.05 mM MES, 16.6 mM acetic acid, 8.9 mM MOPSO, 12.3 mM HEPPSO and 14.4 mM CHES and was titrated with 4 M NaOH to the required pH between 5 and 9 (HI-3220, HANNA instruments US, Woonsocket, Rhode Island, USA). As precipitant or respectively salt component, lithium sulfate, ammonium sulfate and sodium sulfate were used. For the B_{22} -measurements the buffer was prepared using the desired salt concentration and pH. For a more detailed information on preparation of the buffer system see Rakel et al. [6].

All prepared buffers and protein samples were filtered with a 0.2 μm cellulose membrane to avoid contamination and dust particles in the solutions.

5.2.2 Determination of B_{22}

The B_{22} was determined from changes in averaged scattered light intensities using an automated-batch composition gradient multiangle light scattering system with seven SLS detectors at different angles and an additional dynamic light scattering detector to indicate aggregation in solution (CG-MALS, Calypso, DAWN[®] HELEOS[™] 8+, Optilab[®] reX, Wyatt Technology Corp., Santa Barbara, CA, USA, Software CALYPSO Version 1.2.8.5, ASTRA Version 5.3.4.20). The experiments were conducted and analyzed according to Rakel et al. [31]. The flow rate was set to 0.6 mL/min and the delay time to a minimum of 60 sec for the measurement at each concentration step. The background scattering of pure solvent was subtracted. The protein concentration was determined with the refractometer by applying the refractive index increment $dn/dc_P = 0.185$. The B_{22} was calculated according to Zimm [32]. A protein concentration dependency of the apparent molecular weight comparable to that of mAb2 as published by Scherer et al. [33] was detected for all antibodies. However, the extrapolation to infinite dilution resulted in deviations of the molecular weight M_w comparable to the literature data [34]–[36].

5.2.3 Determination of macroscopic phase behavior

The analysis of macroscopic phase behavior is described in detail in Rakel et al. [6]. Therefore only a brief description is given below. The preparation of the screening conditions was conducted with a robotic platform (Freedom EVO[®] 100, Tecan Group, Männedorf, Switzerland). Ammonium and lithium sulfate were used as precipitants with maximal salt concentrations of 3 M and 2.5 M in the salt buffer. First the precipitation buffer was prepared in 2 mL scale in 96 deep well plates (Nalgene Nunc, Rochester, NY, USA, product no. 260252) by mixing different ratios of pH 5 and pH 9 salt-free and salt buffers (maximal salt concentrations for lithium sulfate 2.5 M and ammonium sulfate 3 M). Accordingly, the starting buffer containing different antibody concentrations and different pH-values was prepared in 100 μ L scale (1.5 mL Safe-Lock tubes[™], Eppendorf AG, Hamburg, Germany, product no. 0030 120.086). To finally reach the screening conditions 10 μ L starting buffer and 10 μ L precipitation buffer were mixed in microbatch plates (MRC Under Oil 96 Well Crystallization Plate, Swissci AG, Neuheim, Switzerland; Crystal Clear Sealing Tape, Hampton Research CORP., Aliso Viejo, CA, USA, product no. HR4-506). The phase behavior was analyzed with an imaging system (Formulatrix, Waltham, MA, USA, Software Rock Maker) over 40 days and classified in clear, precipitate, LLPS, gelation and crystals according to Bergfors [37]. The mean of the longest side of 5 - 10 crystals was determined as mean crystal size. With an investigation of the time at which phase transition was visible, information about the kinetic could be achieved.

The second aggregation line was determined according to Dumetz et al. [28]. It characterizes the protein concentration at which the aggregation is instantaneously visible for a constant salt concentration. For mAb04c this data was extracted from former kinetic measurements for lithium sulfate at pH 8 and ammonium sulfate pH 8.5 ± 0.2 [6]. The concentrations were converted into volume fractions with equation (5.12).

5.2.4 Determination of solubility (s)

Batch experiments were conducted in a 2 mL scale at the conditions listed in table 5.1. Protein and salt in the respective buffer were mixed in the concentrator body of a Vivaspin 2 (Cut off 300 kDa, PES-membrane, VS0222, Sartorius Stedim Biotech, Göttingen, Germany), which was sealed completely. The initial protein concentration of the screening condition $c_{pro,ini}$ was determined from UV-absorption measurements at 280 nm. Under the assumption that after 2 weeks of storage at room temperature equilibrium was reached, phase composition was analyzed in respect of protein concentration in the liquid phase. To do so, the sealing of the concentrator body was removed and the supernatant was collected in the filtrate tube by centrifugation of the Vivaspin at 4,000 g as long as liquid phase remained in the concentrator body. The solid phase (crystals or precipitate) was retained in the concentrator body. Protein concentration $c_{pro,liq}$ of the obtained filtrate (the supernatant of the experiment) was determined from UV-absorption measurements at 280 nm. The experiments were conducted in duplicates when not otherwise mentioned. The determined values were used for the solubility line determination applying equations (5.2) and (5.4) as described in detail below.

In addition, the reproducibility and the dependency of the solubility on the initial protein concentration of the experiments were analyzed. Therefore, quadruplicate measurements were conducted with $c_{pro,ini} = 10$ mg/mL mAb04c for final lithium sulfate concentrations of 0.6 M and 1 M (pH 8) as well as final ammonium sulfate concentrations of 0.6 M (pH 9) and duplicate measurements for solubility determination for initial mAb04c concentrations of 10, 8, 7.5, 7, 6, 5, 3.5 mg/mL in 0.6 M lithium sulfate and pH 8. The average is plotted in figure 5.5. Since the standard deviation for the reproducibility for one condition as well as for different initial protein concentrations was below 0.2 mg/mL, these parameters are not further discussed.

Table 5.1: Investigated mAb04c-Salt Systems for Solubility Determination; *single experiment

| Salt | Buffer pH [-] | c_{Salt} [M] |
|---|---------------|-----------------------------------|
| Li ₂ SO ₄ | 7 | 0.4*, 0.5*, 0.625*, 0.75* |
| Li ₂ SO ₄ | 8 | 0.3, 0.4, 0.5, 0.6, 0.8, 1 |
| Li ₂ SO ₄ | 9 | 0.375*, 0.5*, 0.625*, 0.75*, 0.8* |
| (NH ₄) ₂ SO ₄ | 7 | 0.5, 0.6, 0.7*, 0.8* |
| (NH ₄) ₂ SO ₄ | 9 | 0.6, 0.8*, 1* |

5.2.5 Determination of volume fractions (ϕ_P)

To establish a more quantitative phase diagram for the mAb04c the protein fractions in the solid $\phi_{pro,crs}$ and liquid phase $\phi_{pro,liq}$ after phase separation ($_{eql}$) were determined.

The protein volume fraction in the crystal phase $\phi_{pro,crs}$ and liquid phase $\phi_{pro,liq}$ are defined according to equation (5.11) and equation (5.12) respectively:

$$\phi_{pro,crs} = \frac{V_{pro,crs}}{V_{crs,eql}} = \frac{m_{pro,crs}}{\rho_{pro,crs}} \cdot \frac{\rho_{crs,eql}}{m_{crs,eql}} \quad (5.11)$$

$$\phi_{pro,liq} = \frac{V_{pro,liq}}{V_{liq,eql}} = \frac{m_{pro,liq}}{\rho_{pro,liq}} \cdot \frac{\rho_{liq,eql}}{m_{liq,eql}} \quad (5.12)$$

where $V_{crs,eql}$ describes the volume of the obtained solid phase (crystals), $V_{pro,crs}$ the volume of protein in the crystal, $m_{crs,eql}$, $m_{pro,crs}$, $\rho_{crs,eql}$ and $\rho_{pro,crs}$ the respective masses and densities. Respectively, $V_{liq,eql}$ describes the volume of the “supernatant” liquid phase, $V_{pro,liq}$ the volume of protein in the liquid phase, $m_{liq,eql}$, $m_{pro,liq}$, $\rho_{liq,eql}$ and $\rho_{pro,liq}$ the respective masses and densities.

The system points analyzed in the protein phase diagram contained varying lithium sulfate concentrations of 0.4, 0.5, 0.6 and 1 M while the initial protein concentration $c_{pro,ini}$ was set to either 8 mg/mL or 10 mg/mL. The pH was set to pH 8.

As volumetric measurements are rather difficult to perform a mass based analysis was chosen. All weight measurements were carried out with an analytical balance (Talent TE214S, reproducibility $\leq \pm 0.1$ mg, Sartorius AG, Göttingen, Germany). For each initial liquid system ($_{liq,ini}$) – containing varying concentrations of water, buffer salts, salt and protein – the mass $m_{liq,ini}$ of a set volume $V_{liq,ini}$ and thus density $\rho_{liq,ini}$ were determined before each experimental procedure. Additionally the mass of the empty filtration device

and parts thereof used (Vivaspin 2, Cut off 300 kDa, PES-membrane, VS0222, Sartorius Stedim Biotech, Göttingen, Germany) were determined before each experimental procedure.

For the analysis of a system point the experimental procedure described above for the determination of protein solubility s is followed.

After equilibration and centrifugation the remaining solid phase mass in the concentrator body $m_{crs,eql}$ and the mass of the liquid phase $m_{liq,eql}$ collected in the filtration body were weighted subtracting the weight of the empty devices. Remaining liquid attached to the concentrator body of the filtration device is neglected.

The protein mass $m_{pro,liq}$ in the liquid phase – as collected in the filtrate – was calculated from the total mass $m_{liq,eql}$ collected, its density $\rho_{liq,eql}$ and protein concentration $c_{pro,liq}$. Protein concentration in the filtrate $c_{pro,eql}$ was determined by UV 280 measurements as described above.

The protein mass in the crystal $m_{pro,crs}$ was determined using an simple mass balance according to equation (5.13):

$$m_{pro,crs} = m_{pro,ini} - m_{pro,liq} \quad (5.13)$$

The mean crystal density $\rho_{crs,eql}$ was determined to 1.36 mg/mL using a 1 mL pycnometer (30642.09, Klaus Hofmann GmbH, Staudt, Germany). Protein density ρ_{pro} was assumed to be the same in both phases ($\rho_{pro,crs}$ and $\rho_{pro,liq}$) and set to 1.44 mg/mL [27]. The determination of the solid phase has in general shown difficulties and the overall failure is comparable to those in the literature [27]. The deviation in the solid phase can have a variety of reasons including experimental handling procedures such as filtration, weighting and evaporation.

The theoretical solubility (equation (5.2)) is divided by the protein density ($\rho_{pro} = 1.44$ g/mL [27]) to gain the protein volume fraction of the saturated solution.

5.2.6 Model application

The solubility line was determined using the solubility values and respective B_{22} -values for the system points described above. For interpolation of B_{22} -values not determined experimentally, the linear slope between the neighboring points was used. The non-linear fitting of both models for solubility line determination (equation (5.2) and (5.4)) was conducted with a Levenberg-Marquardt iteration. The iteration converged and was terminated when a Chi-square tolerance of 10^{-9} was reached.

For using the HDW-model (5.2) for the solubility line determination the value of $\Omega = 166.5 \text{ nm}^3$ was adopted from Ahamed et al. [27], the Avogadro number N_A is $6.022 \cdot 10^{23} \text{ 1/mol}$ and $V_W = 18.051 \text{ cm}^3/\text{mol}$. The density of the protein crystal was experimentally determined to $\rho_c = 1.36 \text{ g/mL}$, which matches the postulated value for proteins of Haas et al. [38]. As starting points the coordination number z was set to 4 and A to 0.01 according to the determined values for lysozyme of Haas et al. [25].

The missing parameters for the RSL-model (5.4) were set to $V_P = \Omega \cdot N_A = 100266.3 \text{ mL/mol}$, the dn/dc_P was set to 0.185 mL/g and $n_0 = 1.34$ was adopted from Mehta et al. [39], since small variations in the refractive index have only little influence on the results. The starting values of $K = 0.9709$ and $A_c = -0.4150$ were set according to the determined values for lysozyme [24].

The binodal and spinodal were modeled according to equations (5.5) - (5.10). The parameters $\Omega = 166.5 \text{ nm}^3$ [3,27], $\phi_c = 0.37$ [40] and $m = 5552.8$ [27] were adopted from literature. The non-linear set of equation (5.7) and (5.8) was solved for ϕ_α and ϕ_γ as a function of B_{22} -values using Microsoft Excel Solver. Equation (5.9) and (5.10) were fitted separately for the respective volume fraction. The fits were terminated when a tolerance of 10^{-9} was reached.

5.3 Results and Discussion

5.3.1 Electrostatic interactions: Influence of pH on B_{22} -values

The influence of pH on B_{22} -values was analyzed in the buffer system described above for antibodies mAb04c (IgG4), mAb02a (IgG1) and mAb05a (IgG1) with a constant buffer capacity of 10 mM. The results are plotted in figure 5.2. At pH 5 positive B_{22} -values in the same range are obtained for all antibodies. From pH 5 to 7 mAb04c shows a stronger decrease with increasing pH to negative B_{22} -values compared to the IgG1 candidates mAb05a and mAb02a. A slight increase in the B_{22} between pH 8 and 9 for mAb04c results finally in B_{22} -values comparable with those of mAb05a and mAb02a, which are decreasing from pH 7 - 9.

Overall the results confirm common understanding that an increased net charge leads to repulsion and thereby an increase in B_{22} -values [41,42], as shown by the B_{22} -values at pH 5. While a pH dependency of the B_{22} -value is expected due to the varying net charge of the antibodies we see a distinct difference for the different mAbs investigated. The two IgG1 antibodies mAb02a and mAb05a were characterized by a mostly positive B_{22} . Close to the isoelectric point (pI) of the antibodies ($8.2 < \text{pH} < 8.9$) the lowest absolute B_{22} -values are detected. mAb04c in contrast shows a clear shift to negative B_{22} -values with a

minimum at pH 7 - 8. This behavior implies additional hydrophobic forces between mAb04c molecules. The obtained data further suggests a subclass specific behavior; however this could not be confirmed by a statistically relevant number of mAbs [29]. According to Lewus et al. [29] charged residues near the complementarity-determining regions (CDR) as well as the hypervariable region may be responsible for these differences. Nevertheless both IgG1 antibodies seem to follow a similar pattern when considering pH dependency.

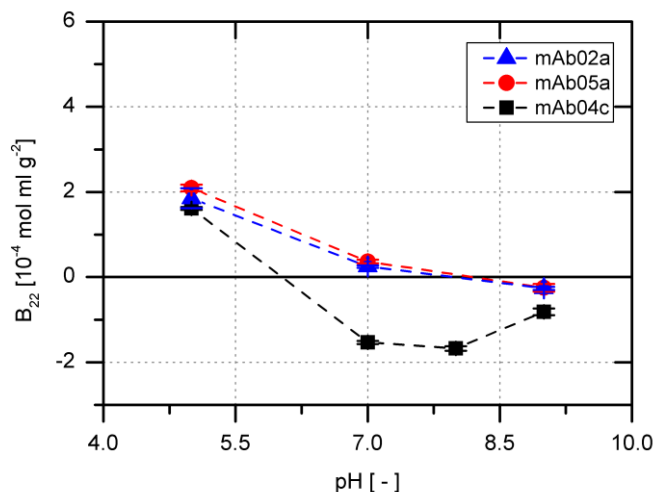


Figure 5.2: B_{22} -values over the pH-range of 5 to 9 for mAb02a, mAb04c and mAb05a at 10 mM buffer capacity

5.3.2 Hydrophobic interactions: Influence of kosmotropic salts on B_{22} -values

In addition to the evaluation of patterns responsible for electrostatic interactions, hydrophobic contributions to the protein-protein interactions were analyzed by increasing the concentration of kosmotropic salts at constant pH. The two salts ammonium and lithium sulfate were chosen for this evaluation. These salts were also successfully applied for the crystallization of IDEC-152 [17]. According to the Hofmeister Series the kosmotropic effect of lithium sulfate is stronger than of ammonium sulfate, since lithium is a kosmotropic and ammonium a chaotropic cation. The pH was set to pH = 9 because the electrostatic interactions are minimal between the antibodies and the differences between the B_{22} -values without salt small. The obtained B_{22} -values for mAb05a, mAb02a and mAb04c are plotted for increasing ammonium sulfate and lithium sulfate concentrations at pH 9 in figure 5.3. Over the measured salt concentration range all B_{22} -values are negative and slightly decreasing. Attraction occurs between the molecules. The trend for mAb02a is comparable to mAb05a. For mAb04c, the B_{22} -values decrease continuously and the behavior is again more pronounced than for both IgG1 antibodies. The latter reflecting the clear difference in behavior of this mAb.

By increasing the kosmotropic strength of the added salt (lithium sulfate) the B_{22} -values for all antibodies are in a comparable range between 0 and 0.4 M lithium sulfate (figure 5.3 b). With a further increase in salt concentrations the deviations are for the first time considerable between all antibodies. While the B_{22} -values for mAb05a are further decreasing constantly with increasing lithium sulfate concentration, the B_{22} -values for mAb02a remain on a comparable level as seen for the case with ammonium sulfate. The most pronounced decrease is again shown by the system with mAb04c.

Given the difference detected for the two IgG1 and lithium sulfate depicted in figure 5.3 for lithium sulfate concentrations above 0.4 M one might postulate that mAb05a is characterized by a slightly higher hydrophobic interaction potential than mAb02a. The latter is however only triggered by a strong kosmotropic environment. mAb04c clearly shows the highest potential for hydrophobic interactions.

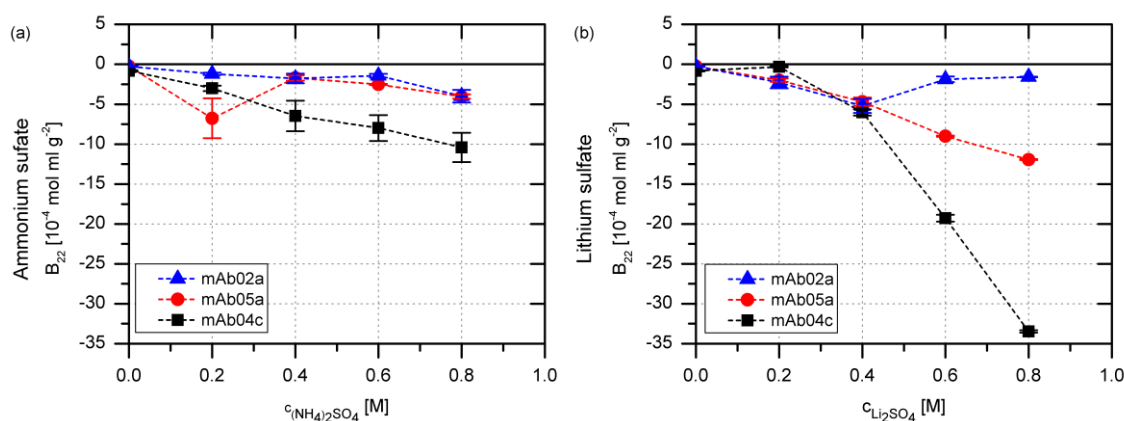


Figure 5.3: B_{22} -values of mAb05a, mAb02a and mAb04c for varying ammonium sulfate (a) and lithium sulfate concentrations (b) at pH 9

5.3.3 Detailed analysis: Salt and pH influence on B_{22} -values of mAb04c

Given the pronounced behavior of the IgG4 antibody mAb04c a detailed investigation of electrostatic and hydrophobic influences was performed. The differences in self-interaction of mAb04c in the presence of the three salts sodium chloride, ammonium sulfate and lithium sulfate in the pH range pH 5 - 9 were investigated by determining B_{22} -values for all systems. The results are plotted in figure 5.4.

At 0 M salt the differences in B_{22} -values for the three pH-values is in the extent of electrostatic interactions. The increase in ionic strength due to the increasing salt concentration leads to a shielding of electrostatic interactions, while the type and concentration of salt additives modulate the extent of hydrophobic interactions. With the salt sodium chloride only weak self-interactions (slightly negative B_{22} -values) were detected due to the chaotropic character of Cl^- figure 5.4 (a). Although a salt induced

increase in hydrophobic interactions might be expected, an increase in sodium chloride leads to constant B_{22} -values due to the weak kosmotropic strength of sodium chloride for all three different pH-values. This can be explained by the shielding of electrostatic interactions with increasing content of sodium chloride.

The corresponding B_{22} -values for ammonium sulfate and lithium sulfate showed stronger attraction ($B_{22} < 0$) with increasing salt concentration (figure 5.4 b, c). When investigating the influence of ammonium sulfate and lithium sulfate on the interaction the salt concentration range was limited due to protein aggregation at higher salt contents, which itself indicates strong attractions. The dominant factor is the presence of the kosmotropic sulfate ion. According to Hofmeister, the anion dominates the salting out effect [43,44] and therefore the stronger self-attraction. The anion effect is observed, but the cation influence on mAb04c is quantified in form of the B_{22} . At the same salt concentrations the B_{22} -values for mAb04c with lithium sulfate were lower than those with ammonium sulfate. According to the Hofmeister series [41,44–46] self-attraction of mAb04c-molecules is stronger induced by the more kosmotropic cation Li^+ than the NH_4^+ . This effect is further influenced by the pH-value. While the differences detected with increasing salt concentration at pH 5 are small, they are the more pronounced the higher the pH-values. At pH-values close to the pI of the protein (8.3 - 8.8) the decrease of B_{22} -values is most distinct for the antibody mAb04c. The development of B_{22} as a function of salt type and pH-value corresponds qualitatively to data reported for other mAbs [29].

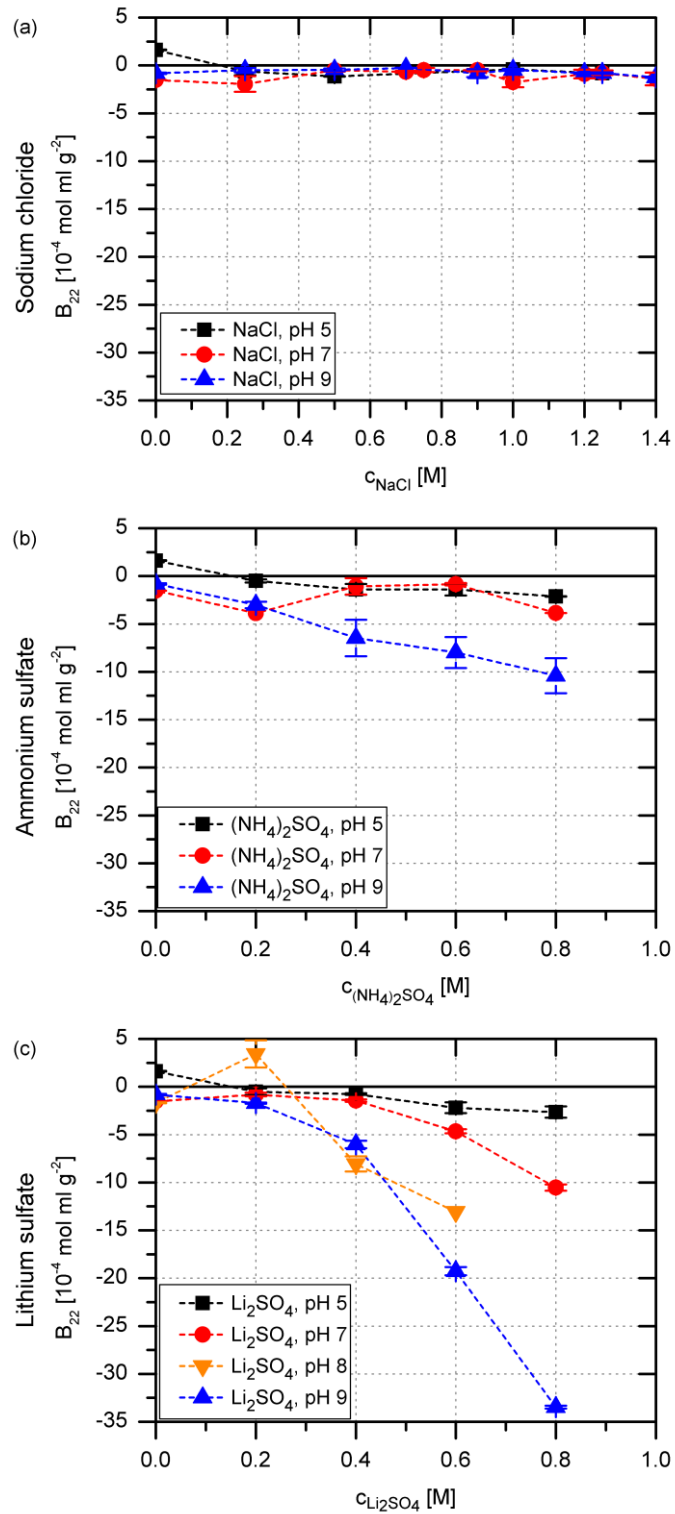


Figure 5.4: B_{22} -values for mAb04c as a function of sodium chloride (a), ammonium sulfate (b) and lithium sulfate (c) concentration for varying pH-values

5.3.4 Crystallization slot: Correlation of B_{22} -values and macroscopic phase behavior

To evaluate the validity of various reports of crystallization slots for antibodies [17,20,27], selected 2D-phase diagrams extracted from a multiparameter screening program [6] combined with measured B_{22} -values and experimental solubility data for mAb04c are shown in figure 5.5. Illustrated cases for mAb04c combine experimentally determined B_{22} , solubility values and macroscopic phase behavior for lithium sulfate at pH 7, 8 and 9. For ammonium sulfate B_{22} -values and solubility data are plotted at pH 7 and 9. Macroscopic phase behavior for the two systems with ammonium sulfate was determined at pH 7.2 ± 0.2 and pH 8.5 ± 0.2 respectively. Protein concentration values for the different phase states and the solubility line refer to the left axis and B_{22} -values to the right axis. From all plots the same qualitative picture arises. Clear solutions are present at low salt concentrations and B_{22} -values close to zero. The higher the salt concentration is, the higher is the aggregation probability, the lower is the negative B_{22} and the lower is the solubility of the protein. This decrease in B_{22} and solubility is more pronounced at pH-values close to the pI of the protein as shown for mAb04c (pI 8.3 - 8.8) and lithium sulfate. In general the absolute level of solubility and B_{22} are lower with lithium sulfate than with ammonium sulfate at the same salt concentrations. Moreover, the aggregation of mAb04c in the presence of lithium sulfate is induced at lower salt concentrations than for ammonium sulfate.

Although the B_{22} -decrease is stronger for lithium sulfate, the crystallization probability is higher and needle-shaped crystals were formed. The crystallization probability for lithium sulfate is high in a pH-range from 7 to 9 and salt concentrations of 0.35 - 0.9 M. These crystals were obtained from white-gray aggregates which were built first in solution. No LLPS in form of droplets was visible and crystals were obtained from aggregates in solution. With increasing salt concentration the phase transition started earlier and the crystal size was decreasing. In the presence of ammonium sulfate, crystallization of mAb04c occurred only near the pI of mAb04c (pH 8.5) with salt concentrations of 0.5 - 0.75 M, whereby the first phase transition was delayed. In all cases the precipitation occurred instantaneously.

The corresponding B_{22} -values in figure 5.5 are in the span from 0 to a broad range of negative values, especially for lithium sulfate at pH 8 and pH 9. Some of these B_{22} -values are in the postulated crystallization slot of $-8 \cdot 10^{-4} < B_{22}/(\text{mol mL g}^{-2}) < -1 \cdot 10^{-4}$ of George and Wilson [13], but crystals are also detected for systems with B_{22} -values outside this range. Analogous stable conditions or precipitation occurred for values within the George and Wilson crystallization slot. Overall crystallization was only achieved for mAb04c with lithium sulfate and ammonium sulfate (data for mAb02a and mAb05a not shown).

In summary, a comparison of the crystallization probability and B_{22} -values within the crystallization slot cannot be considered satisfactory as for various systems with model proteins [14]. For some conditions, crystallization did not occur within the crystallization slot while for others crystals were obtained over a broad range of negative B_{22} -values, also well below the crystallization slot. A shift of the crystallization slot to B_{22} -values closer to zero as Haas et al. [20] propagated could neither be observed for the antibodies in this work nor for other mAbs [17,29]. In contrary, an expansion to lower B_{22} -values seems reasonable for different mAbs including mAb04c. Therefore, the classical crystallization slot of George and Wilson [13] is not applicable for mAb04c. A potential explanation might lie in the fact that antibodies are larger in size compared to most model proteins used by George and Wilson [13]. Moreover mAbs have a higher molecular surface area to molecular weight ratio than other proteins. According to Lewus et al. [29,17] further parameters such as kinetics influence the type of phase transition. This might go hand in hand with the high anisotropy of mAb04c, which is implied by the low determined A-value. Finally, molecular flexibility as introduced through the hinge region of antibodies might be an important factor determining the ability to crystallize.

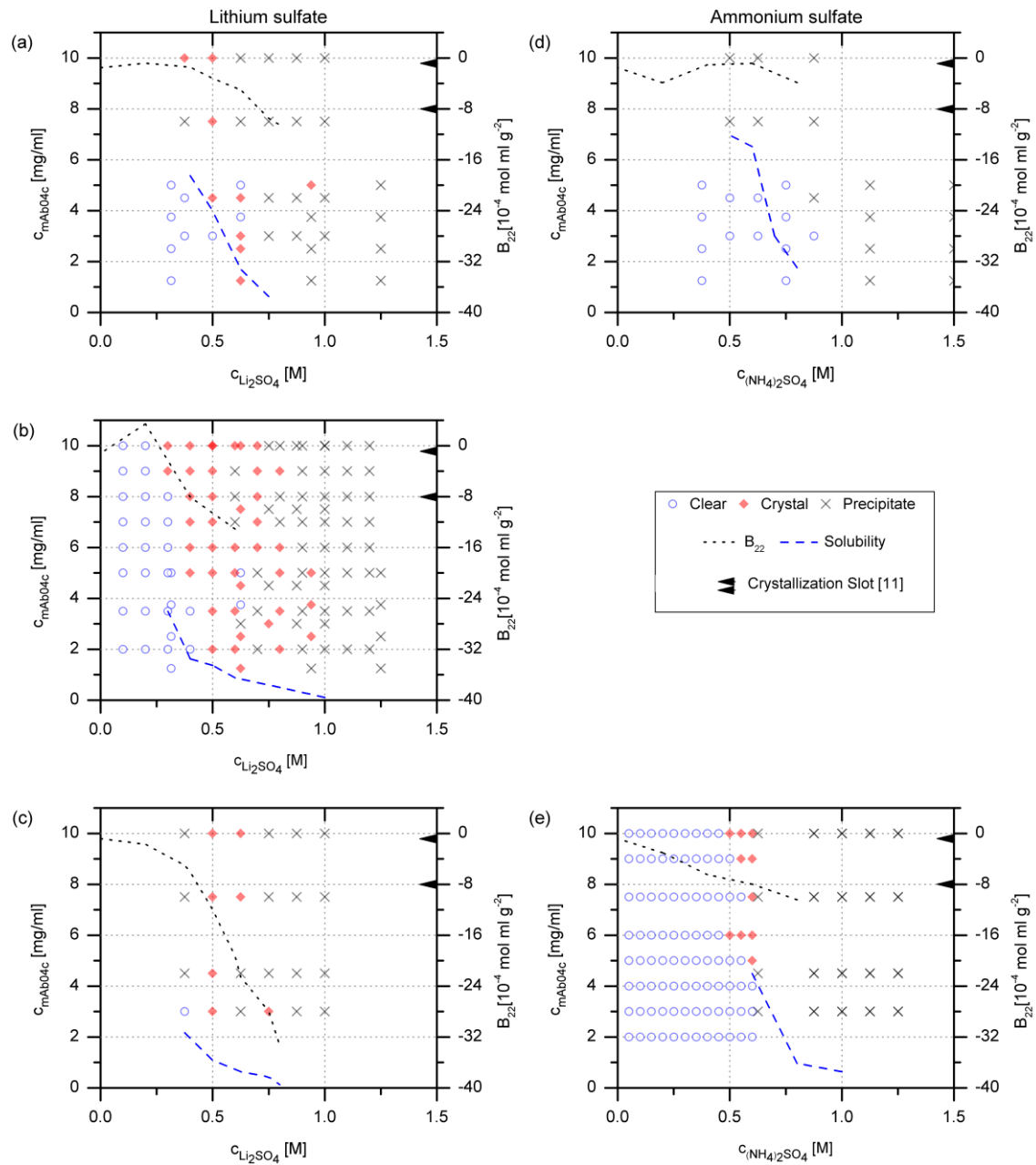


Figure 5.5: left y-axes: Phase diagram dependent on antibody and sulfate salt concentration, dashed line: solubility, right y-axes: dotted line: the corresponding B_{22} -value, arrows: crystallization slot according to George and Wilson [13]; mAb04c (a-c) lithium sulfate (pH 7, 8, 9) (d, e) ammonium sulfate (pH 7, phase diagram pH 7.2 ± 0.2 ; pH 9; phase diagram pH 8.5 ± 0.2)

5.3.5 Phase diagram: Correlation of B_{22} -values and solubility

Thermodynamic correlations between B_{22} and solubility have been postulated by several researchers [24,25,39]. A detailed investigation of the applicability of these models to antibody structures is however still missing. The solubility of mAb04c under different conditions is plotted as a function of B_{22} -values in figure 5.6. The broad B_{22} range includes mainly crystallizing but also precipitating conditions, the systems comprise variations in the type and concentration of added salt at various pH values (see table 5.1). An increase in B_{22} correlates closely to an increase in solubility for all investigated conditions. In figure

5.6 (a) data were fitted with the HDW-model (equation (5.2)) using a Levenberg-Marquardt iteration. The A -value was determined to $5.57 \cdot 10^{-6}$ and the coordination number z to 2. The corresponding corrected R^2 was calculated to 82 %. In addition, the literature data for universal solubility lines determined with the HDW-model of Lysozyme ($A = 0.01$, $z = 4$) [25], equine serum albumin ($A = 0.072$, $z = 6$) and ovalbumin ($A = 0.084$, $z = 6$) [47] are plotted in figure 5.6 (a). The A -value is a factor 10^3 higher for the three proteins and the coordination number varies compared with mAb04c. These differences cause a higher solubility for negative B_{22} -values closer to zero compared with mAb04c. However, lysozyme shows a higher solubility for B_{22} -values between -30 and $-5 \cdot 10^{-4}$ mol mL g^{-2} in comparison to ESA and Ovalbumin, whose solubility reach comparable values to mAb04c. Toward lower B_{22} -values the solubility lines converge for all proteins.

In figure 5.6 (b) the same data were used in combination with the RSL-model [24]. The literature data [24,39] for Lysozyme, ESA and Ovalbumin are additionally plotted. The mAb04c-data fulfill the requirements of solubilities lower than 30 mg/mL. The Levenberg-Marquardt iteration results in expected ranges for a K -value close to unity ($K = 0.888$) and a negative A_c -value of -2.147 . With a corrected R^2 of 84 % the data points are well represented by the RSL-model. Compared with the other proteins the solubility is lower for the same B_{22} -values above a B_{22} -value of $-7 \cdot 10^{-4}$ mol mL g^{-2} . These deviations result from the determined A_c and K -values, which seem to reflect charge and molecular weight differences of the proteins [24]. However, a relation to specific molecular properties could not be identified in this work nor by Ruppert et al. [24]. At low B_{22} -values the model shows a sharp increase in the B_{22} -values to lower solubility, whereby the unique model character is not fulfilled. As shown by the literature data, this increase is found in all other systems [24], whereby the corresponding lowest modeled B_{22} -value depends on the protein. At present we agree with Ruppert et al. [24] that this seems to be a mathematical artifact of the model formulation. We thus did not further apply this model. Likewise empirical models from Mehta et al. [39] are not discussed, since the corrected R^2 was smaller than 80 % and no additional information was gained.

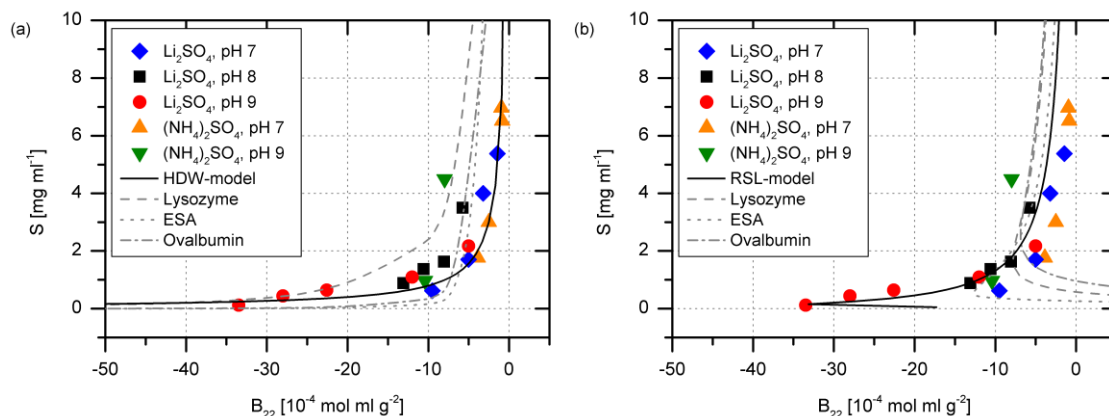


Figure 5.6: Experimental and theoretical solubility line for mAb04c with lithium sulfate and ammonium sulfate: (a) HDW-model: $A = 5.57 \cdot 10^{-6}$ and $z = 2$, literature data [25,47], (b) RSL-model: $K = 0.888$ and $A_C = -2.147$, literature data: [24,39]

The HDW-model shows the possibility to fit the solubility data for mAb04c in various solvent conditions with a general solubility line dependent on B_{22} -values (figure 5.6 a). The fact that crystallization and precipitation are represented by the same solubility line has variable explanations. Technically precipitate or microcrystals can often not clearly be differentiated visually by a microscope [48]. Moreover, no B_{22} -determination with SLS was possible for strong precipitating conditions with salt concentrations above 0.8 M. Thus systems incorporated in the data were considered to be nearby crystallization conditions, so that microcrystalline structures below the resolution limit are possible. The position of the transition from crystallization to precipitation in these systems is considered to be explicitly determined [48]. Therefore the structure of the protein probably remains and the transition from precipitate to crystal might also be possible in this regime [49]. Given that the phase separation between solid phase and liquid phase should be thermodynamically controlled as long as no denaturation has taken place, almost the same solubility line might be reached for precipitate and crystals for low B_{22} -values as shown in figure 5.1. The latter is not valid if the system is kinetically hindered [50] or if the solubility varies with different crystal forms respectively different coordination numbers obtained [24,25,51]. In case of mAb04c it thus seems to be more appropriate to classify the precipitated samples as a liquid-solid than a liquid-liquid phase separation, as Ahamed et al. [27] proposed for the system with IDEC-152. An extrapolation of the solubility line toward the precipitation points in the phase diagram (figure 5.7) confirms the further decrease in solubility for precipitating solution conditions.

The model fit of the solubility data resulted in a coordination number of $z = 2$ and $A = 5.57 \cdot 10^{-6}$ at a corrected error square $R^2 = 82\%$. The coordination number of $z = 2$ is not common for proteins, but neither exceptional for antibodies as shown in the Biological Macromolecule Crystallization Database (BMCD)-entries 1FL5_37948 [52] and 1IGT_52583 [40] (<http://xpdb.nist.gov:8060/BMCD4/index.faces>). The needle form of the crystals obtained further justifies the low coordination number.

In protein crystallization the proteins need to adjust their orientation to each other [20,22]. Crystallization ability is dependent on the anisotropy of the protein structure [25,28]. Rising protein anisotropy ($A \ll 1$) causes progressively directionally dependent interactions between the protein molecules. mAb04c has an A -value of $5.57 \cdot 10^{-6}$, which is by a factor of 10^3 smaller than for lysozyme ($A = 0.01$, $z = 4$) [25]. This implies a relatively high anisotropy. Demoruelle et al. [47] determined the molecular solubility as a function of B_{22} with A -values of 0.072 and 0.084 for equine serum albumin ($z = 6$) and ovalbumin ($z = 6$) applying the same HDW-model. Nevertheless the differences of these molecules to antibodies are significant, since antibodies are more complex and with about 150 kDa larger in size than the three other proteins [25,47]. Moreover, the high anisotropy and molecular flexibility in the hinge region of antibodies might explain partly why it is more difficult to crystallize antibodies and if one succeeds crystals with a low coordination number are obtained.

For mAb05a and mAb02a, no crystallization was observed in the investigated systems (data not shown), although the B_{22} -values were in the range of the crystallization slot. In both cases precipitation as well as gelation occurred. The latter is described as a state in which a further orientation of the molecules to each other is kinetically hindered and dynamically arrested [17]. Therefore solubility line was not determined, but the behavior implies a high anisotropy.

5.3.6 Phase diagram of mAb04c

It would be beneficial to have a universal protein phase diagram to control phase behavior. In theory a universal phase diagram can be obtained from thermodynamics if simplifications and assumptions are applied as stated by Haas and Drenth [20]. The result is a correlation of the B_{22} and the protein volume fraction to describe the different aggregation states in a phase diagram as shown in equations (5.5) - (5.10). However, these models have to be correlated and validated with experimental data. Crystallization processes rely heavily on the coordinates and extension of the metastable region [48,53]. Thus, it is mandatory to determine the layout of the metastable region as exact as possible.

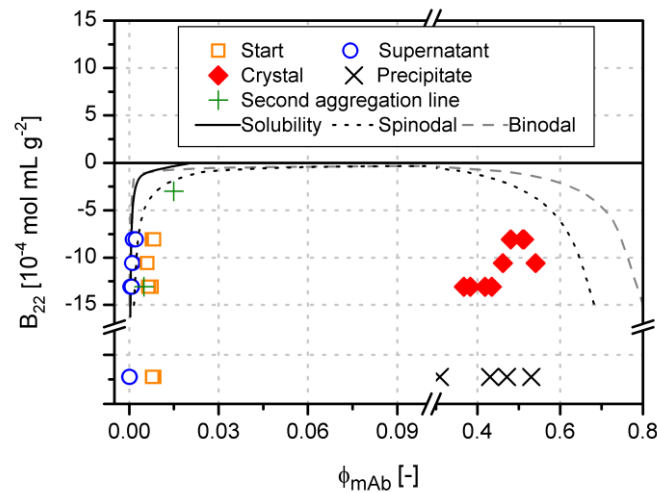


Figure 5.7: Phase diagram of the B_{22} over the volume fraction for mAb04c with lithium sulfate at pH 8, the x and y -axis are broken; solubility, binodal and spinodal are modeled according to Haas and Drenth [20,25]

In figure 5.7 this is attempted exemplarily for mAb04c with lithium sulfate at pH 8. From theory the B_{22} is independent of protein concentration in diluted solutions but dependent on the applied salt concentration. Hence, we fitted the B_{22} -values obtained for pH 8 and lithium sulfate depicted in figure 5.4 (c). To expand the phase diagram with precipitating conditions, additional experimental data from phase behavior studies for a lithium sulfate concentration of 1 M are plotted without a corresponding B_{22} -value. For these conditions the experimental B_{22} -determination with SLS was impossible due to aggregation in solution. From theoretical considerations and comparison of the phase behavior their qualitative position should be below the B_{22} -values obtained for 0 - 0.6 M lithium sulfate. The systems chosen (starting conditions) showed initially a one-phase system which separated into a protein lean phase (supernatant) and a protein rich phase in form of white gray aggregates. From the latter crystals formed under different conditions. The time frame and the trends are described in detail in Rakel et al.[6]. For both phases the volume fraction of the mAb after equilibration was determined as described above. Resulting equilibrium compositions of the supernatant feature a varying protein fraction of $0.4 \cdot 10^{-3}$ - $2.2 \cdot 10^{-3}$ with a mean standard deviation of $2.8 \cdot 10^{-4}$. The protein volume fraction of the solid phase (crystals and precipitate) was determined to 0.34 - 0.54 and tends to decrease with decreasing B_{22} . These volume fractions of the solid phase (crystals and precipitate) correspond to a mean protein concentration of $620 (\pm 101)$ mg/mL. The determined mean antibody volume fraction of the crystal (0.43 ± 0.065) is in the range of reported protein the literature values of 0.37 [27] and 0.5 [26]. Higher values for protein volume fractions were obtained with higher B_{22} -values. This might be the result of a slower crystal growth rate and a more compact crystal structure with less integrated water in the crystal. The second aggregation line was defined by systems showing instantaneous precipitation as described above and defined as such by Dumetz et al [28] and Lewus et al [17]. As shown

for the system mAb04c and lithium sulfate at pH 8 in figure 5.7, crystallization occurred mainly in the range between solubility line and second aggregation line. The composition of the binodal could not be measured, since the crystallization kinetic is fast and the metastable equilibrium not distinguishable.

The binodal and spinodal were determined according to the introduction and are integrated in figure 5.7. The lean phase of the modeled binodal intersects the solubility line at a B_{22} value of about $-1 \cdot 10^{-4} \text{ mol mL g}^{-2}$ and converges to a volume fraction of 0. The lean phase of the spinodal lies between the second aggregation line and the solubility line. The binodal and the spinodal run almost parallel to x-axis and over the critical point, which is the contact point of binodal and spinodal, until they decrease faster at protein volume fractions above 0.4. Overall, the comparison of experimental with modeled data shows that the differences between theory and reality are quite high. According to figure 5.1, the positions of the binodal and spinodal are expected to be in between solubility line and the solid phase. The volume fractions of the protein rich phases of binodal and spinodal are modeled significantly too high. The course of the binodal on the protein lean side adopts values for the protein volume fraction lower than described by the solubility line which is thermodynamically not reasonable. Hence, the model does not give additional information about the system behavior. Overall, the results prove that the simplifications of thermodynamic principles including the B_{22} are not applicable to describe phase behavior of complex and large molecules such as monoclonal antibodies.

To analyze the reasons, we take a closer look on the parameters necessary to solve the binodal and spinodal according to equations (5.5) - (5.10):

- Ω : the volume of an intact mAb molecule was adopted to $\Omega=166.5 \text{ nm}^3$ from Ahamed et al. [27]. This value was calculated from experimental data of a mAb crystal with a unit cell volume (2 molecules/unit cell) of 900 nm^3 , and the protein volume fraction of the crystal of 0.37 [54].
- m : $m = \Omega/\omega$ is the number of water molecules, which have the same volume like one protein molecule, whereby ω is the molar volume of the water (18.016 mL/mol) divided by the Avogadro number and is assumed as 5552.8.
- ϕ_c : the volume fraction of a mAb crystal was assumed as 0.37 [40].

Following parameters vary depending on the systems and can be compared with experimental data:

- $g_\lambda = kT\phi_c(B_{22}M\rho_P^{-4})$: This parameter describes protein-protein interactions in solution and is determined with the B_{22} .
- ϕ_α, ϕ_β : The protein volume fractions ϕ_α and ϕ_β represent the protein lean phase respectively the protein dense phase the binodal.

- $\phi^*_\alpha, \phi^*_\beta$: The corresponding volume fractions of the protein for the spinodal.

It is appropriate to assume Ω and m as constant parameters, since these values should not strongly change over the analyzed range. The deviation due to a false value would impact all results in the same way. From experimental data it seems that ϕ_c is dependent on the B_{22} -value. This is not surprising, since the size and the structure of the crystals vary. These differences are expected to be bigger for systems with varying crystal habits in the analyzed range. However, as long as g_λ is substituted by equation (5.6) this parameter will not influence the results as it can be eliminated as shown in equation (5.14):

$$G_\lambda(\phi_P) = \frac{k_B T}{\Omega} \left[\phi_P^2 (B_{22} M_W \rho_P - 4) + \phi_P (\ln(\phi_P) - \ln(m)) - \left\{ \frac{\phi_P - 6\phi_P^2 + 4\phi_P^3}{(1 - \phi_P)^2} \right\} \right] \quad (5.14)$$

The B_{22} -value is a parameter which describes interactions between two molecules in a diluted solution. We used SLS for its determination. Differences exist in the results compared to other techniques, but the results are qualitatively comparable [31,55]. In our case and in the literature it is quite often, that experimental B_{22} -determination is only possible for a small B_{22} -range below 0, because of aggregation in solution with stronger attraction. Hence, only a part of the phase diagram could be determined as shown by the missing B_{22} -values. Moreover, it is questionable, if this parameter can solely describe a solution composition in which aggregation occurs or if such a solution has to be characterized as a non-diluted system. Then, a truncation of the virial expansion after a higher order term has to be considered and additional virial coefficients have to be determined [56,57]. Especially for macromolecular precipitants the use of osmotic second virial cross coefficients is also discussed in the literature [58]–[61]. This value describes cross-interactions between protein and precipitant. Whether or not this parameter can be neglected needs further investigation.

For experimental determination of the volume fractions of the binodal a LLPS is essential. A LLPS as stated by Haas and Drenth [20] should appear as two clear liquid phases in form of droplets with their metastable equilibrium on the binodal. In real systems, the appearance of two phases in protein solutions differ from droplets to gray or white precipitate depending on the protein and the systems used [27,28,62]. The boundaries are not clear and some authors define aggregates, flocks and/or precipitate as dense phase of a LLPS [27,63,64]. Sometimes it is not distinguished between LLPS and gelation in literature as demonstrated by Dumetz et al. [28]. According to Cheng et al. [65] and Dumetz et al. [28] precipitate and gel is a non-equilibrium state and can be defined as a frustrated liquid-liquid phase separation, which is kinetically trapped and, hence, not

consistent with the dense phase of the LLPS. Different experimental techniques in the literature exist to determine the composition of the two phases of a LLPS. Often cloud-point measurements are conducted [62,66], but these do not represent an equilibrated state (binodal), since the range between spinodal and binodal is metastable and the separation starts somewhere in between. Moreover experimental determination of the cloud-point as a function of precipitant concentration is extremely difficult, because all parameters except the precipitant concentration have to be kept constant [27,50]. Another method uses centrifugation to separate the two phases after equilibration, which involves an impact of external forces on the system and disturbed the equilibria [28]. Moreover, centrifugation cannot be used to determine the binodal for systems in which crystallization processes are fast or in which centrifugation induces heterogeneous nucleation [67]. The analysis of a LLPS with confocal laser scanning microscopy seems to be advantageous [67]. However, dye is coupled on the protein and additive surface and influences the equilibrium as well.

The volume fractions of the spinodal cannot be analyzed, since instantaneous separation occurs and the concentrations of the two phases are not determinable. Moreover, in every real system kinetic phenomena are present [50,68], so that theoretical values cannot be reached. A qualitative picture is obtained with the experimental determination of the second aggregation line in the literature and this work.

Finally, we have to mention, that for other conditions with varied salt type and/or pH, the crystallization range is shifted to the solubility line with respect to B_{22} and protein volume fraction as demonstrated in figure 5.4. For these examples the crystallization range is smaller, respectively crystallization success is not guaranteed. In addition instantaneous separation and therefore the position of the second aggregation line is shifted to lower volume fractions [6]. Thus, the crystallization range and the second aggregation line depend on the sample composition, although the solubility line is universal and describes different conditions. One reason is the cross influence of kinetic phenomena [50,68]. According to this, the used models cannot describe the antibody phase behavior in a universal phase diagram by means of B_{22} and protein volume fraction.

The validation of theoretical models with experimental data is still difficult due to a combination of missing precise experimental data and techniques and simplified thermodynamic models. However, it could be shown, that theory and reality vary in a non-acceptable range. The conditions used are complex due to different ingredients and complex large protein molecules in solution. Under these aspects it is understandable, that different protein molecules and varying solvent conditions cannot fit in such a simple scheme. The complexity of the protein and kinetic phenomena has to be considered. This could be shown for the monoclonal antibody, as the theoretical binodal and spinodal do not

represent the reality. However, the established solubility line can be seen as universal. Thus, the solubility of native proteins is driven thermodynamically.

5.4 Conclusion

The B_{22} -value is commonly used to describe protein phase behavior, but there is still a lack in between what we expect the B_{22} value is able to describe and what the B_{22} can describe. Therefore this work tends to identify the current application limits.

The B_{22} was successfully applied to describe antibody interactions in solution. Corresponding correlations agree with the Hofmeister Series of kosmotropic strength. The probability of aggregation is described, but on the basis of this work a constitutional differentiation between crystals and precipitation in form of a crystallization slot is not possible. The application of the thermodynamic model according to Haas and Drenth [20] to describe a whole phase diagram is not possible since the modeled binodal and spinodal do not represent the reality. Kinetic phenomena and the complexity of the systems analyzed have to be taken into account. However, the theoretical approach of Haas et al. [25] to correlate the solubility with the B_{22} was successfully applied for mAb04c. The determined values for coordination number and anisotropy are conclusive. Thus, the solubility seems to be thermodynamically driven.

The conducted extensive study on the protein phase behavior of a monoclonal antibody will help on the way of understanding mechanisms on the molecular and thermodynamic basis. A fundamental understanding is the key for a reduction of experimental effort in regard to screening of crystallization conditions and especially for all steps in downstream processing.

5.5 Acknowledgements

The authors are grateful for support from the BMBF (Federal Ministry of Education and Research), grant no. 0315338B and Boehringer Ingelheim Pharma GmbH & Co. KG, Biberach, Germany.

5.6 Abbreviations

| | | |
|----------|---------------------------------|-----------------------------------|
| B_{22} | $10^{-4} \text{ mol mL g}^{-2}$ | Osmotic second virial coefficient |
| π | Pa | Osmotic pressure |
| R | 8.31 J/(mol K) | Universal gas constant |

| | | |
|--------------------------|--|---|
| T | K | Temperature |
| R_{θ} | cm^{-1} | Rayleigh ratio |
| N_A | $6.022 \cdot 10^{23} \text{ mol}^{-1}$ | Avogadro constant |
| M_W | g/mol | Molecular weight |
| n_0 | - | Refractive index of the solvent |
| dn/dc_P | mL/g | Refractive index increment |
| k | $1.381 \cdot 10^{-23} \text{ J/K}$ | Boltzmann constant |
| $m = \Omega/\omega$ | - | Number of water molecules, which have the equivalent volume as one protein molecule |
| Ω | nm^3 | Volume of one protein molecule |
| ω | nm^3 | Molar volume of water V_W divided by the Avogadro number N_A |
| V_W | 18.051 mL/mol | Molar volume of water |
| z | - | Coordination number of the protein crystals |
| A | - | Adjustable parameter in HDW-model |
| ν | - | Range of interaction |
| $V_P = \Omega \cdot N_A$ | mL/mol | Partial molar volume of the protein at infinite dilution in the aqueous solution |
| A_C, K | - | Adjustable parameters in RSL-model |
| G_{λ} | J | Gibbs energy |
| g_{λ} | J | Parameter for protein-protein interactions |
| s | mg/mL | Solubility |
| ϕ | - | Volume fraction |
| c | mg/mL or M | Concentration |
| ρ | mg/mL | Density |
| m | mg | Mass |

General Indices

| | |
|-------------|--------------------|
| P | Protein |
| <i>Salt</i> | Salt |
| α | Protein lean phase |
| γ | Protein rich phase |
| * | Spinodal |
| c | Crystal |

Indices for experimental data

| | |
|------------|--|
| <i>pro</i> | Protein |
| <i>ini</i> | Initial |
| <i>liq</i> | Obtained filtrate |
| <i>crs</i> | Crystal |
| <i>eql</i> | After phase separation and equilibration |

Notations

| | |
|-------------|---|
| <i>BMCD</i> | Biological Macromolecule Crystallization Database |
| <i>HDW</i> | Haas-Drenth-Wilson |
| <i>RSL</i> | Ruppert-Sandler-Lenhoff |
| <i>SLS</i> | Static light scattering |

5.7 Literature Cited

- [1] Lightfoot EN, Moscariello JS. Bioseparations. *Biotechnol Bioeng.* 2004;87:259–73.
- [2] Randolph TW, Carpenter JF. Engineering challenges of protein formulations. *AIChE J.* 2007;53:1902–1907.
- [3] Bondos SE, Bicknell A. Detection and prevention of protein aggregation before, during, and after purification. *Anal Biochem.* 2003;316:223–231.
- [4] Rupp B. Maximum-likelihood crystallization. *J Struct Biol.* 2003;142:162–169.
- [5] Jaenicke R. Stability and stabilization of globular proteins in solution. *J Biotechnol.* 2000;79:193–203.
- [6] Rakel N, Baum M, Hubbuch J. Moving through three-dimensional phase diagrams of monoclonal antibodies. *Biotechnol Prog.* 2014;30:1103–13.
- [7] Arakawa T, Timasheff SN. Mechanism of protein salting in and salting out by divalent cation salts: balance between hydration and salt binding. *Biochemistry.* 1984;23:5912–5923.
- [8] Van Oss CJ. Hydrophobicity of biosurfaces - Origin, quantitative determination and interaction energies. *Colloid Surf B Biointerfaces.* 1995;5:91–110.
- [9] Leckband D, Israelachvili J. Intermolecular forces in biology. *Q Rev Biophys.* 2001;34:105.
- [10] Neal BL, Lenhoff AM. Excluded volume contribution to the osmotic second virial coefficient for proteins. *AIChE J.* 1995;41:1010–1014.
- [11] Johnson DH, Parupudi A, Wilson WW, DeLucas LJ. High-throughput self-interaction chromatography: applications in protein formulation prediction. *Pharm Res.* 2009;26:296–305.
- [12] Le Brun V, Friess W, Bassarab S, Mühlau S, Garidel P. A critical evaluation of self-interaction chromatography as a predictive tool for the assessment of protein-protein interactions in protein formulation development: a case study of a therapeutic monoclonal antibody. *Eur J Pharm Biopharm.* 2010;75:16–25.

- [13] George A, Wilson WW. Predicting protein crystallization from a dilute solution property. *Acta Crystallogr D Biol Crystallogr*. 1994;50(Pt 4):361–365.
- [14] Wilson WW. Light scattering as a diagnostic for protein crystal growth—A practical approach. *J Struct Biol*. 2003;142:56–65.
- [15] Pjura PE, Lenhoff AM, Leonard SA, Gittis AG. Protein crystallization by design: chymotrypsinogen without precipitants. *J Mol Biol*. 2000;300:235–239.
- [16] Gabrielsen M, Nagy LA, DeLucas LJ, Cogdell RJ. Self-interaction chromatography as a tool for optimizing conditions for membrane protein crystallization. *Acta Crystallogr D Biol Crystallogr*. 2010;66(Pt 1):44–50.
- [17] Lewus RA, Darcy PA, Lenhoff AM, Sandler SI. Interactions and phase behavior of a monoclonal antibody. *Biotechnol Prog*. 2010;27:280–289.
- [18] Vivarès D, Bonneté F. X-ray scattering studies of *Aspergillus flavus* urate oxidase: towards a better understanding of PEG effects on the crystallization of large proteins. *Acta Crystallogr Sect D Biol Crystallogr*. 2002;58:472–479.
- [19] Ebel C, Faou P, Zaccai G. Protein–solvent and weak protein–protein interactions in halophilic malate dehydrogenase. *J Cryst Growth*. 1999;196:395–402.
- [20] Haas C, Drenth J. The protein–water phase diagram and the growth of protein crystals from aqueous solution. *J Phys Chem B*. 1998;102:4226–4232.
- [21] Elcock AH, McCammon JA. Calculation of weak protein-protein interactions: the pH dependence of the second virial coefficient. *Biophys J*. 2001;80:613–25.
- [22] Neal BL. Molecular origins of osmotic second virial coefficients of proteins. *Biophys J*. 1998;75:2469–2477.
- [23] Neal BL, Asthagiri D, Velev OD, Lenhoff AM, Kaler EW. Why is the osmotic second virial coefficient related to protein crystallization? *J Cryst Growth*. 1999;196:377–387.
- [24] Ruppert S, Sandler SI, Lenhoff AM. Correlation between the osmotic second virial coefficient and the solubility of proteins. *Biotechnol Prog*. 2001;17:182–187.
- [25] Haas C, Drenth J, Wilson WW. Relation between the solubility of proteins in aqueous solutions and the second virial coefficient of the solution. *J Phys Chem B*. 1999;103:2808–2811.
- [26] Haas C, Drenth J. The interface between a protein crystal and an aqueous solution and its effects on nucleation and crystal growth. *J Phys Chem B*. 2000;104:368–377.
- [27] Ahamed T, Esteban BNA, Ottens M, et al. Phase behavior of an intact monoclonal antibody. *Biophys J*. 2007;93:610–619.

- [28] Dumetz AC, Chockla AM, Kaler EW, Lenhoff AM. Protein phase behavior in aqueous solutions: crystallization, liquid-liquid phase separation, gels, and aggregates. *Biophys J*. 2008;94:570–583.
- [29] Lewus R a, Levy NE, Lenhoff AM, Sandler SI. A comparative study of monoclonal antibodies. 1. phase behavior and protein-protein interactions. *Biotechnol Prog*. 2014;3–11.
- [30] Roux KH, Strelets L, Michaelsen TE. Flexibility of human IgG subclasses. *J Immunol*. 1997;159:3372–3382.
- [31] Rakel N, Schleining K, Dismar F, Hubbuch J. Self-interaction chromatography in pre-packed columns: a critical evaluation of self-interaction chromatography methodology to determine the second virial coefficient. *J Chromatogr A*. 2013;1293:75–84.
- [32] Zimm BH. The scattering of light and the radial distribution function of high polymer solutions. *J Chem Phys*. 1948;16:1093.
- [33] Scherer TM, Liu J, Shire SJ, Minton AP. Intermolecular interactions of IgG1 monoclonal antibodies at high concentrations characterized by light scattering. *J Phys Chem B*. 2010;114:12948–12957.
- [34] Sahin E, Grillo AO, Perkins MD, Roberts CJ. Comparative effects of pH and ionic strength on protein-protein interactions, unfolding, and aggregation for IgG1 antibodies. *J Pharm Sci*. 2010;99:4830–4848.
- [35] Salinas BA, Sathish HA, Bishop SM, Harn N, Carpenter JF, Randolph TW. Understanding and modulating opalescence and viscosity in a monoclonal antibody formulation. *J Pharm Sci*. 2010;99:82–93.
- [36] Muschol M, Rosenberger F. Interactions in undersaturated and supersaturated lysozyme solutions: static and dynamic light scattering results. *J Chem Phys*. 1995;103:10424.
- [37] Bergfors T. *Protein Crystallization*, 2nd ed. Bergfors T, editor. La Jolla: International University Line; 2009.
- [38] Fischer H, Polikarpov I, Craievich AF. Average protein density is a molecular-weight-dependent function. *Protein Sci*. 2004;13:2825–2828.
- [39] Mehta CM, White ET, Litster JD. Correlation of second virial coefficient with solubility for proteins in salt solutions. *Biotechnol Prog*. 2011;28:163–170.
- [40] Harris LJ, Larson SB, Hasel KW, McPherson A. Refined structure of an intact IgG2a monoclonal antibody. *Biochemistry*. 1997;36:1581–1597.
- [41] Chernov A. Protein crystals and their growth. *J Struct Biol*. 2003;142:3–21.
- [42] Wang W. Instability, stabilization, and formulation of liquid protein pharmaceuticals. *Int J Pharm*. 1999;185:129–188.

- [43] Zhang Y, Cremer PS. Chemistry of Hofmeister anions and osmolytes. *Annu Rev Phys Chem.* 2010;61:63–83.
- [44] Collins KD. Ions from the Hofmeister series and osmolytes: effects on proteins in solution and in the crystallization process. *Methods.* 2004;34:300–311.
- [45] Baldwin RL. How Hofmeister ion interactions affect protein stability. *Biophys J.* 1996;71:2056–2063.
- [46] Curtis RA, Ulrich J, Montaser A, Prausnitz JM, Blanch HW. Protein-protein interactions in concentrated electrolyte solutions. *Biotechnol Bioeng.* 2002;79:367–380.
- [47] Demoruelle K, Guo B, Kao S, et al. Correlation between the osmotic second virial coefficient and solubility for equine serum albumin and ovalbumin. *Acta Crystallogr Sect D Biol Crystallogr.* 2002;58:1544–1548.
- [48] Chayen NE, Saridakis E. Protein crystallization: from purified protein to diffraction-quality crystal. *Nat Methods.* 2008;5:147–153.
- [49] Ng JD, Lorber B, Witz J, Théobald-Dietrich A, Kern D, Giegé R. The crystallization of biological macromolecules from precipitates: evidence for Ostwald ripening. *J Cryst Growth.* 1996;168:50–62.
- [50] Asherie N. Protein crystallization and phase diagrams. *Methods.* 2004;34:266–272.
- [51] Muschol M, Rosenberger F. Liquid–liquid phase separation in supersaturated lysozyme solutions and associated precipitate formation/crystallization. *J Chem Phys.* 1997;107:1953.
- [52] Yin J, Mundorff EC, Yang PL, et al. A comparative analysis of the immunological evolution of antibody 28B4. *Biochemistry.* 2001;40:10764–10773.
- [53] Durbin SD, Feher G. Protein crystallization. *Annu Rev Phys Chem.* 1996;47:171–204.
- [54] Harris LJ, Skaletsky E, McPherson A. Crystallization of intact monoclonal antibodies. *Proteins.* 1995;23:285–289.
- [55] Ahamed T, Ottens M, Van Dedem G, Van der Wielen LAM. Design of self-interaction chromatography as an analytical tool for predicting protein phase behavior. *J Chromatogr A.* 2005;1089:111–124.
- [56] Guo B. Correlation of second virial coefficients and solubilities useful in protein crystal growth. *J Cryst Growth.* 1999;196:424–433.
- [57] Haynes CA, Tamura K, Korfer HR, Blanch HW, Prausnitz JM. Thermodynamic properties of aqueous α -chymotrypsin solution from membrane osmometry measurements. *J Phys Chem.* 1992;96:905–912.

- [58] Yu M, de Swaan Arons J, Smit JA. A simple model for estimating protein solubility in aqueous polymer solutions. *J Chem Technol Biotechnol*. 1994;60:413–418.
- [59] Yu M, de Swaan Arons J. Phase behaviour of globular protein and flexible polymer in an aqueous medium. *Fluid Phase Equilib*. 1996;120:121–129.
- [60] Antipova AS, Semenova MG. Influence of sucrose on the thermodynamic properties of the 11S globulin of *Vicia faba*-dextran-aqueous solvent system. *Food Hydrocoll*. 1997;11:415–421.
- [61] Rakel N, Galm L, Bauer KC, Hubbuch J. Influence of macromolecular precipitants on phase behavior of monoclonal antibodies. *Biotechnol Prog*. 2015;31:145–153.
- [62] Wang Y, Lomakin A, Latypov RF, et al. Phase transitions in human IgG solutions. *J Chem Phys*. 2013;139:121904.
- [63] Shih YC, Prausnitz JM, Blanch HW. Some characteristics of protein precipitation by salts. *Biotechnol Bioeng*. 1992;40:1155–1164.
- [64] Coen CJ, Blanch HW, Prausnitz JM. Salting out of aqueous proteins: phase equilibria and intermolecular potentials. *AIChE J*. 1995;41:996–1004.
- [65] Cheng YC, Lobo RF, Sandler SI, Lenhoff AM. Kinetics and equilibria of lysozyme precipitation and crystallization in concentrated ammonium sulfate solutions. *Biotechnol Bioeng*. 2006;94:177–188.
- [66] Jion AI, Goh L, Oh SKW. Crystallization of IgG1 by mapping its liquid-liquid phase separation curves. *Biotechnol Bioeng*. 2006;95:911–918.
- [67] Vivarès D, Kaler EW, Lenhoff AM. Quantitative imaging by confocal scanning fluorescence microscopy of protein crystallization via liquid-liquid phase separation. *Acta crystal. Sect D, Biol Crystallogr*. 2005;6:819-825
- [68] Jacobsen C, Garside J, Hoare M. Nucleation and growth of microbial lipase crystals from clarified concentrated fermentation broths. *Biotechnol Bioeng*. 1998;57:666–675.

6 Influence of Macromolecular Precipitants on Phase Behavior of Monoclonal Antibodies

Natalie Rakel^{1,2}, Lara Galm¹, Katharina Christin Bauer¹, Juergen Hubbuch¹

¹Section IV: Biomolecular Separation Engineering, Institute of Engineering in Life Sciences, Karlsruhe Institute of Technology, Engler-Bunte-Ring 1, 76131 Karlsruhe, Germany

²Roche Diagnostics GmbH, 68305 Mannheim, Germany

Published in Biotechnology Progress, 2015, 31(1), 145-153

Corresponding author:

Juergen Hubbuch
Karlsruhe Institute of Technology
Institute of Engineering in Life Sciences
Section IV: Biomolecular Separation Engineering
Engler-Bunte-Ring 1, 76131 Karlsruhe, Germany
Phone: +49-721-608-42557, fax: +49-721-608-46240
E-mail: juergen.hubbuch@kit.edu.

Keywords: Protein interactions, Phase behavior; Monoclonal antibody; Static light scattering; Crystallization

Abstract

For the successful application of protein crystallization as a downstream step, a profound knowledge of protein phase behavior in solutions is needed. Therefore a systematic screening was conducted to analyze the influence of macromolecular precipitants in the form of polyethylene glycol (PEG). First, the influence of molecular weight and concentration of PEG at different pH-values were investigated and analyzed in three-dimensional (3-D) phase diagrams to find appropriate conditions in terms of a fast kinetic and crystal size for downstream processing. In comparison to the use of salts as precipitant, PEG was more suitable to obtain compact 3-D crystals over a broad range of conditions, whereby the molecular weight of PEG is, besides the pH-value, the most important parameter. Second, osmotic second virial coefficients as parameters for protein interactions are experimentally determined with static light scattering to gain a deep insight view in the phase behavior on a molecular basis. The PEG-protein solutions were analyzed as a pseudo-one-compartment system. As the precipitant is also a macromolecule, the new approach of analyzing cross-interactions between the protein and the macromolecule PEG in form of the osmotic second cross-virial coefficient (B_{23}) was applied. Both parameters help to understand the protein phase behavior. However, a predictive description of protein phase behavior for systems consisting of monoclonal antibodies and PEG as precipitant is not possible, as kinetic phenomena and concentration dependencies were not taken into account.

6.1 Introduction

Biopharmaceutical proteins gain rising attention in the modern medicine. Especially monoclonal antibodies (mAb) are of interest for therapeutic and diagnostic reasons. While substantial progress is made in designing and producing antibodies, the downstream part during manufacturing is still a cost intensive and challenging task [1,2]. Moreover high product purity requirements set by the Food and Drug Administration have to be fulfilled, while in the same time dealing with large macromolecular proteins with a high degree of segmental flexibility and chemical heterogeneity [3]. To date only little is known about the phase behavior of antibodies under various solvent conditions, and still, a high effort is laid into trial and error screening experiments.

Protein phase behavior results from interactions of inhomogeneously distributed patches on the protein surface. Whether these interactions are attractive or repulsive strongly depends on the orientation of the protein molecules to each other [4]. The sum of all interaction potentials can be influenced by the type of precipitant and additive in solution. The addition of salts can cause an electrostatic double layer around the protein surface charges which involves a shielding and reduction of repulsive interactions. Moreover, the salt ions compete with the protein for water molecules and dehydrate the protein. While salts induce the protein aggregation by mainly electrostatic and hydrophobic interactions, polymers bring the protein molecules together due to preferential interactions and an osmotic potential. Preferential hydration of the protein results in a steric exclusion of polymers from the protein domain [5]. Moreover, an attractive osmotic potential results from a smaller distance between protein molecules compared with the diameter of the macromolecule, which hinders the polymer to enter the intermediate space [6,7]. The protein molecules attempt to further decrease the distance between each other to reduce the osmotic pressure produced by local concentration gradients [6]. Conversely, polymers as excipients might have an ambivalent character. Polymers with a strong nonpolar character like polyethylene glycol (PEG) can bind to hydrophobic patches on the protein surface, which decreases the hydrophobic interactions between the proteins [5,8]. Compared with salts as precipitant, polymers have the advantage that the aggregation probability and the strength of protein interactions can be controlled by the molecular weight besides the polymer concentration and the type of polymer [9,10]. However, the protein separates more often into a protein rich and a protein poor phase, the so called liquid-liquid phase separation (LLPS) [11]. Starting from this phase separation crystallization is still possible, if the protein rich phase is in a metastable condition. Complex proteins are often crystallized using polymers as precipitant. These polymers are also macromolecules and influence the protein interactions by other forces compared to salts as precipitants [12].

George and Wilson [13] formulated an empirical correlation between protein interactions and crystallization probability of model proteins using the osmotic second virial coefficient (B_{22}) as descriptor. It is part of the virial expansion of the osmotic pressure and describes the pair interaction between protein molecules. The B_{22} can be determined from a dilute solution with methods such as self-interaction chromatography, membrane osmometry, or static light scattering (SLS). In their study a so called “crystallization slot” was defined as a region of slight negative B_{22} -values in which the crystallization probability for the protein under investigation is high. However, it could be shown in several studies that the proposed crystallization slot determined by George and Wilson [13] for small molecules is not directly transferable to more complex and larger molecules such as antibodies [14–17].

Up to now, interactions between proteins and PEG have often been neglected in thermodynamic approaches analyzing protein phase behavior, although, Vivarès et al. [18] proved in simulation of potentials the existence of these interactions. They clearly showed repulsive interactions between protein-PEG and PEG-PEG. These interactions are measurable and might be characterized with the osmotic second cross-virial coefficient (B_{23}) [19]. Attractive interactions between two macromolecules correspond to a negative B_{23} , and complementary results in positive B_{23} -values. Thus, a strong correlation between protein phase behavior and the B_{23} might be expected [20–22]. However, only few publications exist, which deal with the influence of this value on crystallization and precipitation of proteins. McCarty et al. [23] and Cheng et al. [22] confirmed the applicability of the B_{23} for downstream process optimization for a mixture of the model proteins lysozyme and ovalbumin. Accordingly, a negative B_{22} for lysozyme, a positive B_{33} for ovalbumin and a positive B_{23} should lead to conditions where lysozyme crystallizes while ovalbumin stays in solution. When the B_{23} besides the B_{22} and/or B_{33} is slightly negative, the kinetics of a phase transition can be delayed and the selectivity as well as the yield reduced [22,24]. Moreover, for strong negative B_{23} -values the proteins associate and precipitate in a mixture, whereas the formation of mixed crystals is improbable [22]. Besides optimization of crystallization conditions, other separation problems were attempted to be explained using the B_{23} . A correlation between the diafiltration sieving behavior of lysozyme-bovine serum albumin (BSA) mixtures and the B_{23} was found by Tessier et al. [25]. Haynes et al. [19] applied the B_{23} to predict liquid-liquid equilibria, as well as the protein partition coefficients in aqueous two-phase systems. Other authors used the B_{23} to predict phase separation between proteins and polysaccharides by the demixing criterion [26,27]:

$$B_{22}B_{33} < B_{23}^2 \quad (6.1)$$

Given the above it is not clear how and if the use of B_{22} and B_{23} leads to a predictive description of protein phase behavior for systems consisting of mAbs and PEG as precipitant.

In this work, the phase behavior of three antibodies was investigated in three-dimensional (3-D) phase diagrams in dependency of pH, concentration and molecular weight of PEG and protein concentration. The protein interactions were analyzed as a pseudo-one-component system [28] in terms of the B_{22} via SLS neglecting protein-polymer interactions. In a second approach taking protein-polymer interactions into account, the determination of cross-interactions was conducted via SLS, assuming a two component system in solution with interactions between alike molecules (B_{22} for protein, B_{33} for PEG) and unlike molecules in form of the osmotic second cross-virial coefficient (B_{23}). Finally, correlations between the interaction parameters and the protein phase behavior were analyzed

6.2 Material and Methods

6.2.1 Materials

Protein A-purified mAb mAb04c (type IgG4), mAb05a (type IgG1), and mAb02a (type IgG1) in solution were kindly provided from Boehringer Ingelheim Pharma GmbH & Co. KG, Biberach, Germany.

The following chemicals were used: acetic acid, sodium hydroxide (NaOH), 2-(N-morpholino)ethanesulfonic (MES), and PEG 1000 (PEG 1000; Merck KGaA, Darmstadt, Germany); 3-Morpholino-2-Hydroxy-Propanesulfonic Acid (MOPSO), 2-(N-Cyclohexylamino)-Ethanesulfonic Acid (CHES), and ammonium sulfate (Applichem GmbH, Darmstadt, Germany) and 4-(2-Hydroxyethyl)-Piperazine-1-(2-Hydroxy)-Propanesulfonic Acid (HEPPSO) (molekula Germany., Taufkirchen, Germany), PEG 400, 3350, 8000 (PEG 400, PEG 3350, PEG 8000; Sigma-Aldrich GmbH, St. Louis, MO, USA).

6.2.2 Determination of phase diagrams

The preparation, storage and analysis of the samples were conducted according to Rakel et al. [17,29]. The composition of the buffer system with five monoprotic acid components and a constant buffer capacity of 10 mM in the pH-range of 5 - 9 was: 10.05 mM MES, 16.6 mM Acetic acid, 8.9 mM MOPSO, 12.3 mM HEPPSO and 14.4 mM CHES. The required pH-value was titrated with 4 M NaOH. As precipitant PEG of different molecular

weights (400, 1000, 3350, and 8000 Da) were used. A detailed description of the buffer preparation is described in Rakel et al. [17]. The buffer exchange of the antibody samples was conducted several times at 8,000 g and 20°C with Vivaspin 20, Vivaspin 2, or Vivaspin 500 (30 kDa Cutoff PES-membrane, VS2022, VS0222 and VS0122, Sartorius Stedim Biotech, Göttingen, Germany). The desired protein concentration was then adjusted. All prepared buffers and protein samples were filtrated with a 0.2 µm cellulose membrane to avoid contamination and dust particles in the solutions.

The precipitation buffers were produced with the buffer system and the respective precipitant PEG 400 (40 m/V %), 1000 (30 m/V %), 3350 (25 m/V %) or 8000 (25 m/V %). Initial protein concentrations in the starting buffer were 5, 10, 15 and 20 mg/mL. With variation in pH and protein concentration various screening buffer compositions were tested (see table 6.1). Every PEG concentration was combined with every protein concentration at every pH listed in the same row for 20 µl scale experiments in microbatch plates (MRC Under Oil 96 Well Crystallization Plate, Swissci AG, Neuheim, Switzerland) using a robotic platform (Tecan infinite®M200, Tecan Group, Crailsheim, Germany). The visual examination of the protein phase behavior was conducted with an imaging system (Rock Imager 54, Formulatrix, Waltham, MA, USA, Software Rock Maker) as described in detail in Rakel et al. [17] Following classification for the protein phase behavior according to Bergfors [30] was used:

1. Clear,
2. light precipitate,
3. heavy precipitate,
4. LLPS,
5. gelation,
6. microcrystals smaller than 20 µm, and
7. crystals (needles).

Structures, smaller than the microscopic resolution limit of 3 µm, were classified as precipitate. The resulting information was used to establish 3-D phase diagrams. Additionally, the time of first visible structures, the crystal size, and the phase behavior after 40 days were determined.

Table 6.1: Screening Buffer Composition Including the PEG and Protein Content as well as the Screening pH for the Experiment Number

| No | Protein | C_{PEG} [m/V %] | c_P [mg/mL] | pH |
|----|------------------------------|-------------------------|-----------------|---------------|
| 1 | PEG 400, 1000, 3350, 8000 | 2.5, 5, 7.5, 10 | 2.5, 5, 7.5, 10 | 5, 6, 7, 8, 9 |
| | PEG 400 | 12.5, 15, 17.5, 20 | | 5, 6, 7, 8, 9 |
| 2 | PEG 1000 | 1, 1.5, 2, 3, 12.5, 15 | 2.5, 5, 7.5, 10 | 6, 7, 8, 9 |
| | PEG 3350 | 0.5, 1, 1.5, 2, 3, 12.5 | | |
| | PEG 8000 | 0.5, 12.5 | | |

6.2.3 Determination of B_{22} , B_{33} and B_{23} with SLS

The SLS is a noninvasive method to determine osmotic second virial coefficients in diluted solutions. Thereby, the change in the averaged intensity of scattered light can be correlated with interactions between macromolecules. Evaluating the correlation of scattered light intensity to protein concentration and detection angle for one molecule species allows the determination of protein molecular weight M_W and osmotic second virial coefficient B_{22} according to Zimm [7].

The B_{ij} in combination with B_{22} and the B_{33} can be calculated with the following equation [31]:

$$\frac{K^*}{R_\theta} = \left(\sum_i^n M_i \left(\frac{dn}{dc} \right)_i^2 c_i \right)^{-1} + \frac{2 \sum_i^n \sum_j^n B_{ij} M_i M_j c_i c_j \left(\frac{dn}{dc} \right)_i \left(\frac{dn}{dc} \right)_j}{\left(\sum_i^n M_i \left(\frac{dn}{dc} \right)_i^2 c_i \right)^2} \quad (6.2)$$

The parameter R_θ is the Rayleigh ratio, c the concentration, M_i , M_j the weight-average molar mass, the refractive index increment dn/dc of the respective species i and/or j . The modified optical constant K^* is defined in equation (6.3)

$$K^* = \frac{4\pi^2 n_0^2}{N_A \lambda^4} \quad (6.3)$$

With the refractive index of the solvent n_0 and the wavelength of the incident vertically polarized light in vacuum λ .

For the determination of the osmotic second virial coefficients an automated-batch composition gradient multiangle light scattering system and an additional dynamic light scattering detector (CG-MALS: Calypso, DAWN[®] HELEOS[™] 8+ with $\lambda=658$ nm, Optilab[®] reX, Wyatt Technology Corp., Santa Barbara, CA, USA, Software CALYPSO

Version 1.2.8.5, ASTRA Version 5.3.4.20) were used. Applying a flow rate of 0.6 mL/min and the delay time to minimum 60 sec the protein concentration and the scattered light at seven angles could be measured at each concentration step. In the case of aggregation in solution the additional dynamic light scattering detector in the system indicated the aggregation.

The calibration for the SLS instrument to determine absolute R_{θ} was done with toluene, which has an established Rayleigh ratio R_{90} at an angle of 90° of $1.406 \cdot 10^{-5} \text{ cm}^{-1}$ at a wavelength λ of 633 nm [30,31]. The background scattering of pure solvent was subtracted.

Under the assumption that PEG does not interact with the protein B_{22} -values in PEG-solutions were determined and analyzed according to Rakel et al. [29,34] using the Zimm equation [35]. As the refractive index dn/dc of the protein is dependent on the respective PEG molecular weight and its concentration, this value was adjusted for the protein concentration determination with the refractometer. The B_{22} -values of mAb04c with PEG 400 - PEG 8000 at pH 7, and pH 9 were determined in solutions containing up to 3 % PEG. At higher concentrations aggregation was detected.

For the description of interactions assuming cross-interactions B_{22} , B_{33} , and B_{23} were determined with the same CG-MALS-system. In a stepwise gradient an ascending gradient of increasing PEG-concentration (for B_{33}) is followed by a crossover gradient (for B_{23}), where the concentration of PEG is descending and the concentration of the protein is ascending. The measurement is terminated by a descending stepwise gradient of the protein concentration (for B_{22}). For further information see Some et al. [36,37]. B_{22} , B_{33} and B_{23} were determined with equation (6.2). Analyzed systems were PEG 3350 and PEG 8000 and pH 5, 7, and 9 with mAb04c. The light scattering signal for PEG 1000 and PEG 400 was too small to get reliable data.

6.3 Results and Discussion

6.3.1 Macroscopic phase behavior of mAb04c in dependency of macromolecular precipitants

For complex molecules, like antibodies, polymers are often used as precipitant. But still a detailed knowledge of how parameters like pH-value, PEG molecular weight and concentration affect their phase behavior is missing. Therefore a detailed experimental analysis is conducted with the antibody mAb04c in a buffer system with a constant buffer capacity from pH 5 - 9. This buffer system has the advantage that over a broad pH-range only one buffer is used, which minimizes influences due to changing buffer components

[17,38]. Hence, it is possible to investigate the phase behavior of the antibody mAb04c and the polymer PEG in dependency of pH, PEG molecular weight and their concentrations. In figure 6.1 the phase diagrams of mAb04c with PEG are plotted for pH 5 - 9 and the respective molecular weight of the PEG.

The results show a clear dependence on all analyzed factors, whereby the protein concentration has the smallest influence. Overall, a higher PEG-concentration increases the crystallization probability. At high PEG-concentrations precipitation is also observed. Exceptions are the ambiguous phase behavior in the presence of PEG 400 and few experiments for PEG 8000 and pH 9 which result in LLPS.

An increasing pH-value resulted in crystallization of mAb04c at slightly lower PEG-concentrations and a broader crystallization range for all PEG molecular weights. No crystallization was observed in the analyzed conditions at pH 5 and for PEG 400 at pH 6 mAb04c. The precipitation region was comparable for pH-values 6 - 9 for a respective molecular weight of PEG. This behavior can be explained by electrostatic interactions at the isoelectric point of mAb04c at pH 8.2 - 8.5. The antibody is positively charged at pH-values lower than 8, while the net charge of the antibody at pH 9 is already negative. These net charges induce electrostatic repulsive interactions between the protein molecules. The higher the net charge of the proteins the higher is the repulsion [18]. This can be confirmed by the B_{22} -results in pure buffer [29]. From these B_{22} -results, it can also be shown, that the differences in B_{22} -values for mAb04c in pure buffer from pH 7 to 9 are small, as additional attractive forces like hydrophobic interaction influence the proteins. This is also reflected in the phase diagrams, as only small differences exist between pH 7 and 9. Overall, the electrostatic repulsion for pH 5 compared with the osmotic attraction seems to stronger influence the phase behavior than for pH 6 - 9.

The phase behavior depends also on the PEG molecular weight. A higher molecular weight induced crystallization at lower PEG-concentrations. Moreover precipitation occurs at lower PEG-concentrations over the whole pH-range. This is associated with depletion forces induced by an osmotic potential due to the PEG. According to Asakura and Oosawa [6] these attractive forces due to a local concentration gradient with an unbalanced osmotic pressure gradient are developed by macromolecules, when the distance between two protein molecules is smaller than the diameter of the solute macromolecules. An attractive potential between the protein molecules arises for a higher PEG molecular weight at lower PEG concentrations attempting the protein molecules to further decrease the distance between each other to reduce the osmotic pressure difference.

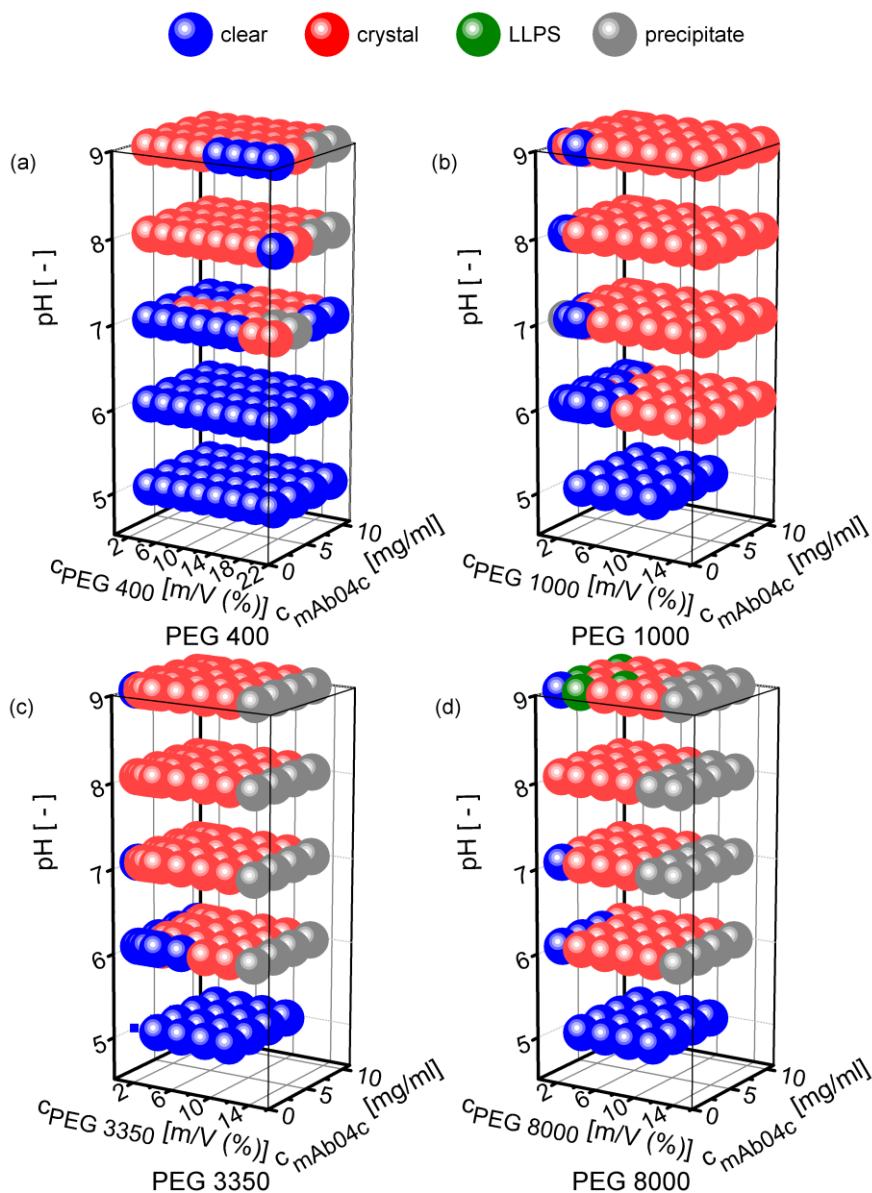


Figure 6.1: Phase diagrams for mAb04c in 10 mM CFBS-buffer at pH 5-9 and PEG 400 (a), 1000 (b), 3350 (c), and 8000 (d)

6.3.2 Nucleation kinetics, crystal size and form

Further important parameters for screening conditions with respect to downstream processing are the size of crystals as well as the kinetic of the nucleation respectively the crystallization. As already shown in Rakel et al.⁸³ the method used here enables us to gain additional information about these parameters. In figure 6.2 the size of the crystals after 40 days and the time of first visible structures are plotted for all four PEG molecular weights. The first visible structures can be LLPS or other structures, which end in crystals. A protein dense and protein poor phase developed due to short range and strong anisotropic protein interactions. The phase separation is metastable as crystals were formed out of this separation and Ostwald ripening occurred [39,40]. Few conditions for PEG 8000 at pH 9 were arrested in this LLPS (see figure 6.1).

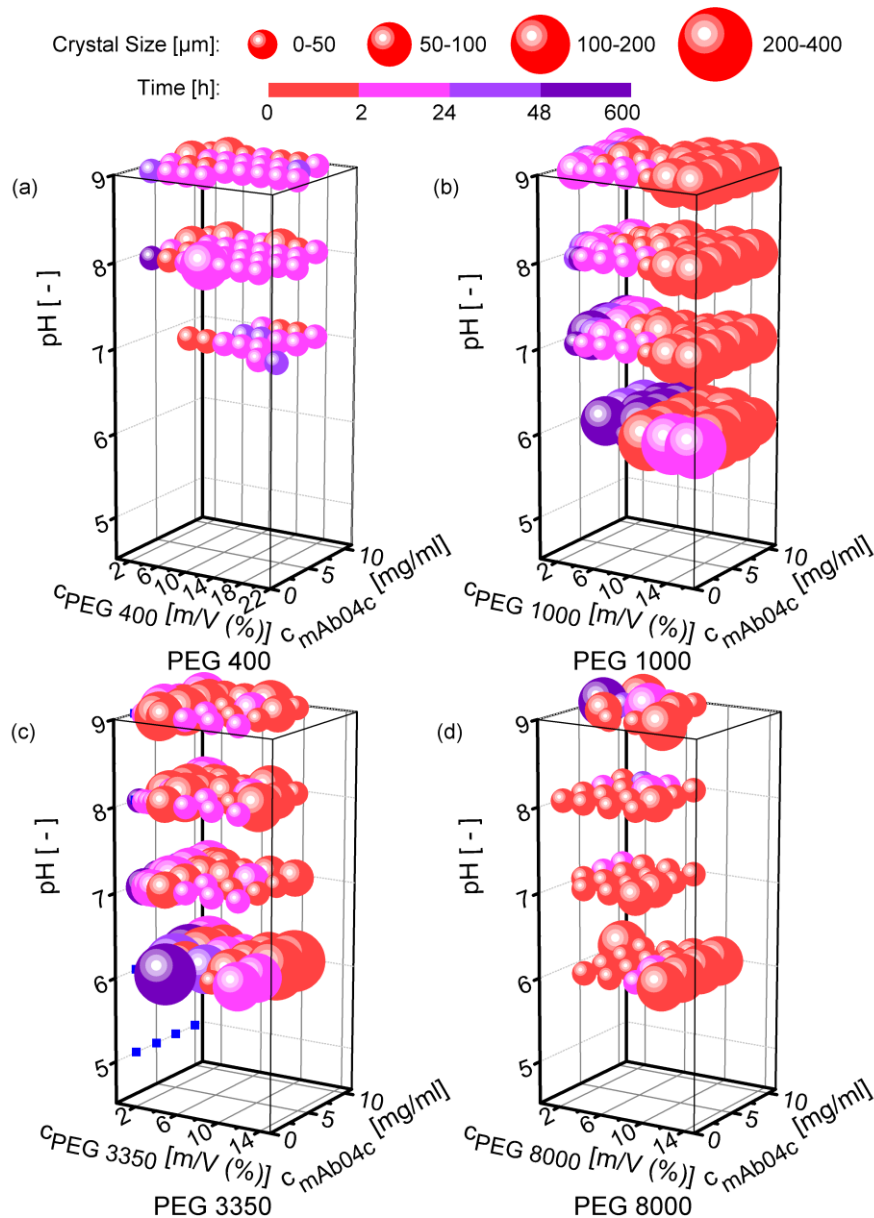


Figure 6.2: Crystal size and time of first visible phase transition for mAb04c in 10 mM CFBS-buffer at pH 5 – 9 and PEG 400 (a), 1000 (b), 3350 (c), and 8000 (d)

For all mAb04c and PEG-combinations no phase aggregation was observed for pH 5. Except the systems with PEG 400, all other systems show a pH-dependency for the crystal size and the timespan to first visible structures. At pH 6 the biggest crystals are obtained, but the timespan is comparably long. With pH-values from 7 to 9, the timespan is smaller and the crystal size is decreased, but comparable to each other for one PEG molecular weight. Thus, a lower electrostatic potential favors smaller crystals. A direct correlation between the size of the crystals and the PEG concentration at one pH was not found for PEG 400 and PEG 8000. For PEG 1000 the crystal sizes tend to increase with increasing PEG concentration, while the crystal sizes slightly decrease for PEG 3350 and pH 7 - 9. For PEG 1000, and 3350 a slight mAb04c concentration effect could be observed. With

increasing protein concentration in the investigated concentration range the crystal size for PEG 1000 and 3350 tend to increase. According to the results of Jion et al. [41] for an IgG1 antibody the size and the amount of nuclei which form out of the solution during LLPS are protein concentration dependent.

The size of the crystals varies with the PEG molecular weight. The application of PEG 400 and PEG 8000 causes smaller crystals compared with PEG 1000 and 3350. One reason can be the longer range of interaction [42,43]. The higher the molecular weight of the PEG, the longer is the range of interaction. A short-range attractive potential is desirable as the rate of crystal nucleation, and the degree of supersaturation can be controlled [10]. However, for PEG 400, no clear dependency of the crystal size on protein and PEG concentration could be determined. One reason for smaller crystals with PEG 400 might be the ambivalent character of PEG 400 as stabilizer as well as precipitant. In studies analyzing the efficacy of precipitants it was shown that no clear preferred concentration exists for protein crystallization with PEG 400 [44].

Observations made during the experiments are illustrated with representative crystal images in figure 6.3. Given conclusions are based on all experiments. Overall the coffin-shaped crystals developed from a LLPS or other structures. The resulting 3-D crystals are smaller in the presence of PEG 400 (a) and PEG 8000 (d) compared to PEG 1000 (b), and PEG 3350 (c). The higher the PEG-concentration the rougher is the surface of the crystals for all PEG molecular weights. The same picture arises for a higher molecular weight of PEG at the same PEG and protein concentration. The higher range of interaction and strength of depletion attraction due to a higher polymer size and concentration result in a faster crystal growth kinetic. This causes optical inhomogeneities which are defective regions in the crystal lattice [10,45].

On the way toward stirred batch crystallization, nonagitated diffusion-driven systems represent an intermediate screening step. For downstream processing, compact large crystals to simplify crystal separation and a fast kinetic to reduce the process time are favored. Overall, a broad crystallization region for mAb04c with varying PEG concentration, molecular weight, and pH was obtained. Hence, PEG is an adequate precipitant to generate compact mAb04c crystals. For PEG 1000, the resulting crystals were large in size especially at a higher negative charge of the protein (pH 6). However, a high amount of precipitant was needed to obtain these crystals with a fast kinetic, which might influence the later separation. The presence of PEG 3350 resulted also in acceptable crystals sizes under the advantage of lower PEG concentration needed to crystallize mAb04c. Therefore, PEG molecular weights from 1000 to 3350 are recommended for a broad crystallization range, comparably fast crystallization combined with large crystal sizes. How these parameters can be scaled up needs further investigation.

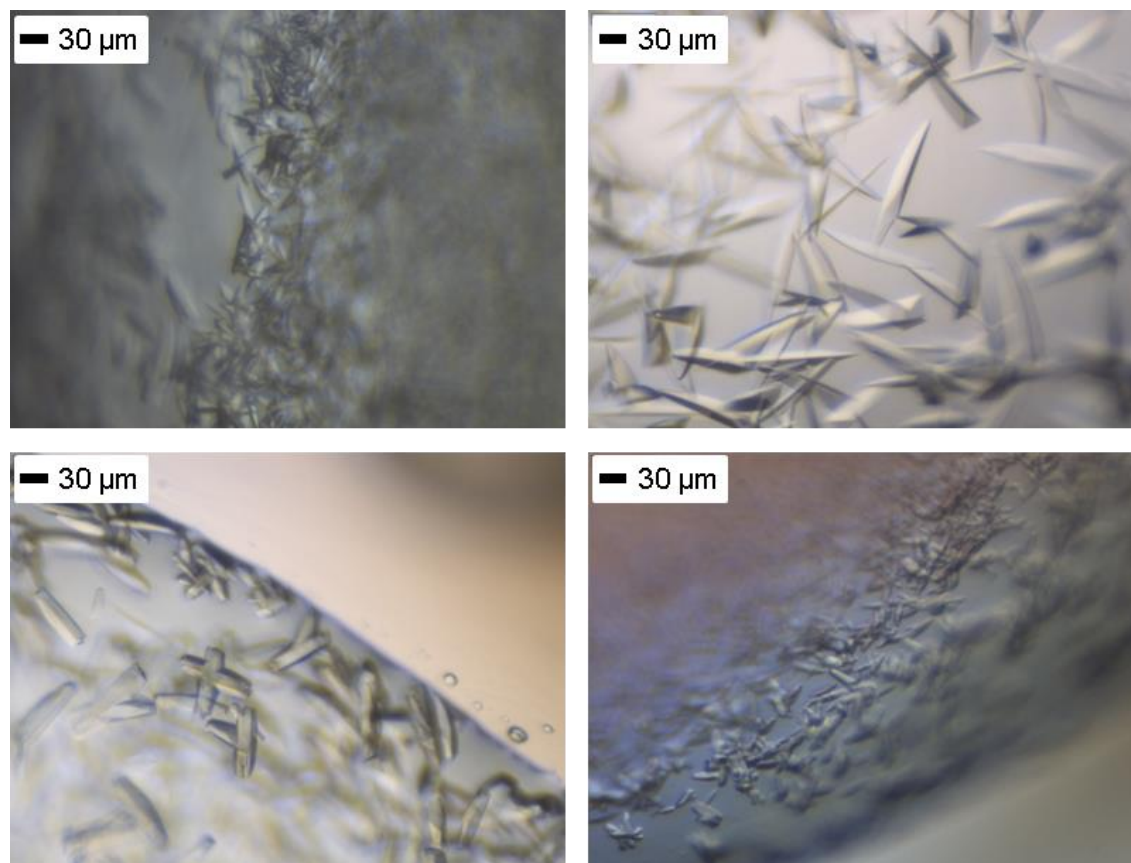


Figure 6.3: Crystal-images: 7.5 m/V % PEG, 10 mg/mL mAb04c at pH 8 (a) PEG 400, (b) PEG 1000, (c) PEG 3350, (d) PEG 8000

6.3.3 Comparison of PEG and salt influence on antibody phase behavior

A comparison of the influence of PEG and salt is possible, as the phase behavior of mAb04c in the presence of PEG was analyzed in the same buffer system used in earlier works to investigate the phase behavior of mAb04c with salts. Overall, the influence of the precipitant has a strong influence on the out coming results. One main difference is the crystal form. While with salts as precipitant needles are obtained, PEG induces a 3-D crystal growth with a higher crystal volume due to the coffin-shaped form. The reason might be different interaction potentials. As the phase behavior of proteins is influenced by Hofmeister effects for salts, PEG induces phase separation due to depletion forces. Thereby the molecular weight of PEG is an important parameter to control the crystallization. Moreover, a clear difference between salts and PEG as precipitant exist in the optimal pH-value for mAb04c crystallization. With sulfate salts the largest crystals and the highest yields were obtained close to the pI, while the crystallization range with PEG is remarkably broader. Crystals were obtained over a broad range of conditions with varying pH, molecular weight and concentration of the PEG. A higher protein net charge results in bigger crystals. The influence of the pH slows down the nucleation kinetic, which results in increasing crystal size with raising net charge and the later timespan for first visible phase

transition (figure 6.2). Overall, the higher probability of crystallization for large molecules in the presence of PEG compared to salts is consistent with the findings of Finet et al. [10].

6.3.4 Characterization of macroscopic phase behavior of mAb04c using the osmotic second virial coefficient

Osmotic second virial coefficients are often used to describe protein interaction in solution. The most famous example is the crystallization slot of George and Wilson [13]. With the so called crystallization slot they suggest a negative B_{22} -range of high crystallization probability. However, it is ambiguous to state that this crystallization slot is transferable to antibodies. Therefore B_{22} -values were determined for mAb04c in dependency of the PEG-concentration and molecular weight. The results are plotted in figure 6.4 for pH 7 and pH 9. At pH 7 and pH 9 the B_{22} is already below zero, if no PEG is in solution. All B_{22} -values remain slightly negative and decrease with increasing PEG concentration, except with PEG 400 at pH 9. The B_{22} -trend for PEG 400 is opposite to pH 7 and reaches positive values at 3 m/V % PEG. B_{22} -values are sorted by the PEG molecular weight, whereby the differences rise with higher PEG concentration. The highest B_{22} -value is determined for PEG 400 and the lowest for PEG 3350 and 8000. Nevertheless, PEG 3350 and 8000 feature similar values at 2 and 3 m/V % PEG. Above 3 m/V % PEG B_{22} could not be determined with SLS due to aggregation of the antibody.

The influence of PEG and pH shows a synergistic effect on the phase behavior of mAb04c. First, the charge of the protein is changed due to the distance to the pI at different pH-values, second the molecular weight and concentration of PEG influence the range of interaction [12,46]. As shown in figure 6.4 these effects of electrostatic and osmotic interactions do not simply add up, as the differences in B_{22} -values between pH 7 (a) and 9 (b) for the same molecular weight are smaller without PEG (0 m/V % PEG) than in the presence of PEG. The higher the PEG concentrations, the higher are the differences. As shown by the determined B_{22} -values the interactions are dependent on the molecular weight as well as the concentration of the PEG. The higher the molecular weight and/or the concentration, the higher is the attraction between the molecules. The only PEG for which the B_{22} -value rises with increasing PEG concentration for pH 9 is PEG 400. This might go on hand with the stabilizing and precipitating effect of PEG 400 [44].

In figure 6.4 the crystallization slot according to George and Wilson [13] defines the range of high crystallization probability. Comparing these conditions with the phase behavior of mAb04c in figure 6.1 the same picture arises like with salts [29]. Most of these experiments show crystallization within this range, few do not separate and others are crystallizing below this range. For pH 5, positive B_{22} -values correspond to nonseparating

conditions (data not shown). However, also crystallizing conditions with positive B_{22} -values were found for mAb04c with PEG 400 at pH 9.

Overall, the results confirm that an application of the crystallization slot is not possible for mAb04c. Neither a shift to higher B_{22} -values for the crystallization slot as postulated by Haas et al. [16] is recommended for mAb04c, nor a direct correlation between B_{22} -values and crystallizing conditions was found. In contrast to salts as precipitant, the systems with PEG showed as well positive B_{22} -values for crystallizing conditions. Different reasons can explain these results. First, intact mAbs are complex molecules with a higher molecular weight and flexibility compared to the most model proteins used by George and Wilson [13]. Therefore, attractive interaction potentials between different groups on the surface of two protein molecules might result in local attraction which induces crystallization, while the overall interactions represent repulsive interactions. Bonneté et al. [47] explained this with a subtle balance between attractive and repulsive potentials. Conversely, repulsion between different groups can inhibit crystallization, although the B_{22} -value is in a promising range. Moreover, further parameters like the protein concentration or nucleation and crystallization kinetics have to be taken into account as already proposed by different authors [29,48,49]. Intact mAbs are in general difficult to crystallize, as shown by the small number of positive examples [48,50]. Second, with PEG as precipitant for proteins, two macromolecules are in solution. When determining the B_{22} -value interactions between protein and polymer are neglected. This approximation might influence the results. For example, also positive B_{22} -values are obtained for crystallizing conditions in contrast to salt as precipitant [29]. In literature more examples for positive B_{22} -values for crystallizing conditions exist, like for urate oxidase or the Brome Mosaic Virus [47,51]. These conditions were also obtained with PEG as precipitant in solution. The determination of cross-interactions between protein and PEG in form of the B_{23} might show if this approximation is applicable.

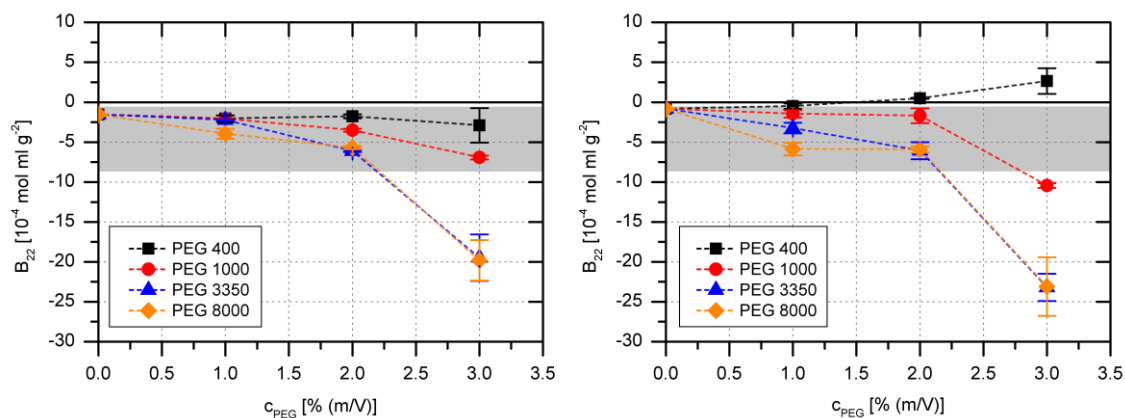


Figure 6.4: B_{22} -values for mAb04c as a function of PEG-concentration and molecular weight at (a) pH 7 and 9 (b); in gray crystallization slot according to George and Wilson [13]

6.3.5 Characterization of phase behavior using cross-interaction determination

From the results of figure 6.4 the question arises, whether or not cross-interactions between proteins and macromolecular precipitants can be neglected or if they can give additional information about how the protein behaves. For macromolecules with a sufficient molecular size, it is possible to determine the osmotic second cross-virial coefficient as a parameter for cross-interactions via SLS. Therefore, the systems containing PEG 3350 and PEG 8000 with mAb04c used in this work were analyzed as two component system with the macromolecules PEG and protein. Interactions between alike molecules (mAb04c - mAb04c: B_{22} , PEG - PEG: B_{33}) and unlike molecules (mAb04c - PEG: B_{23}) for the pH-values 5, 7, 9 were determined. They are measured in the pure buffer system at the respective pH-value, by varying the PEG and mAb04c concentrations as described in chapter 6.2.3. The results are plotted in figure 6.5. The determined B_{22} -values for the pseudo-one-component system at 0 % PEG (figure 6.4) and the B_{22} for the two component system PEG-mAb04c represent by definition the same value at the same pH-value. The determined values are consistent with each other, as the overall averaged B_{22} -values show a standard deviation of $0.173 \cdot 10^{-4} \text{ mol mL g}^{-2}$. This result shows the applicability of the SLS method for the two component system.

For pH 5 the B_{22} is positive while for pH 7 and pH 9 negative B_{22} -values were determined. The B_{33} values are positive over the pH-range and values higher than $20 \cdot 10^{-4} \text{ mol mL g}^{-2}$ are determined, while the mean values for PEG 3350 and PEG 8000 differ by approximately $10 \cdot 10^{-4} \text{ mol mL g}^{-2}$. The B_{23} is decreasing with increasing pH, but remains positive. The B_{23} -values for PEG 3350 at all measured pH-values are averaged $0.7 \cdot 10^{-4} \text{ mol mL g}^{-2}$ smaller compared with those of PEG 8000.

For the pH-values of 7 and 9, negative B_{22} -values and positive B_{33} -values are obtained, while the B_{23} are positive. In phase behavior experiments, mAb04c crystallizes over a broad PEG concentration range. These cases are comparable to the phase behavior of lysozyme and ovalbumin in solution described by McCarty et al. [23] and Cheng et al. [22]. Both postulate a high probability of purified crystals of the target protein - here mAb04c -, whereas the other macromolecule - here PEG 3350 or PEG 8000 - stays in solution. As B_{22} as well as B_{33} are positive, the LLPS which initializes crystallization results from the repulsion between PEG and protein. Thus, PEG is not attached in the crystal which can be generally confirmed by Finet et al. [10] for protein-PEG systems. Positive B_{23} -values and B_{33} -values are also expected for other protein and PEG systems in aqueous buffers, as PEG is a hydrophilic nonionic polymer. The B_{23} for PEG 3350 and mAb04c is smaller compared to the B_{23} for PEG 8000 and mAb04c. This might explain the faster kinetic of the latter system. However, the B_{23} cannot be analyzed as single

parameter, as the decrease of B_{23} -values with increasing pH for one PEG molecular weight is not reflected in the kinetics and the strength of the phase transitions. Conversely, no phase transition of mAb04c occurred at pH 5. In contrast to pH 7 and 9, the only difference is a positive B_{22} -value. With regard to the demixing criterion in equation (6.1) the virial coefficients predict that the systems of mAb04c and PEG 3350 as well as PEG 8000 at pH 5 do not separate.

From the earlier, it is clear that interactions between protein and PEG exist. Moreover the combination of B_{22} , B_{33} , and B_{23} could be used to better understand the protein phase behavior. It helps in analyzing the kinetics of phase transition, if phase transition occurs and predicts selective crystallization. Thereby a negative B_{22} -value in combination with positive B_{23} - and B_{33} -values increases the probability of phase transition as shown by the application of the demixing criterion on the obtained results. However, this demixing criterion gives neither the additional information about the type of phase transition nor the corresponding PEG and/or protein concentration. A prediction of protein phase behavior, respectively, the desired crystallization with B_{22} , B_{33} , and B_{23} over the analyzed range seems not possible. These three parameters are protein and PEG concentration independent and try to describe complete 2-D phase diagram at constant pH-value and varying protein and PEG concentration. Thus, three parameters are supposed to describe every possible phase state such as stable solutions, crystallization, precipitation as well as an arrested LLPS as shown for PEG 8000 at pH 9. B_{22} , B_{33} , and B_{23} are derived from the non-ideality of the osmotic pressure and, hence, hardly capable of predicting complete phase diagrams. To gain further information about the protein phase behavior, additional parameters like the PEG/protein concentration dependency and kinetics have to be taken into account as already mentioned for the analysis with the B_{22} -value in chapter 1.3.4.

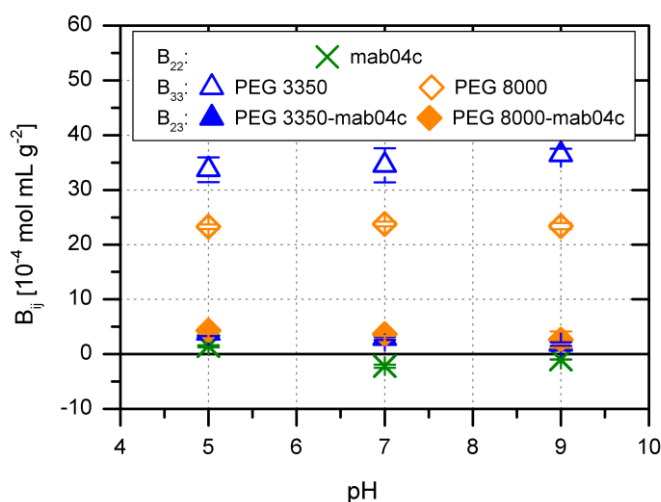


Figure 6.5: B_{22} , B_{33} and B_{23} for mAb04c and PEG 3350 and 8000 in dependency of the pH

6.4 Conclusion

In this work, a detailed and systematic analysis of the phase behavior of mAb04c in dependency of different pH-values and PEG molecular weights as well as concentrations in a buffer system is presented. The phase behavior as well as the time for the first occurrence and the size of the crystals can be controlled by the PEG molecular weight and the pH-value. Overall, the use of PEG as precipitant for antibodies is more promising compared with salts due to the success in finding crystallization conditions by an easy variation of the depth and range of the osmotic attraction, simply by changing the polymer size and concentration⁸². PEG molecular weights of 1000 or 3350 in combination with mAb04c are preferred due to a larger crystal size, the fast phase transition and the broad crystallization range.

The approach of considering the protein in a PEG solution as a pseudo-one-component system to determine the protein interactions in form of the B_{22} and the approach of using the B_{23} for analyzing the protein-PEG interactions were successfully applied to establish further theoretical understanding. However, these osmotic second virial coefficients are neither capable of prediction crystallization probability, for example, in the form of a crystallization slot nor the type of phase transition. B_{ii} and B_{ij} describe the non-ideality of the osmotic pressure and, therefore, cannot describe kinetic processes or concentration dependencies of the protein phase behavior.

6.5 Acknowledgements

The authors are grateful for support by the BMBF (Federal Ministry of Education and Research), grant no. 0315338B and Boehringer Ingelheim Pharma GmbH & Co. KG, Biberach, Germany.

6.6 Literature Cited

- [1] Birch JR, Racher AJ. Antibody production. *Adv Drug Deliv Rev.* 2006;58(5-6):671–685.
- [2] Thömmes J, Etzel M. Alternatives to chromatographic separations. *Biotechnol Prog.* 2007;23(1):42–5.
- [3] Low D, O’Leary R, Pujar NS. Future of antibody purification. *J Chromatogr B Analyt Technol Biomed Life Sci.* 2007;848(1):48–63.
- [4] Drenth J, Dijkstra K, Haas C, Ohlenschla O. Effect of molecular anisotropy on the nucleation of lysozyme. *J Phys Chem. B* 2003;4203–4207.

- [5] Arakawa T, Timasheff SN. Mechanism of poly(ethylene glycol) interaction with proteins. *Biochemistry*. 1985;24(24):6756–62.
- [6] Asakura S, Oosawa F. Interaction between particles suspended in solutions of macromolecules. *J Polym Sci*. 1958;33(126):183–192.
- [7] Zimm BH. The scattering of light and the radial distribution function of high polymer solutions. *J Chem Phys*. 1948;16(12):1093.
- [8] Timasheff SN. The control of protein stability and association by weak interactions with water: how do solvents affect these processes? *Annu Rev Biophys Biomol Struct*. 1993;22(1):67–97.
- [9] Tanaka S, Ataka M. Protein crystallization induced by polyethylene glycol: a model study using apoferritin. *J Chem Phys*. 2002;117(7):3504.
- [10] Finet S, Vivarès D, Bonneté F, Tardieu A. Controlling biomolecular crystallization by understanding the distinct effects of PEGs and salts on solubility. *Methods Enzymol*. 2003;368:105–129.
- [11] Anderson VJ, Lekkerkerker HNW. Insights into phase transition kinetics from colloid science. *Nature*. 2002;416(6883):811–815.
- [12] Tardieu A, Bonneté F, Finet S, Vivarès D. Understanding salt or PEG induced attractive interactions to crystallize biological macromolecules. *Acta Crystallogr D Biol Crystallogr*. 2002;58(10):1549–1553.
- [13] George A, Wilson WW. Predicting protein crystallization from a dilute solution property. *Acta Crystallogr D Biol Crystallogr*. 1994;50(Pt 4):361–365.
- [14] Vivarès D, Bonneté F. X-ray scattering studies of *Aspergillus flavus* urate oxidase: towards a better understanding of PEG effects on the crystallization of large proteins. *Acta Crystallogr D Biol Crystallogr*. 2002;58(3):472–479.
- [15] Ebel C, Faou P, Zaccai G. Protein–solvent and weak protein–protein interactions in halophilic malate dehydrogenase. *J Cryst Growth*. 1999;196(2-4):395–402.
- [16] Haas C, Drenth J. The Protein–Water Phase Diagram and the Growth of Protein Crystals from Aqueous Solution. *J Phys Chem B*. 1998;102(21):4226–4232.
- [17] Rakel N, Baum M, Hubbuch J. Moving through three-dimensional phase diagrams of monoclonal antibodies. *Biotechnol Prog*. 2014 submitted for publication.
- [18] Vivarès D, Belloni L, Tardieu A, Bonneté F. Catching the PEG-induced attractive interaction between proteins. *Eur Phys J E Soft Matter*. 2002;9(1):15–25.
- [19] Haynes CA, Benitez FJ, Blanch HW, Prausnitz JM. Application of integral-equation theory to aqueous two-phase partitioning systems. *AIChE J*. 1993;39(9):1539–1557.
- [20] Choi SH, Bae YC. Osmotic cross second virial coefficient (B_{23}) of unfavorable proteins: modified Lennard-Jones potential. *Macromol Res*. 2009;17(10):763–769.

- [21] Tessier PM, Sandler SI. Direct measurement of protein osmotic second virial cross coefficients by cross-interaction chromatography. *Protein Sci.* 2004;13(5):1379–90.
- [22] Cheng YC, Bianco CL, Sandler SI, Lenhoff AM. Salting-Out of Lysozyme and Ovalbumin from Mixtures: predicting Precipitation Performance from Protein–Protein Interactions. *Ind Eng Chem Res.* 2008;47(15):5203–5213.
- [23] McCarty BW, Adams ET. Osmotic pressure measurements of ovalbumin and lysozyme mixtures. *Biophys Chem.* 1987;28(2):149–159.
- [24] Zang Y. Development of a crystallization step for monoclonal antibody purification : screening , optimization and aggregation control. PhD Thesis. Karlsruhe Institute of Technology, Germany; 2013.
- [25] Tessier PM, Verruto VJ, Sandler SI, Lenhoff AM. Correlation of diafiltration sieving behavior of lysozyme-BSA mixtures with osmotic second virial cross-coefficients. *Biotechnol Bioeng.* 2004;87(3):303–10.
- [26] Schaink H, Smit JA. Protein–polysaccharide interactions: the determination of the osmotic second virial coefficients in aqueous solutions of β -lactoglobulin and dextran. *Food Hydrocoll.* 2007;21(8):1389–1396.
- [27] Doublier J-L, Garnier C, Renard D, Sanchez C. Protein–polysaccharide interactions. *Curr Opin Colloid Interface Sci.* 2000;5(3-4):202–214.
- [28] Mahadevan H, Hall CK. Statistical-mechanical model of protein precipitation by nonionic polymer. *AIChE J.* 1990;36(10):1517–1528.
- [29] Rakel N, Galm L, Bauer K, Hubbuch J. From osmotic second virial coefficient (B_{22}) to phase behavior of a monoclonal antibody. *Biotechnol Prog*; in press.
- [30] Bergfors T, editor. *Protein Crystallization*. 2nd ed. La Jolla, CA: International University Line; 2009.
- [31] Comper WD, Laurent TC. An estimate of the enthalpic contribution to the interaction between dextran and albumin. *Biochem J.* 1978;175(2):703–708.
- [32] Rosenbaum DF, Zukoski CF. Protein interactions and crystallization. *J Cryst Growth.* 1996;169(4):752–758.
- [33] Wilson WW. Light scattering as a diagnostic for protein crystal growth—a practical approach. *J Struct Biol.* 2003;142(1):56–65.
- [34] Rakel N, Schleining K, Dismer F, Hubbuch J. Self-interaction chromatography in pre-packed columns: a critical evaluation of self-interaction chromatography methodology to determine the second virial coefficient. *J Chromatogr A.* 2013;1293:75–84.
- [35] Zimm BH. Application of the methods of molecular distribution to solutions of large molecules. *J Chem Phys.* 1946;14(3):164.

- [36] Some D, Hanlon A, Sockolov K. Characterizing protein-protein interactions via static light scattering: reversible heteroassociation. *Am Biotechnol Lab*. 2008;26(4):18–20.
- [37] Some D, Hitchner E, Ferullo J. Characterizing protein-protein interactions via static light scattering: nonspecific interactions. *Am Biotechnol Lab*. 2009;27(2):2–6.
- [38] Ries-Kautt MM, Ducruix AF. Relative effectiveness of various ions on the solubility and crystal growth of lysozyme. *J Biol Chem*. 1989;264(2):745–748.
- [39] Ng JD, Lorber B, Witz J, Théobald-Dietrich A, Kern D, Giegé R. The crystallization of biological macromolecules from precipitates: evidence for Ostwald ripening. *J Cryst Growth*. 1996;168(1-4):50–62.
- [40] Ten Wolde PR, Frenkel D. Homogeneous nucleation and the Ostwald step rule. *Phys Chem Chem Phys*. 1999;1(9):2191–2196.
- [41] Jion AI, Goh L, Oh SKW. Crystallization of IgG1 by mapping its liquid-liquid phase separation curves. *Biotechnol Bioeng*. 2006;95(5):911–918.
- [42] Lekkerkerker HNW, Poon WC-K, Pusey PN, Stroobants A, Warren PB. Phase behaviour of colloid + polymer mixtures. *Europhys Lett*. 1992;20(6):559–564.
- [43] Ilett SM, Orrock A, Poon WC-K, Pusey PN. Phase behavior of a model colloid-polymer mixture. *Phys Rev E*. 1995;51(2):1344–1352.
- [44] Peat TS, Christopher JA, Newman J. Tapping the protein data bank for crystallization information. *Acta Crystallogr D Biol Crystallogr*. 2005;61(Pt 12):1662–1669.
- [45] Durbin SD, Feher G. Protein crystallization. *Annu Rev Phys Chem*. 1996;47:171–204.
- [46] Budayova M, Bonneté F, Tardieu A, Vachette P. Interactions in solution of a large oligomeric protein. *J Cryst Growth*. 1999;196(2-4):210–219.
- [47] Bonneté F, Vivarès D, Robert C, Colloc'h N. Interactions in solution and crystallization of *Aspergillus flavus* urate oxidase. *J Cryst Growth*. 2001;232(1-4):330–339.
- [48] Lewus RA, Darcy PA, Lenhoff AM, Sandler SI. Interactions and phase behavior of a monoclonal antibody. *Biotechnol Prog*. 2010;27(1):280–289.
- [49] Ahamed T, Esteban BNA, Ottens M, Van Dedem G, Van der Wielen LAM, Bisschops MAT, Lee A, Pham C, Thömmes J. Phase behavior of an intact monoclonal antibody. *Biophys J*. 2007;93(2):610–619.
- [50] Zang Y, Kammerer B, Eisenkolb M, Lohr K, Kiefer H. Towards protein crystallization as a process step in downstream processing of therapeutic antibodies: screening and optimization at microbatch scale. *PLoS One*. 2011;6(9):e25282.

- [51] Bonneté F, Vivarès D. Interest of the normalized second virial coefficient and interaction potentials for crystallizing large macromolecules. *Acta Crystallogr D Biol Crystallogr*. 2002;58(10):1571–1575.

7 Conclusion and Outlook

This work shows the importance of optimization and simplification of reliable screening methods for the analysis of protein phase behavior to gain transferable information for further studies. A screening method using a buffer system with a constant buffer capacity from pH 5 – 9 was established to systematically analyze protein phase behavior. The main advantages of such a screening are the comparability between different conditions and the possibility to analyze the influence of single parameters on the protein phase behavior. Additional information such as nucleation and crystallization kinetics was obtained by using an automated imaging system during the screening. This developed screening method can now be expanded to different kinds of precipitants and mixtures. With a transfer of this methodology to different proteins the setup of databases is essential to be able to interlink information in the future.

With the here developed screening method, the influence of salts and PEG on antibody phase behavior was analyzed and differences between the two precipitant types were highlighted. Appropriate crystallization conditions for downstream processing could be found for mAb04c with PEG due to a compact crystal appearance, large crystal size and a broad crystallization range. Since the experiments were conducted in microbatch experiments with low vibration storage, the influence of additional process parameters like stirring and filtration of crystals have to be investigated in further upscale studies.

These results were supported and supplemented by an extensive study of protein-protein interactions using the osmotic virial coefficients. Additional information from the correlation of B_{22} -values to antibody phase behavior fosters the understanding of mechanisms on a molecular and thermodynamic basis. A constitutional differentiation between crystallization and precipitation in form of a crystallization slot was neither possible nor a description of the binodal and the spinodal with the thermodynamic model.⁴³ Kinetic phenomena and complexity of the analyzed antibody molecules have to be taken into account. However, the theoretical HDW-model⁴⁰ was successfully applied for mAb04c to correlate solubility to the B_{22} . Thus, the solubility seems to be thermodynamically driven. Such information can be applied for optimization of different downstream processing steps.

The determination of B_{22} with SLS, however, is still protein and time consuming, which is a disadvantage when a high throughput screening is considered. Since the SIC is not applicable for a quantitative determination of the B_{22} , more time and effort should be invested to optimize non-invasive methods like the SLS to reduce time and protein consumption. The use of a dual-detector cell for simultaneous measurement of scattered

light intensity and concentration in Size Exclusion Chromatography-HPLC for SLS as postulated by Bajaj et al.⁸⁴ might be a possibility.

Unfortunately, no structural information was available for the three antibodies investigated in this study, even though structure based approaches seem to be very powerful⁵³ in finding correlations to crystallization probability. The combination of thermodynamic and statistic considerations will help to further increase the understanding of what happens in protein solutions. Moreover the quantification of protein-protein interactions via B_{22} as an additional parameter to differentiate protein phase behavior simplifies the use of statistical methods like multivariate data analysis.

Overall, it could be shown in this thesis, that it is still a long way to go to completely understand protein phase behavior in solution. Due to an extensive and systematic analysis, the phase behavior of monoclonal antibodies is better understood in detail now. The established screening method and the knowledge gained for antibody phase behavior will simplify the analysis of protein phase behavior in the future. Moreover, this work also points out the limits of the existing experimental screening methods as well as empirical and theoretical models. Strategies were suggested for further investigations. A fundamental understanding is not only the key to reduce experimental effort in crystallization condition screening, but also in optimization of all steps in downstream processing.

References

1. Zider A, Drakeman DL. The future of monoclonal antibody technology. *MAbs*. 2010;2(4):361–364.
2. Stockwin LH, Holmes S. The role of therapeutic antibodies in drug discovery. *Biochem Soc Trans*. 2003;31(2):433–436.
3. Stockwin LH, Holmes S. Antibodies as therapeutic agents: vive la renaissance! *Expert Opin Biol Ther*. 2003;3(7):1133–1152.
4. Birch JR, Racher AJ. Antibody production. *Adv Drug Deliv Rev*. 2006;58(5-6):671–685.
5. Mather JP. Engineered antibody therapeutics. *Adv Drug Deliv Rev*. 2006;58(5-6):631–632.
6. Thömmes J, Etzel M. Alternatives to chromatographic separations. *Biotechnol Prog*. 2007;23(1):42–45.
7. Manning MC, Chou DK, Murphy BM, Payne RW, Katayama DS. Stability of protein pharmaceuticals: an update. *Pharm Res*. 2010;27(4):544–575.
8. Kozlowski S, Swann P. Current and future issues in the manufacturing and development of monoclonal antibodies. *Adv Drug Deliv Rev*. 2006;58(5-6):707–722.
9. Gottschalk U. Downstream processing of monoclonal antibodies: from high dilution to high purity. *Biopharm Int*. 2005;18(6):42–58.
10. Low D, O’Leary R, Pujar NS. Future of antibody purification. *J Chromatogr B Analyt Technol Biomed Life Sci*. 2007;848(1):48–63.
11. Roque ACA, Lowe CR, Taipa MA. Antibodies and genetically engineered related molecules: production and purification. *Biotechnol Prog*. 2004;20(3):639–654.
12. Schmidt S, Havekost D, Kaiser K, Kauling J, Henzler HJ. Kristallisation für die Aufarbeitung von Proteinen. *Chemie Ing Tech*. 2004;76(6):819–822.
13. Salinas BA, Sathish HA, Bishop SM, Harn N, Carpenter JF, Randolph TW. Understanding and modulating opalescence and viscosity in a monoclonal antibody formulation. *J Pharm Sci*. 2010;99(1):82–93.
14. Haas C, Drenth J. The interface between a protein crystal and an aqueous solution and its effects on nucleation and crystal growth. *J Phys Chem B*. 2000;104(2):368–377.
15. McMillan WG, Mayer JE. The statistical thermodynamics of multicomponent systems. *J Chem Phys*. 1945;13(7):276.

16. Leckband D, Israelachvili J. Intermolecular forces in biology. *Q Rev Biophys.* 2001;34(2):105.
17. Neal BL, Lenhoff AM. Excluded volume contribution to the osmotic second virial coefficient for proteins. *AIChE J.* 1995;41(4):1010–1014.
18. Van Oss CJ. Hydrophobicity of biosurfaces - Origin, quantitative determination and interaction energies. *Colloids surfaces B Biointerfaces.* 1995;5(3-4):91–110.
19. Derjaguin B, Landau L. Theory of the stability of strongly charged lyophobic sols and of the adhesion of strongly charged particles in solutions of electrolytes. *Prog Surf Sci.* 1941;43(1-4):30–59.
20. Verwey EJW. Theory of the stability of lyophobic colloids. *J Phys Colloid Chem.* 1947;51(3):631–636.
21. Roth CM, Neal BL, Lenhoff AM. Van der Waals interactions involving proteins. *Biophys J.* 1996;70(2):977–987.
22. Prausnitz JM. Molecular thermodynamics for some applications in biotechnology. *Pure Appl Chem.* 2003;75(7):859–873.
23. Asakura S, Oosawa F. Interaction between particles suspended in solutions of macromolecules. *J Polym Sci.* 1958;33(126):183–192.
24. Zimm BH. The scattering of light and the radial distribution function of high polymer solutions. *J Chem Phys.* 1948;16(12):1093.
25. Neal BL. Molecular origins of osmotic second virial coefficients of proteins. *Biophys J.* 1998;75(5):2469–2477.
26. Dill KA. Dominant forces in protein folding. *Biochemistry.* 1990;29(31):7133–7155.
27. Dong A, Prestrelski SJ, Allison SD, Carpenter JF. Infrared spectroscopic studies of lyophilization- and temperature-induced protein aggregation. *J Pharm Sci.* 1995;84(4):415–424.
28. Arakawa T, Timasheff SN. Mechanism of protein salting in and salting out by divalent cation salts: balance between hydration and salt binding. *Biochemistry.* 1984;23(25):5912–5923.
29. Tanaka S, Ataka M. Protein crystallization induced by polyethylene glycol: A model study using apoferritin. *J Chem Phys.* 2002;117(7):3504.
30. Moon YU, Anderson CO, Blanch HW, Prausnitz JM. Osmotic pressures and second virial coefficients for aqueous saline solutions of lysozyme. *Fluid Phase Equilib.* 2000;168(2):229–239.
31. Zimm BH. Application of the methods of molecular distribution to solutions of large molecules. *J Chem Phys.* 1946;14(3):164.

32. Rosenbaum DF, Zukoski CF. Protein interactions and crystallization. *J Cryst Growth*. 1996;169(4):752–758.
33. Ahamed T, Esteban BNA, Ottens M, et al. Phase behavior of an intact monoclonal antibody. *Biophys J*. 2007;93(2):610–619.
34. Jones MJ, Ulrich J. Industrielle Kristallisation von Proteinen - Eine Frage der Aktivität. *Chemie Ing Tech*. 2005;77(10):1527–1534.
35. Durbin SD, Feher G. Protein crystallization. *Annu Rev Phys Chem*. 1996;47:171–204.
36. Thakur AS, Robin G, Guncar G, et al. Improved success of sparse matrix protein crystallization screening with heterogeneous nucleating agents. *PLoS One*. 2007;2(10):e1091.
37. Ng JD, Lorber B, Witz J, Théobald-Dietrich A, Kern D, Giegé R. The crystallization of biological macromolecules from precipitates: evidence for Ostwald ripening. *J Cryst Growth*. 1996;168(1-4):50–62.
38. Asherie N. Protein crystallization and phase diagrams. *Methods*. 2004;34(3):266–272.
39. Chayen NE, Saridakis E. Protein crystallization: from purified protein to diffraction-quality crystal. *Nat Methods*. 2008;5(2):147–153.
40. Haas C, Drenth J, Wilson WW. Relation between the solubility of proteins in aqueous solutions and the second virial coefficient of the solution. *J Phys Chem B*. 1999;103(14):2808–2811.
41. Lewus RA, Darcy PA, Lenhoff AM, Sandler SI. Interactions and phase behavior of a monoclonal antibody. *Biotechnol Prog*. 2010;27(1):280–289.
42. Anderson VJ, Lekkerkerker HNW. Insights into phase transition kinetics from colloid science. *Nature*. 2002;416(6883):811–815.
43. Haas C, Drenth J. The protein–water phase diagram and the growth of protein crystals from aqueous solution. *J Phys Chem B*. 1998;102(21):4226–4232.
44. Ruppert S, Sandler SI, Lenhoff AM. Correlation between the osmotic second virial coefficient and the solubility of proteins. *Biotechnol Prog*. 2001;17(1):182–187.
45. Rupp B. Maximum-likelihood crystallization. *J Struct Biol*. 2003;142(1):162–169.
46. Chayen NE. Turning protein crystallisation from an art into a science. *Curr Opin Struct Biol*. 2004;14(5):577–583.
47. McPherson A. Introduction to protein crystallization. *Methods*. 2004;34(3):254–265.
48. Brzozowski AM, Walton J. Clear strategy screens for macromolecular crystallization. *J Appl Crystallogr*. 2001;34(2):97–101.

49. Jancarik J, Kim SH. Sparse matrix sampling: a screening method for crystallization of proteins. *J Appl Crystallogr.* 1991;24(4):409–411.
50. Carter C. Statistical design of experiments for protein crystal growth and the use of a precrystallization assay. *J Cryst Growth.* 1988;90(1-3):60–73.
51. Ries-Kautt MM, Ducruix AF. Relative effectiveness of various ions on the solubility and crystal growth of lysozyme. *J Biol Chem.* 1989;264(2):745–748.
52. George A, Wilson WW. Predicting protein crystallization from a dilute solution property. *Acta Crystallogr Sect D Biol Crystallogr.* 1994;50(Pt 4):361–365.
53. Price WN, Chen Y, Handelman SK, et al. Understanding the physical properties that control protein crystallization by analysis of large-scale experimental data. *Nat Biotechnol.* 2009;27(1):51–57.
54. Hui R. High-throughput protein crystallization. *J Struct Biol.* 2003;142(1):154–161.
55. Chayen NE. Comparative studies of protein crystallization by vapour-diffusion and microbatch techniques. *Acta Crystallogr Sect D Biol Crystallogr.* 1998;54(1):8–15.
56. Gabrielsen M, Nagy LA, DeLucas LJ, Cogdell RJ. Self-interaction chromatography as a tool for optimizing conditions for membrane protein crystallization. *Acta Crystallogr Sect D Biol Crystallogr.* 2010;66(Pt 1):44–50.
57. Pjura PE, Lenhoff AM, Leonard SA, Gittis AG. Protein crystallization by design: chymotrypsinogen without precipitants. *J Mol Biol.* 2000;300(2):235–239.
58. Johnson DH, Parupudi A, Wilson WW, DeLucas LJ. High-throughput self-interaction chromatography: applications in protein formulation prediction. *Pharm Res.* 2009;26(2):296–305.
59. Le Brun V, Friess W, Bassarab S, Mühlau S, Garidel P. A critical evaluation of self-interaction chromatography as a predictive tool for the assessment of protein-protein interactions in protein formulation development: a case study of a therapeutic monoclonal antibody. *Eur J Pharm Biopharm.* 2010;75(1):16–25.
60. Choi SH, Bae YC. Osmotic cross second virial coefficient (B₂₃) of unfavorable proteins: Modified lennard-jones potential. *Macromol Res.* 2009;17(10):763–769.
61. Tessier PM, Sandler SI. Direct measurement of protein osmotic second virial cross coefficients by cross-interaction chromatography. *Protein Sci.* 2004;13(5):1379–1390.
62. Cheng YC, Bianco CL, Sandler SI, Lenhoff AM. Salting-out of lysozyme and ovalbumin from mixtures: predicting precipitation performance from protein–protein interactions. *Ind Eng Chem Res.* 2008;47(15):5203–5213.
63. McCarty BW, Adams ET. Osmotic pressure measurements of ovalbumin and lysozyme mixtures. *Biophys Chem.* 1987;28(2):149–159.

64. Tessier PM, Verruto VJ, Sandler SI, Lenhoff AM. Correlation of diafiltration sieving behavior of lysozyme-BSA mixtures with osmotic second virial cross-coefficients. *Biotechnol Bioeng.* 2004;87(3):303–310.
65. Haynes CA, Benitez FJ, Blanch HW, Prausnitz JM. Application of integral-equation theory to aqueous two-phase partitioning systems. *AIChE J.* 1993;39(9):1539–1557.
66. Yousef MA, Datta R, Rodgers VGJ. Model of osmotic pressure for high concentrated binary protein solutions. *AIChE J.* 2002;48(4):913–917.
67. Comper WD, Laurent TC. An estimate of the enthalpic contribution to the interaction between dextran and albumin. *Biochem J.* 1978;175(2):703–708.
68. Ahamed T, Ottens M, Van Dedem G, Van der Wielen LAM. Design of self-interaction chromatography as an analytical tool for predicting protein phase behavior. *J Chromatogr A.* 2005;1089(1-2):111–124.
69. Tessier PM, Vandrey SD, Berger BW, Pazhianur R, Sandler SI, Lenhoff AM. Self-interaction chromatography: a novel screening method for rational protein crystallization. *Acta Crystallogr Sect D Biol Crystallogr.* 2002;58(10):1531–1535.
70. Teske CA, Blanch HW, Prausnitz JM. Measurement of lysozyme–lysozyme interactions with quantitative affinity chromatography. *J Phys Chem B.* 2004;108(22):7437–7444.
71. Patro SY, Przybycien TM. Self-interaction chromatography: a tool for the study of protein-protein interactions in bioprocessing environments. *Biotechnol Bioeng.* 1996;52(2):193–203.
72. Lightfoot EN, Moscariello JS. Bioseparations. *Biotechnol Bioeng.* 2004;87(3):259–273.
73. Wilson WW. Light scattering as a diagnostic for protein crystal growth—A practical approach. *J Struct Biol.* 2003;142(1):56–65.
74. Baldwin RL. How Hofmeister ion interactions affect protein stability. *Biophys J.* 1996;71(4):2056–2063.
75. Lyklema J. Simple Hofmeister series. *Chem Phys Lett.* 2009;467(4-6):217–222.
76. Piazza R, Pierno M. Protein interactions near crystallization: a microscopic approach to the Hofmeister series. *J Phys Condens matter.* 2000;12(8A):A443–A449.
77. Nucci N V., Vanderkooi JM. Effects of salts of the Hofmeister series on the hydrogen bond network of water. *J Mol Liq.* 2008;143(2-3):160–170.
78. Bostrom M, Tavares FW, Finet S, Skouri-Panet F, Tardieu A, Ninham BW. Why forces between proteins follow different Hofmeister series for pH above and below pI. *Biophys Chem.* 2005;117(3):217–224.

79. Collins KD. Ions from the Hofmeister series and osmolytes: effects on proteins in solution and in the crystallization process. *Methods*. 2004;34(3):300–311.
80. Vivarès D, Bonneté F. X-ray scattering studies of *Aspergillus flavus* urate oxidase: towards a better understanding of PEG effects on the crystallization of large proteins. *Acta Crystallogr Sect D Biol Crystallogr*. 2002;58(3):472–479.
81. Ebel C, Faou P, Zaccai G. Protein–solvent and weak protein–protein interactions in halophilic malate dehydrogenase. *J Cryst Growth*. 1999;196(2-4):395–402.
82. Finet S, Vivarès D, Bonneté F, Tardieu A. Controlling biomolecular crystallization by understanding the distinct effects of PEGs and salts on solubility. *Methods Enzymol*. 2003;368:105–129.
83. Rakel N, Baum M, Hubbuch J. Moving through three-dimensional phase diagrams of monoclonal antibodies. *Biotechnol Prog*. 2014;30(5):1103–1113.
84. Bajaj H, Sharma VK, Kalonia DS. Determination of second virial coefficient of proteins using a dual-detector cell for simultaneous measurement of scattered light intensity and concentration in SEC-HPLC. *Biophys J*. 2004;87(6):4048–4055.

Curriculum Vitae

Natalie Rakel née Schnabel

Dipl.-Ing. Life Science Engineering

Professional Experience

| | |
|-----------------|---|
| 03/2014-now | Project manager Manufacturing Science and Technology (MSAT) at Roche Diagnostics GmbH, Mannheim |
| 09/2012-02/2014 | Maternity leave and finalization of PhD thesis |
| 03/2009-09/2012 | Scientific Researcher at the Institute of Engineering in Life Sciences, Chair: Biomolecular Separation Engineering, Karlsruhe Institute of Technology (KIT): <i>“Characterization of Phase behavior and Protein Interactions of Monoclonal Antibodies“</i> |
| 12/2008-01/2009 | Research assistant at the Institute of Thermal Process Engineering, University Karlsruhe (TH) |
| 10/2006-03/2007 | Internship at Bayer Healthcare Pharma, México City |
| 08/2005-07/2006 | Research assistant at the Institute of Technical Thermodynamics, University Karlsruhe (TH) |

Education

| | |
|-----------------|--|
| 09/2003-11/2008 | Studies of Life Science Engineering , University Karlsruhe (TH) |
| 11/2008 | Diploma degree , Majors: Bio- and Food Process Engineering |
| 05/2008-11/2008 | Diploma Thesis at the Institute of Thermal Process Engineering, University Karlsruhe (TH): <i>„Untersuchung der Phasengleichgewichte halbleitender organischer Materialien in der Flüssigphase“</i> |
| 07/2007-01/2008 | Student research project at the Institute of Engineering in Life Sciences, Chair of Bioprocess Engineering, University Karlsruhe (TH): <i>„Experimentelle Untersuchungen zur Detektion der im Product-Sensing-Verhalten involvierten Signalmoleküle der Mikroalge Porphyridium purpureum“</i> |
| 07/2003 | Abitur at Zeppelin-Gymnasium Lüdenscheid |

Publications

Papers

- N. Rakel**, L. Galm, K. C. Bauer, J. Hubbuch
Influence of macromolecular precipitants on phase behavior of monoclonal antibodies
Biotechnology Progress, 2015, 31(1), 145-153
- N. Rakel**, K. C. Bauer, L. Galm, J. Hubbuch
From osmotic second virial coefficient (B_{22}) to phase behavior of a monoclonal antibody
Biotechnology Progress, 2015, 31(2), 438-451
- N. Rakel**, M. Baum, J. Hubbuch
Moving through three-dimensional phase diagrams of monoclonal antibodies
Biotechnology Progress, 2014, 30(5), 1103-1113
- N. Rakel**, K. Schleining, F. Dimer, J. Hubbuch
Self-interaction chromatography in pre-packed columns: a critical evaluation of SIC methodology to determine the second virial coefficient
Journal of chromatography A, 2013, 1293, 75-84
- B. Schmidt-Hansberg, M. Sanyal, M. Klein, M. Pfaff, **N. Schnabel**, S. Jaiser, A. Vorobiev, E. Müller, A. Colsmann, P. Scharfer, D. Gerthsen, U. Lemmer, E. Barrena, W. Schabel
Moving through the phase diagram: morphology formation in solution cast polymer-fullerene-blend films for organic solar cells
ACS Nano, 2011, 5 (11), 8579–8590

Presentations

- N. Schnabel**, S. Hansen, B. Maiser, P. Diederich
A-mAb: a case study in bioprocess development
Workshop, Downstream Days Summer School, 13.-16.09.2011, Wetter a. d. Ruhr, Germany
- B. Schmidt-Hansberg, **N. Schnabel**, K. Peters, P. Scharfer, U. Lemmer, M. Kind, W. Schabel
Phase separation during the drying process of the photoactive layer in polymer solar cells
14th International Coating Science and Technology Symposium, 7.-10.09.2008, Marina del Rey, USA

K. Lang, **N. Rakel**, A. Schaller, F. Dimer, J. Hubbuch
In silico-Charakterisierung der thermischen Stabilität von Proteinen in verschiedenen Puffersystemen
ProcessNet-Jahrestagung und 30. DECHEMA-Jahrestagung der Biotechnologen 2012, 10.-13.09.2012, Karlsruhe, Germany

J. Hubbuch, **N. Schnabel**, F. Dimer, S. Alten, M. Kind, B. Cornehl, H. Nirschl, Y. Zang, M. Eisenkolb, H. Kiefer, S. Ebert, F. Nothelfer
Protein crystallization – from phase diagrams to process
Recovery of Biological Products 29.07.-02.08.2012, Stowe, USA

N. Schnabel, F. Dimer, J. Hubbuch
Self-interaction-chromatography as predictive tool in protein crystallization and the influence of immobilization reaction
1st European Congress of Applied Biotechnology and 8th European Congress of Chemical Engineering, 25.-29.09.2011, Berlin, Germany

N. Schnabel, F. Dimer, J. Hubbuch
Einfluss der Immobilisierung beim Herstellen von Säulen für die Self-Interaction-Chromatographie
Vortrags- und Diskussionstagung: Bioverfahrenstechnik an Grenzflächen, 30.05.2011 - 01.06.2011, Potsdam, Germany

B. Schmidt-Hansberg, **N. Schnabel**, K. Peters, P. Scharfer, W. Schabel
Phasenseparation von Polymer-Fulleren-Lösungen photoaktiver Schichten organischer Polymersolarzellen
ProcessNet-Fachausschuss Kristallisation, 12.-13.03.2009, Dortmund, Germany